The Design of a coupled co-axial resonator filter for Low Earth Orbit Satellites working at Microwave Frequencies

Lwazi Sam

Thesis presented in fulfillment for the requirements of the degree of Master of Science (Eletronic) at the University of Stellenbosch
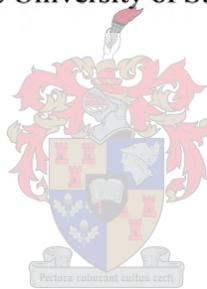
Study Leader: Prof P Meyer

Co-Study Leader: Mr W. J. A van Brakel

December 2002

Declaration

I, the undersigned, hereby declare that the work contained in this thesis is my own original work unless otherwise indicated.

Lwazi Sam   April 2002

Abstract

Keywords: Coupled resonator filters, Co-axial line resonators, Basic Coupling
Design, Co-axial resonator filter

The study of the basic dynamics of filters, with the emphasis on coupled resonator filters, is presented. Special attention is paid to the synthesis of doubly terminated coupling matrices using the Darlington method. Due to restrictions placed on the filter by the equivalent circuit used, a coupling matrix reduction is applied to the resulting coupling matrix.

An investigation is performed on $\lambda/2$ co-axial line resonators, with the emphasis on rectangular co-axial line resonators with a round center conductor. The basic definition of the coupling coefficient is revisited and it is calculated using the method based on Bethe's theory and Cohn's experimental work.

A 4th-order co-axial resonator filter operating at 3 GHz is designed using the theory outlined in this thesis. The measured response is in good agreement with the theory in terms of the center frequency, but disagree in terms of the coupling coefficient, bandwidth and Q-factor. The reasons for this, as well as suggestions for improving the accuracy of the parameters mentioned, are given.

Opsomming

Sleutelwoorde: Gekoppelde resoneerder filters, Ko-aksiale lyn resoneerders, Basiese Koppeling Ontwerp, Ko-aksiale resoneerder filter

Die studie van die basies dinamika van filters, met die klem op gekoppelde resoneerder filters, is voorgelê. Spesiale aandag is gegee aan die sintese van dubbelbelaste koppel matrikse met die gebruik van die Darlington metode. As gevolg van die beperkings wat op die filter geplaas word deur die gebruik van die ekwivalent stroombaan, word 'n koppel matriks vermindering gebruik.

'n Ondersoek is gedoen op $\lambda/2$ ko-aksiale lyn resoneerders, met die klem op reghoekige ko-aksiale lyn resoneerders met 'n ronde binnegeleier. Die basiese definisie van die koppel koëffisiënt is hersien en dit is bereken met die gebruik van die metode wat baseer is op Bethe se teorie en Cohn se experimentele werk.

'n 4de-orde ko-aksiale resoneerder filter wat opereer by 3 GHz is ontwerp met die gebruik van die teorie wat in hierdie tesis gaskets word. Die gemete weergawe is in goeie ooreenkoms met die teorie in terme van die senter frekwensie, maar verskil in terme van die koppel koëffisiënt, bandwydte en Q-faktor. Die rede hiervoor, as ook voorstelle vir die verbetering van die akkuraatheid van die parameters wat genoem is, is gegee.

Acknowledgements

Special thanks must be given to:

The Almighty God, for giving me strength and health to finish this project. My parents and my friends for supporting me through all the years of my education.

The Department of Communications of the Republic of South Africa, for both moral and financial support of this project.

My supervisor, Prof. P. Meyer and Co-supervisor, Mr. Wessel van Brakel for his guidance and constant support through out this research.

Mr. Wessel Croucamp for the construction of filter.

Contents

i

List of Figures

List of Tables

List of Abbreviations and Symbols

A^+, A^-	-	Arbitrary amplitudes of the forward and backward waves, respectively
A-A	-	Symmetry line between two identical cavities
B, Δf	-	bandwidth
c_1	-	Influence of the iris resonance effect on the coupling
c_2	-	Finite iris thickness
c_3	-	Variation of field strength over the iris
DC	-	Direct Current
$D_k(s)$	-	Roots of the transmission coefficient
$D_k^*(s)$	-	Conjugate of $D_k(s)$
e_1	-	Source voltage
e_n	-	Load voltage
E_n	-	Normal electric field vector
E_x, E_y	-	Transverse electric fields
$\overline{e}(x, y)$	-	Transverse variation of the mode
$E_1(s)$, $E_2(s)$	-	Even parts of $D_k(s)$
$E(s)$	-	Poles of the function
E_0	-	Odd part of $E(s)$
E_e	-	Even part of $E(s)$
E_G	-	Generator voltage
E_s	-	Source voltage
$F(s)$	-	Reflection zeros
F_0	-	Even part of $E(s)$
F_e	-	Odd part of $E(s)$
f_c	-	Free space wavelength at the cutoff frequency
f_0	-	Resonant frequency
f	-	Frequency of operation

ix

f_r	-	Resonant frequency of the aperture
f_e	-	Resonant frequency resulting when the the plane A-A is a perfect electric wall
f_m	-	Resonant frequency resulting when the the plane A-A is a perfect magnetic wall
G	-	Conductance
$H(s)$	-	Transfer function
$|H(j\omega)|$	-	Magnitude function
$|H_{LP}(j\omega)|$	-	Low-pass filter magnitude function
$|H_{HP}(j\omega)|$	-	High-pass filter magnitude function
$|H_{BP}(j\omega)|$	-	Band-pass filter magnitude function
$|H_{BR}(j\omega)|$	-	Band-reject filter magnitude function
$|H_{AP}(j\omega)|$	-	All-pass filter magnitude function
$h(t)$	-	Impulse response function
H_t	-	Tangential magnetic field vector
I	-	Identity matrix
I_2	-	Output current
I_1	-	Input current
$I(s)$	-	Current transfer function
I_{1r}	-	Reflected current from port 1
$[I]$	-	Current matrix
$K(s)$	-	Characteristic function
k_c	-	cutoff wavenumber
L	-	Inductance or physical length
ΔL	-	Length of aperture
M	-	Coupling matrix
M_e	-	Even-mode coupling matrix
M_{ij}	-	Coupling coefficient between ith and jth cavities
M_R	-	Complex variable

M_0	-	Magnetic polarizability
M_m	-	Magnetic dipole moment
n_1, n_2	-	Transformer turns
$O_1(s), O_2(s)$	-	Even part of $D_k(s)$
PEC	-	Perfect electric conductor
PMC	-	Perfect Magnetic Conductor
P_ℓ	-	Average power dissipated
P_r	-	Reflected power
P_{max}	-	Maximum amount of power available from the generator
P_1	-	Power that emerge at the load.
p_i	-	Pole of the function
$P(s)$	-	Transmission zeros
P	-	Average power in the system
P_u	-	Internal power dissipation
P_c	-	Power loss by conductors
P_r	-	Power loss by radiation
P_d	-	Power loss by dielectric fills
P_e	-	Power loss due to external drain on the internal energy reserves
P_T	-	Total power loss by the system
P_{Lb}	-	Power delivered to a specified load before inserting the network
P_{La}	-	Power delivered to a specified load after inserting the network
P_0	-	Electric polarizability
Q	-	Quality factor
Q_u	-	Unloaded Q-factor
Q_L	-	Loaded Q-factor
Q_e	-	External Q-factor
Q_s	-	Single loaded Q-factor

R_s, R_1	-	Source resistance
R_r	-	Rotation matrix
R_r^t	-	Transpose of R_r
R_G	-	Generator impedance
R_0	-	Impedance-scaling factor
R_L, R_n	-	Load resistance
$[S]$	-	Scattering Matrix
s	-	Complex variable
S	-	Transformed complex variable
S_{11}, S_{22}	-	Reflection coefficients
$S_{11num}(s)$	-	Numerator of the reflection coefficient
$S_{11den}(s)$	-	Denominator of the reflection coefficient
S_{21}, S_{12}	-	Transmission coefficients
T	-	Orthogonal matrix
T^t	-	Transpose of the orthogonal matrix
$T_d(\omega)$	-	Group delay
$T_p(\omega)$	-	Phase delay
$\Gamma(s)$	-	Power-transmission ratio
$\left|t(j\omega)\right|^2$	-	Normalized low-pass insertion loss ratio
T_{1k}, T_{Nk}	-	Row vectors
U_1	-	Potential of the inner conductor
V_2	-	Output voltage
V_{1i}	-	Incident voltage at port 1
V_{1r}	-	reflected voltage from port 1.
$[V]$	-	Voltage matrix
v_p, c	-	Phase velocity
V_0^+	-	Amplitude of the incident voltage
ω_p	-	Cutoff frequency

ω_L	-	Loaded natural resonant frequency
ω	-	Radian frequency
ω_0	-	Radian resonant frequency
ω_s	-	Stop band frequency
W_0	-	Maximum energy stored by a resonator
W_m	-	Average energy stored by inductance
W_e	-	Average Energy stored by capacitance
w	-	Width
Δw	-	Width of aperture
$X(s)$	-	Laplace transform of the input
X_c	-	Capacitance reactance
X_L	-	Inductance reactance
x	-	Input of the system
y	-	Output of the system
$Y_{12}(s)$	-	Transfer admittance (mhos)
Y_e	-	Even-mode admittance
Y_o	-	Odd-mode admittance
Y_e^*	-	Conjugate of even-mode admittance
$Y(s)$	-	Laplace transform of the output
Y_{in}	-	Input admittance (mhos)
$Z_{12}(s)$	-	Transfer impedance (ohms)
Z	-	Impedance (ohms)
$[Z]$	-	Impedance matrix
Z_L	-	Load impedance
$Z(s)$	-	Open-circuit impedance matrix
Z_n^e, Z_d^e	-	Complex even polynomials for the numerator and denominator of the input impedance, respectively
Z_n^o, Z_d^o	-	Complex odd polynomials for the numerator and denominator of the input impedance, respectively

Z_0	-	Characteristic impedance of transmission line
$Z_{in}(s)$	-	Complex odd polynomials
z_{ij}	-	Open-circuit impedance parameters
z_i	-	Zero of the function
Z_{in}	-	Input impedance (ohms)
α_p	-	Pass-band ripple
α_s	-	Stop band attenuation
$\alpha(\omega)$	-	Attenuation
$\phi(\omega)$	-	Phase function
$\beta(\omega)$	-	Phase-lag angle
Ω_0	-	Desired cutoff frequency
Ω	-	Normalized frequency
Ω_1	-	Lower 3-dB point
Ω_2	-	Upper 3-dB point
Λ	-	Diagonal of the eigenvalues
θ_r	-	Angle of rotation
σ	-	Conductivity
Γ	-	Reflection coefficient
γ	-	Complex propagation constant
β	-	Phase constant
π	-	3.14159265
λ_g	-	Wavelength in guide cavity
μ_0	-	Permeability of air
ε_0	-	Permittivity of air
μ	-	Permeability of the material
ε	-	Permeability of the material
J_{nm}	-	Bessel function of the first kind
$\tan\delta$	-	Loss tangent
λ	-	Wavelength
ℓ/L	-	Ratio of the tap point position to the physical length of cavities

Chapter 1

Introduction.

1.1 The History of Filters in Telecommunications.

The theory and design of microwave filters can be traced back to the period during World War II when pioneering work was done at various institutions, including the Radiation Laboratory of Massachusetts Institute of Technology.

The precise filter design method with two specific design steps was introduced in 1940 [MY 2001]. The first step was the determination of the transfer function that met with the required specifications. The second step was the synthesis of the circuit that realizes the transfer function. Soon, filter design development expanded from the lumped-element LC resonators to the newly discovered distributed coaxial line resonators and waveguide resonators.

In 1939, Richtemeyer [Ri 1939] reported that the dielectric resonator, which utilized the electromagnetic wave resonance, had two special features. These are small size and high Q-factor value. However, the material's lack of temperature stability in those days meant that the filter was insufficient for practical use.

In the 1970s, the development of various kinds of ceramic materials with excellent temperature stability and high Q-factor value increased the viability of practical application of the dielectric filter [Co 1968]. In addition, superconducting materials with high critical temperature discovered in the 1980's are expected to have the possibility of designing novel microwave filters with extremely low loss and small size.

The early stages of filter design were based on passive electrical circuits composed of appropriate combinations of an inductor, L, and a capacitor, C. The LC resonator being a linear resonant system.

In addition, early stages of filter design also suggested that there could be another approach that realizes filter response without utilizing a linear resonant system. The main reasoning behind this was the general view of filters as functional devices which achieve their performance according to a given transfer function. Filtering systems, which employed active circuits, were typical examples.

Moreover, there is also a digital technique, which realizes the transfer function of a filter digitally. Currently almost all digital communications systems adopt these digital filters as the base-band filters.

Due to variety and diversity of filter types, it often becomes necessary for a designer to carefully consider which filter to adopt for particular applications. Filters are classified according to their frequency response and are divided into four basic types, that is, low-pass filters, high-pass filters, band-pass filters and band-stop filters. The low-pass filter provides the basis for other filter types.

1.2 Filters for Wireless Communication

Filters developed during the World War II period were of the band-pass type. They are used to protect receivers from interference signals in the spectral region outside their operating bands and to confine radiation from transmitters within specified spectral limits. These requirements generally translated into specifications on frequency domain amplitude responses, such as passband reflection and stop band rejection.

Similar basic demands regarding amplitude response are made on modern band-pass filters, but in addition there are increasing demands on the phase and/or group delay characteristics, especially of filters intended for use in communication satellites and high capacity terrestrial systems.

Conventional communication satellite transponder designs employ multiplexing systems based upon Chebyscheff or Butterworth waveguide band-pass filters. In order to utilize the allocated frequency spectrum as efficiently as possible, guard bands should be kept very narrow and hence, sharp cut-off filters result. Further, the filters must have flat in-band group delay and a small gain slope in order to minimize distortion and cross talk [BM 1970]. Conventional direct coupled waveguide Chebyscheff filters of high order followed by group delay equalizers have been used in the design of multiplexing systems for such transponders [AW 1967]. Not only do these filters represent a significant percentage of the overall transponder weight, but filtering functions also do not possess optimum frequency selectivity, group delay, or in-band insertion loss.

However, the rise of satellite communications in the late 1960's challenged microwave engineers to reduce the mass and the volume of the communication payload. The result was coupled cavity filters employing more than one resonator per cavity. At microwave frequencies, a single cavity can support an infinite number of modes at different frequencies and it is up to the filter designer to suppress unwanted modes and control the wanted modes independently.

The use of more than two degenerate modes in a single cavity of cylindrical cross section was introduced in a fifth order filter by Lin [Li 1951]. Although the use of more degenerate modes in a single cavity is an obvious attractive solution to reducing the size and weight of a filter, the control of more than three modes is difficult from a practical point of view. However, higher order filters can be constructed by cascading either dual or triple mode cavities.

1.3 Problem Statement

Satellite systems needs small, low-loss, lightweight filters for the definition of bands. This project calls for the design of a coupled co-axial resonator filter for Low Earth Orbit satellite applications working at microwave frequencies. Fig. 1.1 shows a co-axial resonator filter with the lid removed, consisting of identical square coaxial resonators concentric with cylindrical conductor coupled with rectangular apertures.
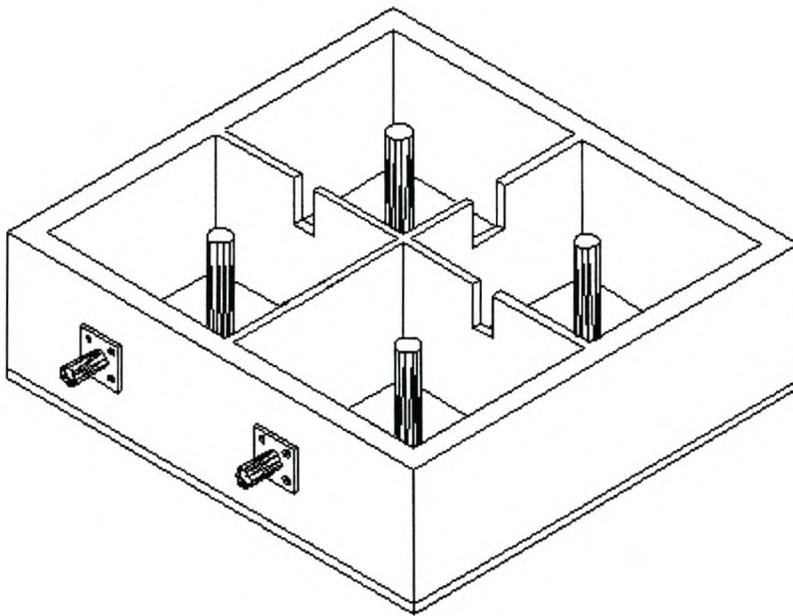
Figure 1.1 Co-axial resonator filter.

The aim of this thesis is to illustrate the design of a co-axial resonator filter, starting with the approximation function and ending in a prototype filter.

1.4 About the Thesis

This thesis main objective is to design a fourth order co-axial band-pass filter working at microwave frequencies.

Chapter 2 describes the roles and the basic concepts of analog filters, their applications in electrical engineering and certain fundamental ideas concerning them.

Introduction to coupled resonator filters, synthesis, reduction and the realization of the coupling matrix is given in Chapter 3.

Since coupled resonator filters are made of n identical cavities, transmission line, cavity and co-axial line resonators are discussed in Chapter 4 with the emphasis on their Q-factors.

Each resonator is coupled to each other through apertures. Chapter 5 gives a basic coupling design that can be used to determine the coupling coefficient between cavity resonators.

The design of a co-axial resonator filter and measurement results are covered in chapter 6.

Lastly, chapter 7 gives the conclusions, discussions and future work.

Chapter 2

Basic Dynamics of Filters

2.1 Introduction

There are many ways of actually implemeting a filter using both active and passive circuits. In general active filters are used at low frequencies where both inductor and capacitor values are impractical, passive filters are used at higher frequencies (MHz or above) where the values become realistic.

The filtering system plays a major role in determining the overall system response. For this reason familiarity with the fundamental aspects of filter response is not only a must for the filter engineer, but it is advantageous for the system designer and those who specify and use filters. Appreciation of the factors that are affecting various responses results in more realistic system and filter requirements.

This chapter describes the role and the basic concepts of analog filters (branch of filter theory that makes use of linear time-invarying elements to perform certain tasks on continuous functions) and their applications at microwave frequencies.

2.2 Basic Filter Types

The theory presented in this section follows the theory set fourth by Su [Su 1996-a]. In Fig. 2.1, five basic filter types, each characterized by its magnitude response as a function of the radian frequency, ω, are (a) low-pass, (b) high-pass, (c) band-pass, (d) band-reject and (e) all pass filters.
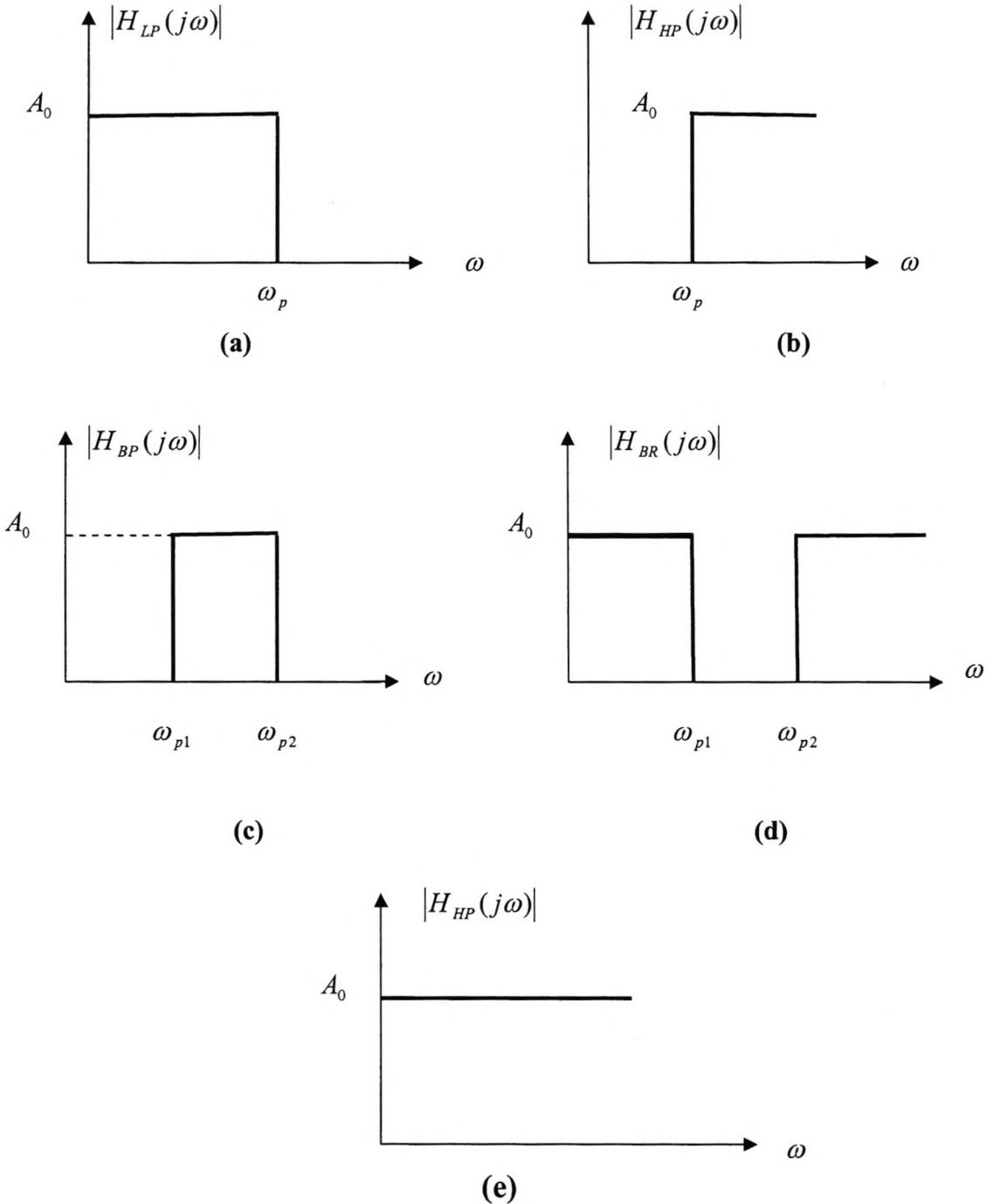
Figure 2.1 Magnitude Characteristics for ideal Filters

The first four filters can be used as frequency selective circuits. Moreover, filters for communication purposes are normally of the band-pass type, and are used to select a frequency band in which a system will receive or transmit a signal. All signals falling outside this band will be rejected and not allowed into the system. Fig. 2.2 shows the application of the band-pass filters as frequency selective circuits at microwave frequencies.
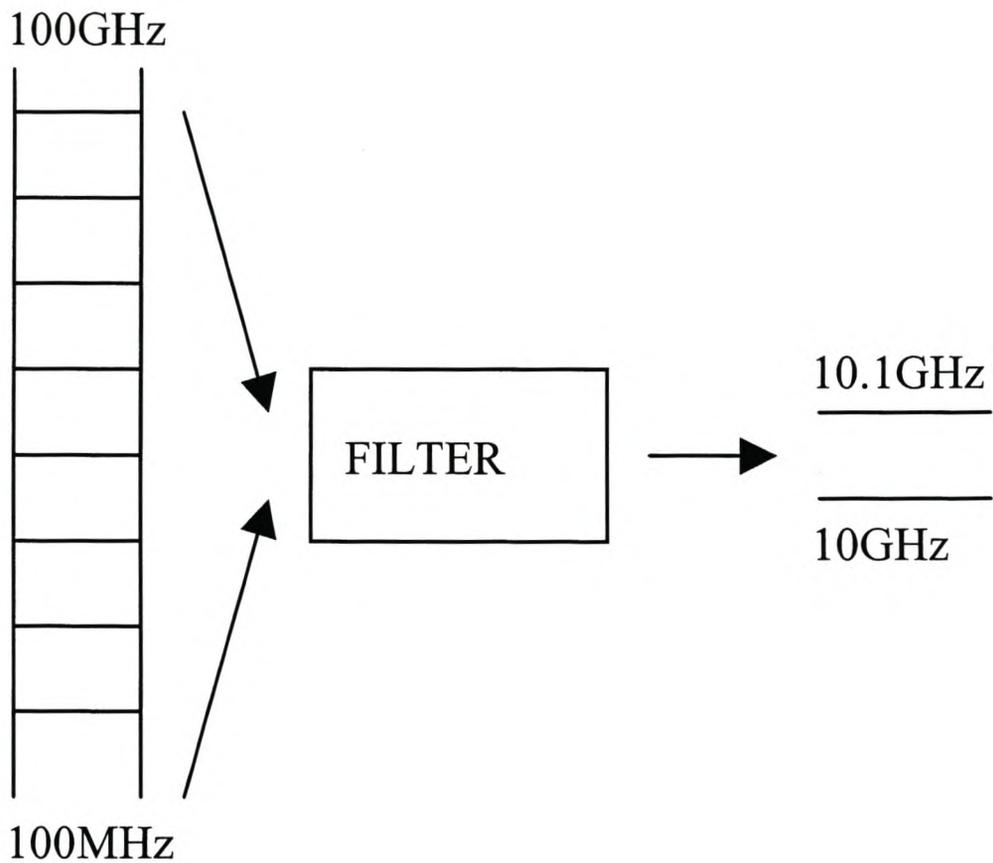
Figure 2.2 Applications of Microwave filters

The all-pass filter is used mainly for its phase-linearization or delay-equalization. Also, these responses are called ideal characteristics since they are not realizable by finite networks.

Fig. 2.3 contains an example of the magnitude of a typical low-pass filter that illustrates the types of characteristics of most low-pass filters. Instead of each

frequency being passed or rejected, there are three regions, i.e., a pass-band, transition band, and a stop-band, which are defined by the cutoff frequency, ω_p, and a stop band frequency, ω_s.
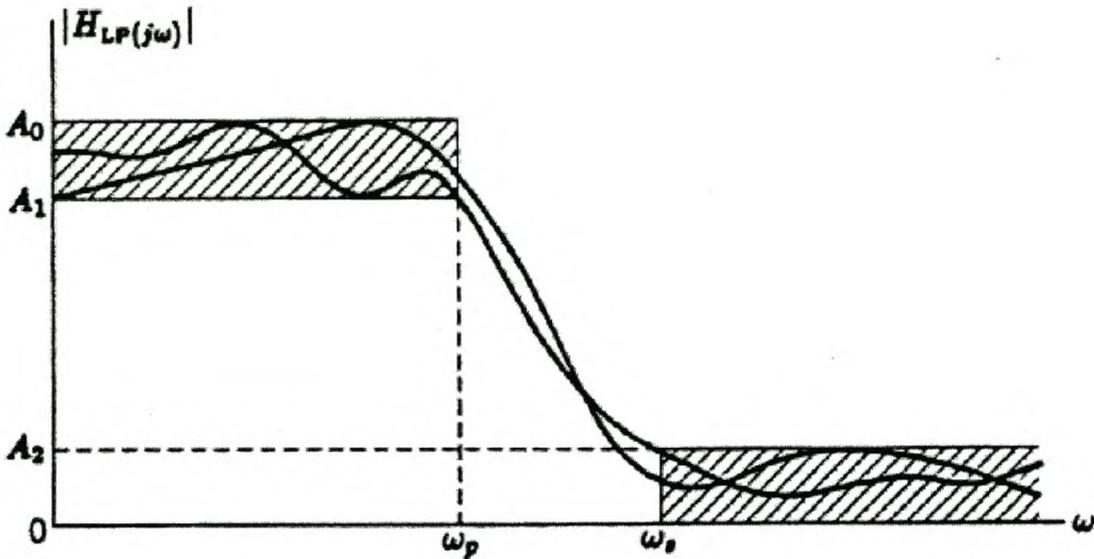
Figure 2.3 Approximate low-pass magnitude characteristics.

The region $0 < \omega < \omega_p$ is considered to be the pass-band in that the gain is relatively high so signals in this range are pass through. The amount of variation in the pass band, which is indicated by the maximum gain variation, is called the pass-band ripple or pass-band variation, α_p, given by the following equation

$$\alpha_p = 20\log\left[\frac{A_0}{A_1}\right] \text{dB} \qquad (2.1)$$

Furthermore, the region $\omega_s < \omega < \infty$, in which the gain is made very small, is called the stop-band. At this region, the filter suppresses signals. Also, the degree of suppression of signals in this range is indicated by the stopband attenuation, α_s, defined as

$$\alpha_s = 20\log\left[\frac{A_0}{A_2}\right] \text{dB} \qquad (2.2)$$

Finally the region $\omega_p < \omega < \omega_s$ is known as the transition band and the quantity ω_s / ω_p is called the transition band ratio.

In this chapter the primary attention will be paid to low-pass filters, as there are other techniques in which the other three types of filters can be derived from basic low-pass ones.

2.3 Transfer Function

The transfer function of a linear, time invariant, differential equation system is defined as the ratio of the Laplace transform of the output (response function) to the Laplace transform of the input (driving function) under assumption that all the initial conditions are zero [Og 1990].

$$a_0 y^n + a_1 y^{n-1} + \cdots + a_{n-1}\dot{y} + a_y y = b_0 x^m + b_1 x^{m-1} + \cdots + b_{m-1}\dot{x} + b_m x \qquad (2.3)$$

where y is the output of the system and x is the input. Taking the Laplace transform of eqn. (2.3), under the assumption that all initial conditions are zero, yields

$$H(s) = \frac{Y(s)}{X(s)} = \frac{b_0 s^m + b_1 s^{m-1} + \cdots + b_{m-1}s + b_m}{a_0 s^n + a_1 s^{n-1} + \cdots + a_{n-1}s + a_n} \quad (n \geq m) \qquad (2.4)$$

where $s = \sigma + j\omega$ and $X(s)$ and $Y(s)$ are regarded as the Laplace transforms of the input and output, respectively.

However, the transfer function defined above is a complex number that can be represented in polar form or in magnitude and phase form as follows

$$H(j\omega) = |H(j\omega)|e^{j\phi(\omega)} \qquad (2.5)$$

where $|H(j\omega)|$ is the magnitude function and $\phi(\omega)$ is the phase function. Because $|H(j\omega)|$ can take on an enormous range of values, the logarithm of eqn. (2.5) is often used to obtain more convenient values. If the natural logarithm is used [BZ 1976]

$$\ln H(j\omega) = \ln\left[|H(j\omega)|e^{j\phi(\omega)}\right] = \ln|H(j\omega)| - j\phi(\omega) = \alpha(\omega) + j\beta(\omega) \quad (2.6)$$

where $\alpha(\omega)$ is the attenuation in nepers given by

$$\alpha(\omega) = \ln|H(j\omega)| \text{ nepers} \tag{2.7}$$

and $\beta(\omega)$ is the phase-lag angle in radians and is the negative of $\phi(\omega)$,

$$\beta(\omega) = -\phi(\omega) \text{ rads} \tag{2.8}$$

In addition, it is more convenient to deal with $|H(j\omega)|^2$ instead of $|H(j\omega)|$. $|H(j\omega)|^2$ can be obtained as follows

$$|H(j\omega)|^2 = H(s)H(-s)\big|_{s=j\omega} = H(j\omega)H(-j\omega) \tag{2.9}$$

A common definition for attenuation is given by Su [Su 1996-a] to be

$$\alpha(\omega) = 20\log|H(j\omega)| \text{ dB} \tag{2.10}$$

Since the design of filters starts from the low-pass filter, the emphasis in this section is to seek magnitude characteristics that approximate the ideal low-pass filter characteristics shown in Fig. 2.1(a). The general approach for obtaining the low-pass characteristic is to seek a function of the form

$$|H(j\omega)|^2 = \frac{A_0}{1 + F(\omega^2)} \tag{2.11}$$

such that

$$\begin{aligned} F(\omega^2) &<< 1 \quad 0 < \omega < \omega_p \\ F(\omega^2) &>> 1 \quad \omega > \omega_s \end{aligned} \tag{2.12}$$

This implies that $|H(j\omega)|^2 \approx A_0$ in the pass band and $|H(j\omega)|^2 << A_0$ in the stop band. These are essential features of a low-pass characteristic that approximate the ideal low-pass characteristics.

From eqn. (2.11), non-ideal low-pass characteristics that are in common use, that is the Butterworth, the Chebyschev, and the elliptic function magnitude characteristics, can be derived.

2.3.1 Derivation

Fig 2.4 shows two equivalent double terminated second order networks. The transfer function for the network shown in Fig. 2.4(a) is obtained by first replacing each element by the generalized impedance, which is shown in Fig. 2.4(b).

(a)   (b)
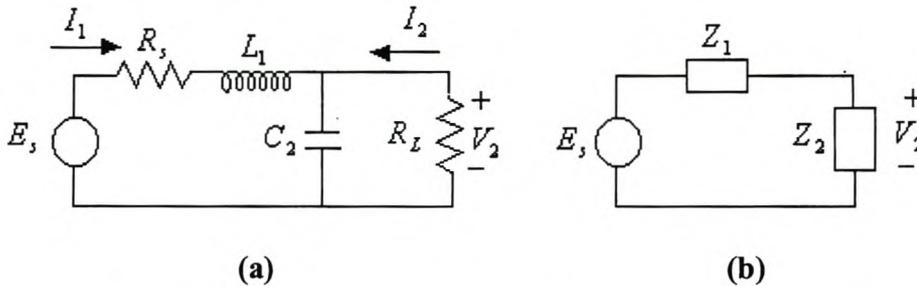
Figure 2.4 Double terminated second-order network

The impedance of the parallel RC and the series RL circuit are given by

$$Z_1 = R_s + sL_1 \qquad (2.13a)$$

and

$$Z_2 = \frac{R_L}{sR_L C_2 + 1} \qquad (2.13b)$$

respectively. The output voltage is obtained by the voltage division of the input as

$$V_2 = \frac{Z_2}{Z_1 + Z_2} E_s = \frac{Z_2}{Z_{in}} E_s = Y_{in} Z_2 E_s \qquad (2.14)$$

with Z_{in} and Y_{in} representing the input impedance and the input admittance, respectively. Then the transfer function, $H(s)$, is given by

$$H(s) = \frac{V_2}{E_s} = \frac{Z_2}{Z_1 + Z_2} \qquad (2.15)$$

Furthermore, the transfer impedance, $Z_{12}(s)$, relates the output voltage to the input current and has the dimension of ohms, while the transfer admittance, $Y_{12}(s)$, relates the output current to the input voltage and has the dimension of mhos. Applying ohms law to Fig. 2.4(a), the output current and input current can be determined to be

$$-I_2 = \frac{V_2}{R_L} \qquad (2.16a)$$

$$I_1 = \frac{E_s}{Z_{in}} \qquad (2.16b)$$

Dividing I_2 by E_s and V_2 with I_1 result to the following equations for $Y_{12}(s)$ and $Z_{12}(s)$.

$$Y_{12}(s) = \frac{I_2}{E_s} = \frac{V_2}{E_s} \times \frac{1}{R_L} \qquad (2.17a)$$

$$Z_{12}(s) = \frac{V_2}{I_1} = \frac{V_2}{E_s} \times Z_{in} \qquad (2.17b)$$

In addition, the ratio of the output current to the input current is called the current transfer function, $I(s)$, and is dimensionless. Dividing I_2 by I_1, the current transfer function is obtained to be

$$I(s) = \frac{I_2}{I_1} = \frac{V_2}{R_L} \times \frac{Z_{in}}{E_s} = \frac{V_2}{E_s} \times \frac{Z_{in}}{R_L} \qquad (2.18)$$

2.3.2 Poles and zeros

By factoring the polynomials of eqn. (2.4), eqn. (2.19) result

$$H(s) = K \frac{\prod_{i=1}^{m} (s - z_i)}{\prod_{i=1}^{n} (s - p_i)} \quad n \geq m \tag{2.19}$$

When $s = z_i$, s is referred to as a zero of the function, and when $s = p_i$, s is referred as a pole of the function.

The locations of the poles and zeros in the s-plane completely determine the transfer function, and this is illustrated in Fig. 2.5. Fig. 2.5 shows a magnitude characteristic of a fifth-order filter formed by the poles that lie in the left-halfplane of the s-plane.
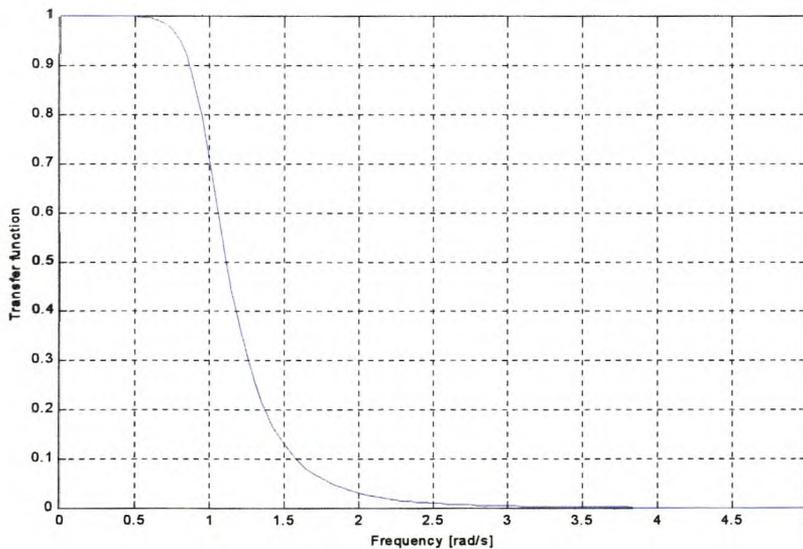
Figure 2.5 Magnitude Characteristics of 5$^{\text{th}}$-order Butterworth Filter

In addition, poles and zeros can be used to compute the corresponding time response and thus identify some responses with pole locations in the s-plane. Furthermore, poles determine whether the time-domain response increases with time, oscillates or decreases with time (this is illustrated in Fig. 2.6).

2.4 Impulse Response

Consider the output (response) of a system to a unit impulse input when the initial conditions are zero. Since the Laplace transform of the unit impulse function is unity, the Laplace transform of the output of the system is just

$$Y(s) = H(s) \qquad (2.20)$$

The inverse Laplace transform of the output given by eqn. (2.20) is the impulse-response function, or

$$y(t) = h(t) \qquad (2.21)$$

The impulse response function $h(t)$ is thus the response of a linear system to a unit impulse input when the initial conditions are zero. From eqn. (2.20) and eqn. (2.21) it is seen that the impulse-response is given by the time function corresponding to the transfer function. Hence it is called the natural response of the system.

In general, the shape of the natural response is determined by the location of the poles of the transfer function. A sketch of these pole locations and corresponding natural responses is given in Fig. 2.6, along with other pole locations including complex ones.
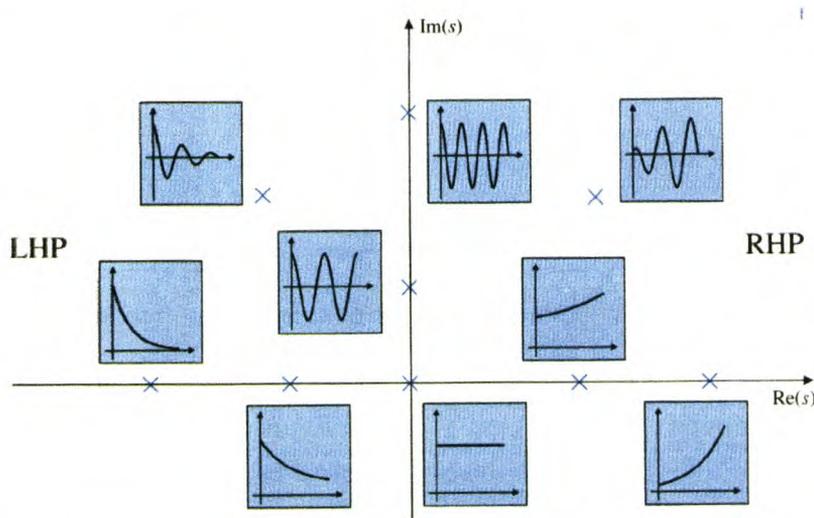
Figure 2.6 Pole locations and corresponding natural responses.

2.5 Group Delay

If a signal is suddenly applied to a system input, the effect is usually not immediately observable at the output, but occurs at a later time. Two useful functions for describing this delay are group delay and phase delay.

In a general sense, the group delay describes the delay of a packet of frequencies, whereas phase delay is the delay of a single sinusoid. The group delay, $T_d(\omega)$, and phase delay, $T_p(\omega)$, are defined by Su [Su 1996-a] and Blinchikoff [BZ 1976], respectively, to be

$$T_d(\omega) = -\frac{d}{d\omega}\phi(\omega) \qquad\qquad (2.22a)$$

$$T_p(\omega) = -\frac{\phi(\omega)}{\omega} \qquad\qquad (2.22b)$$

where $\phi(\omega)$ is the phase function. The group delay four a fifth-order Butterworth filter is shown in Fig. 2.7. In order for the input signal to be recovered at the output of the filter, constant group delay over the passband of a filter is needed.
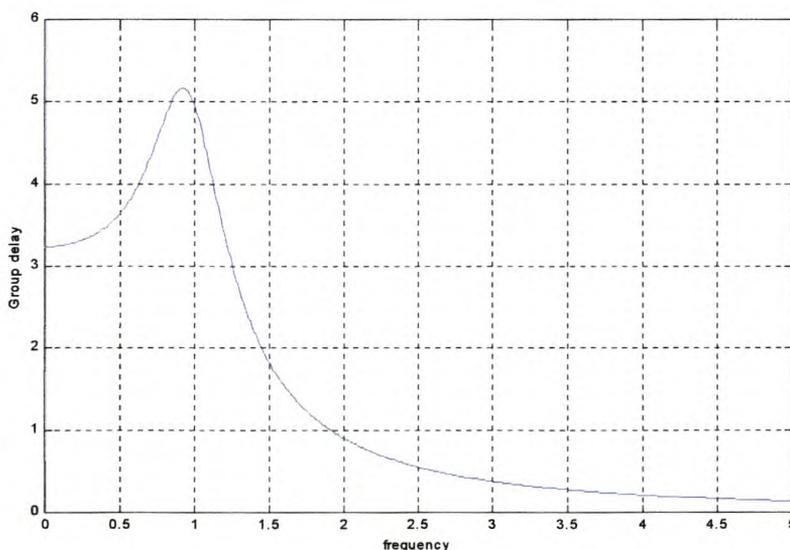
Figure 2.7 Group Delay for 5ᵗʰ order Butterworth filter

2.6 Normalization and Denormalization Scaling

The use of standard units (ohms, henrys, farads, etc) frequently leads to very large or small numbers in circuit analysis and design. Using these normalized values (1 H and 1 F) will produce a transfer function that gives a cutoff frequency of 1 rad/sec. These values are practically unrealizable. In addition, since filters are used for many different frequency ranges and impedance levels, it is desirable to be able to standardize the basic theory and design, and then adapt the filter to different applications.

To allow the use of realistic values and to accomplish different frequency ranges in filters, Frequency Scaling and Impedance Scaling must be applied.

2.6.1 Frequency Scaling

Frequency Scaling is the process of shifting the cutoff frequency of the filter from 1 rad/sec to the desired cutoff frequency, Ω_0. The impedance of an inductor and admittance of a capacitor are given by eqn. (2.23a) and eqn. (2.23b).

$$Z(s) = sL \qquad (2.23a)$$

$$Y(s) = sC \qquad (2.23b)$$

Applying frequency scaling to eqns. (2.23) yields eqn. (2.24a) and eqn. (2.24b)

$$Z'(s') = Z\left(\frac{s}{\Omega_0}\right) = s\frac{L}{\Omega_0} \qquad (2.24a)$$

$$Y'(s') = Y\left(\frac{s}{\Omega_0}\right) = s\frac{C}{\Omega_0} \qquad (2.24b)$$

where the primed letters represent the values after frequency scaling is applied.

It can be seen from eqns. (2.24) that frequency scaling has the effect of dividing every inductance and capacitance by the desired cutoff frequency. Hence the cut off frequency is now at Ω_0. In addition, the transfer function, $H(s)$, becomes, $H(s/\Omega_0)$.

2.6.2 Impedance Scaling

Impedance Scaling is the process of changing the component values to practical ones without changing the cutoff frequency. The impedance-scaling factor is denoted by R_0. Applying the impedance scaling to eqns (2.13, 2.15, 2.17, and 2.18) derived in section 2.2.1, yields the following equations

$$Z'_1 = R_0 R_s + s R_0 L_1 = R_0 Z_1 \qquad (2.25a)$$

$$Z'_2 = \frac{R_0 R_L}{s(R_0 R_L)\left(\dfrac{C_2}{R_0}\right)+1} = R_0 Z_2 \qquad (2.25b)$$

$$H'(s) = \left(\frac{V_2}{E_s}\right)' = \frac{R_0}{R_0\left(Z_1 + Z_2\right)} = \frac{V_2}{E_s} = H(s) \qquad (2.25c)$$

$$Z'_{12}(s) = \left(\frac{V_2}{I_1}\right)' = \left(\frac{V_2}{E_s}\right)' Z'_{in} = \left(\frac{V_2}{E_s}\right)R_0 Z_{in} = R_0 Z_{12}(s) \qquad (2.25d)$$

$$Y'_{12}(s) = \left(\frac{I_2}{E_s}\right)' = \left(\frac{V_2}{E_s}\right)' \frac{1}{R_0 R_L} = Y_{12}(s)\frac{1}{R_0} \qquad (2.25e)$$

$$I'(s) = \left(\frac{I_2}{I_1}\right)' = \left(\frac{V_2}{E_s}\right)' \times \frac{Z'_{in}}{R_0 R_L} = I(s) \qquad (2.25f)$$

where the primed letters represent the values after impedance scaling is applied.

From eqns. ((2.25a)-(2.25f)), it can be seen that, when impedance scaling is applied the following consequences occur

- All the network functions that have the dimension of impedance (such as driving point impedance Z_{in} and the transfer impedance $Z_{12}(s)$) will be multiplied by R_0.

- All network functions that have the dimension of admittance (such as the driving point admittance Y_{in} and the transfer admittance $Y_{12}(s)$) will be divided by R_0.

- All the networks functions that are dimensionless (such as the transfer function $H(s)$ and the current transfer function $I(s)$) will be unaffected.

In conclusion, every element in a network that has the dimension of resistance (this includes the multiplicative constant of the current controlled voltage source) or inductance (this includes the self and mutual inductances) is multiplied by R_0; and the value of every element that has the dimension of the conductance (this includes the multiplicative constant of a voltage controlled current source) or capacitance is divided by R_0.

2.7 Synthesis of Passive Networks

Network synthesis according to Teme [TL 1977-a] is the creation of circuit that provides the desirable response to a given input excitation. This definition is illustrated schematically in Fig. 2.8.
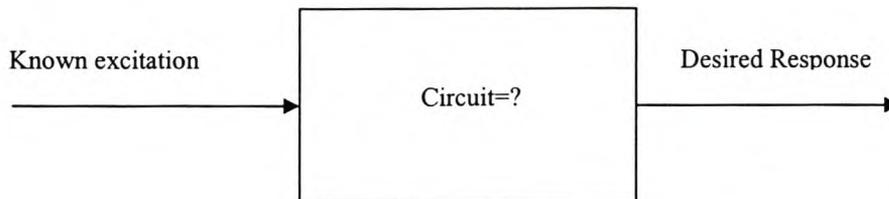
Figure 2.8 Circuit Design

Circuit synthesis depends on the kind of circuit that the designer is interested on designing. The circuit can be classified into various types, however, in this particular section only passive networks are considered.

A network is called passive if it cannot generate or amplify energy, that is, if the energy which it has supplied since the beginning of time, cannot exceed the energy which was fed into it.

Before discussing network synthesis, it is necessary to give an overview of double terminated network properties since they are useful in the design of filters.

2.7.1 Double Terminated Network Properties

The impedance and current of a two-port system can be related to each other by using the impedance and/or admittances of circuit theory, thus essentially arriving at a matrix description of the network. This representation of voltages and current is quite useful in the design of passive components such as couplers and filters. A two-port with its port quantities is shown in Fig. 2.9.
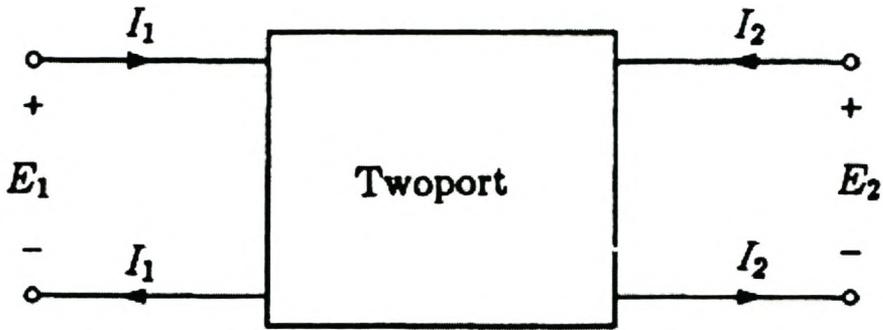
Figure 2.9 Double terminated two-port network

The impedance matrix, $[Z]$ of a two-port network relates the voltages and currents as follows [Su 1996-e]

$$\begin{bmatrix} E_1 \\ E_2 \end{bmatrix} = \begin{bmatrix} z_{11} & z_{12} \\ z_{21} & z_{22} \end{bmatrix} \begin{bmatrix} I_1 \\ I_2 \end{bmatrix} \qquad (2.26)$$

or, in matrix form

$$[V] = [Z][I] \qquad (2.27)$$

The quantities z_{ij} of eqn. (2.26) are called the open-circuit impedance parameters of the two-port and the matrix

$$Z(s) = \begin{bmatrix} z_{11} & z_{12} \\ z_{21} & z_{22} \end{bmatrix} \qquad (2.28)$$

is called the open-circuit impedance matrix. Similarly an admittance matrix, $[Y]$, is defined as

$$\begin{bmatrix} I_1 \\ I_2 \end{bmatrix} = \begin{bmatrix} y_{11} & y_{12} \\ y_{21} & y_{22} \end{bmatrix} \begin{bmatrix} E_1 \\ E_2 \end{bmatrix} \qquad (2.29)$$

or in matrix form

$$[I] = [Y][V] \tag{2.30}$$

The quantities y_{ij} of eqn. (2.26) are called the short-circuit admittance parameters of the two-port. From eqn. (2.29) and eqn. (2.30), it is seen that

$$Y(s) = \begin{bmatrix} y_{11} & y_{12} \\ y_{21} & y_{22} \end{bmatrix} \tag{2.31}$$

is the short-circuit admittance matrix.

Manipulation of eqn. (2.27) yields the following equation

$$Z_{ij} = \left. \frac{V_i}{I_j} \right|_{I_k = 0 \text{ for } k \neq j} \tag{2.32}$$

which implies that Z_{ij} can be found by driving port j with a current I_j, open-circuiting all other ports, and measuring the open circuit voltage at port i. Similarly, from eqn. (2.30), Y_{ij} can be found as

$$Y_{ij} = \left. \frac{I_i}{V_j} \right|_{V_k = 0 \text{ for } k \neq j} \tag{2.33}$$

which states that Y_{ij} can be determined by driving port j with a voltage V_j, short-circuiting all other ports (so $V_k = 0$ for k $\neq$ j), and measuring the short circuit current at port i.

However, the measurement of voltages and currents at microwave frequencies is difficult since direct measurement usually involve the magnitude and phase of a wave traveling in a given direction. In addition, equivalent voltages and currents, and the

related impedance and admittance matrices, become somewhat of an obstruction when dealing with high-frequency networks.

A representation, which is more in accordance with the direct measurements, and with the ideas of incident, reflected and transmitted waves is given by the scattering matrix, [S]. Consider the two-port network shown in Fig. 2.10. Only port 1 is excited in Fig. 2.10.
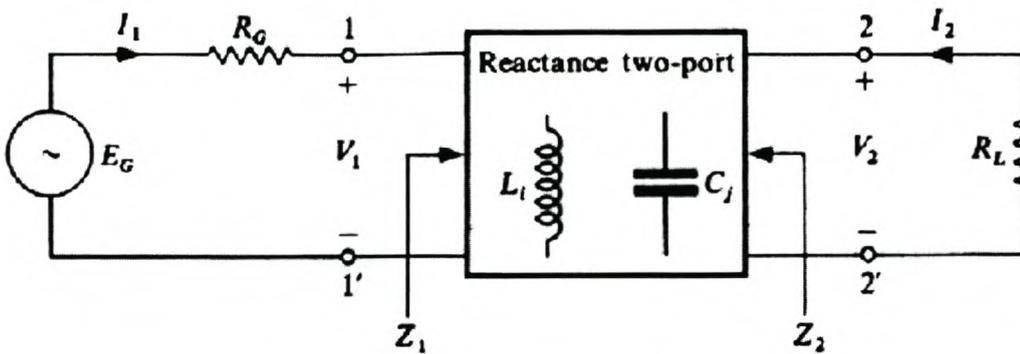
Figure 2.10 Double Terminated Reactance two-port

The equivalent voltages and currents for the incident and reflected wave are denoted by (V_{1i} and I_{1i}) and (V_{1r} and I_{2r}), respectively. These voltages and currents can be expressed in terms of incident and reflected waves as follows

$$V_1 = V_{1i} + V_{1r} \qquad V_2 = V_{2i} + V_{2r} \qquad (2.34a)$$

$$I_1 = I_{1i} - I_{1r} \qquad I_2 = I_{2i} - I_{2r} \qquad (2.34b)$$

Assuming that the source impedance and load are matched, i.e., $R_G = Z_1$ and $Z_2 = R_L$. Then, the following results for a matched load

$$V_{1r} = I_{1r} = 0 \qquad (2.35)$$

Applying eqn. (2.35) to eqns. (2.34a) and eqn. (2.34b), the following equations results

$$V_{1i} = V_1$$
$$I_{1i} = I_1 \tag{2.36}$$

By using the voltage division, the voltage (V_1) and current (I_1) are obtained to be

$$V_1 = \frac{Z_1 E_G}{Z_1 + R_G} \tag{2.37a}$$

$$I_1 = \frac{E_G}{Z_1 + R_G} \tag{2.37b}$$

Substitution of eqns. (2.37a) into eqn. (2.36a) and eqn. (2.37b) into 2.36b), result to the following equations

$$V_{1i} = \frac{E_G}{2} \tag{2.38a}$$

$$I_{1i} = \frac{E_G}{2 R_G} \tag{2.38b}$$

Again, by substituting eqn. (2.38a), eqn. (2.38b), eqn. (2.37a) and eqn. (2.37b) into eqn. (2.34a) and eqn. (2.34b), the following equations for V_{1r} and I_{1r} results, respectively.

$$V_{1r} = \frac{(Z_1 - R_G)}{(Z_1 + R_G)} \frac{E_G}{2} \tag{2.39a}$$

$$I_{1r} = \frac{(Z_1 - R_G)}{(Z_1 + R_G)} \frac{E_G}{2 R_G} \tag{2.39b}$$

The "a" and "b" in the following equations will be used to represent the amplitude and phase of the incident and emerging or reflected traveling waves with the subscripts 1 and 2 referring to the excited ports.

The maximum amount of power available from the generator of the two-port network is [TP 1977-b]

$$P_{max} = \frac{E_G^2}{4R_G} = |a_1|^2 \tag{2.40}$$

From eqn. (2.40), it is seen that

$$a_1 = \frac{V_{1i}}{\sqrt{R_G}} \tag{2.41}$$

Also, maintaining the voltage V_2 across the resistor R_L requires a power input

$$P_2 = \frac{|V_2|^2}{R_L} = \frac{|V_{2r}|^2}{R_L}\bigg|_{V_{2i}=0} = |b_2|^2\bigg|_{a_2=0} \tag{2.42}$$

However, when the mismatch ($R_G \neq Z_1$) occurs, a part of P_{max} is reflected from the two-port, and only the remainder of it pass through to the load. The reflected power P_r is expressed as follows [TL 1977-b]

$$P_r = P_{max} - P_1 = \frac{|E_G|^2}{4R_G} - \text{Re}\left[I_1 I_1^* Z_1\right] \tag{2.43}$$

where I_1^* is the conjugate of I_1. Meadows [PM 1975] give the following property of $|z|$:

$$|z|^2 = z\,z^* \tag{2.44}$$

Applying eqn. (2.44) into eqn. (2.43), eqn. (2.45) result

$$P_r = P_{max} - P_1 = \frac{|E_G|^2}{4R_G} - \text{Re}[Z_1]|I_1|^2 \tag{2.45}$$

Substitution of eqn. (2.37b) into eqn. (2.45) yield eqn. (2.46)

$$P_r = \frac{|E_G|^2}{4R_G} - \text{Re}[Z_1]\frac{|E_G|^2}{|Z_1 + R_G|^2} \tag{2.46}$$

Using the triangle inequality property given by Meadows [PM 1975] to eqn. (2.46) result to the following equation

$$P_r = \frac{|E_G|^2}{4R_G} - \frac{\text{Re}(Z_1)|E_G|^2}{|Z_1|^2 + 2\text{Re}(Z_1)R_G + R_G^2} = \frac{|E_G|^2|Z_1 - R_G|^2}{4R_G|Z_1 + R_G|^2} \tag{2.47}$$

Using eqn (2.39a), eqn. (2.47) can be expressed as follows

$$P_r = \frac{|V_{1r}|^2}{R_G} = |b_1|^2 \tag{2.48}$$

From eqn. (2.48), it is seen that

$$b_1 = \frac{V_{1r}}{\sqrt{R_G}} \tag{2.49}$$

The complex reflection coefficient at port 1, S_{11}, is given by

$$S_{11} = \frac{b_1}{a_1}\bigg|_{a_2=0} = \frac{Z_1 - R_G}{Z_1 + R_G} \tag{2.50}$$

when port 2 is terminated in its characteristics impedance. Eqn. (2.50) can be expressed as follows

$$|S_{11}|^2 = \frac{|Z_1 - R_G|^2}{|Z_1 + R_G|^2} = \frac{P_r}{P_{max}} \tag{2.51}$$

Similarly, the complex transmission coefficient from port1 to port 2, S_{21}, is given by

$$S_{21} = \left. \frac{b_2}{a_1} \right|_{a_2=0} \tag{2.52}$$

Also, eqn. (2.52) can be expressed as follows

$$|S_{21}|^2 = \frac{P_2}{P_{max}} \tag{2.53}$$

By reversing the ports and terminating port 1 in its characteristic impedance, S_{22} and S_{12} can similarly be defined.

The scattering matrix, $[S]$, is defined by Pozar [Po 1998-a] in relation to these incident and reflected waves as

$$\begin{bmatrix} b_1 \\ b_2 \end{bmatrix} = \begin{bmatrix} S_{11} & S_{12} \\ S_{21} & S_{22} \end{bmatrix} \begin{bmatrix} a_1 \\ a_2 \end{bmatrix} \tag{2.54}$$

It is necessary to use the power-transmission instead of the transfer function defined in the previous sections for a double terminated network reactance two-port. The power-transmission ratio (also called transducer factor) is defined as follows by Teme [TL 1977-b]

$$\Gamma(s) = \frac{P_{max}}{P_2} = \left| \frac{1}{2} \sqrt{\frac{R_L}{R_G}} \frac{E_G}{V_2} \right|^2 \tag{2.55}$$

Furthermore, the ratio given by eqn. (2.55) provides a well defined power-transmission efficiency of the two-port. For $\Gamma(s) = 1$, all the power which the generator can supply is transmitted to the load whereas, for $\Gamma(s) = \infty$, none of it is. In addition, it is noticed that $\Gamma(s)$, in contrast with the previous defined transfer functions, is an input-quantity/output-quantity ratio.

The characteristic function, $K(s)$, of the terminated two-port is by definition [TP 1977-b]

$$K(s) = S_{11}(s)\Gamma(s) \tag{2.56}$$

When $s = j\omega$ in eqn. (2.56), the following equation results

$$|K(j\omega)|^2 = |S_{11}(j\omega)|^2 |\Gamma(j\omega)|^2 = \frac{P_r}{P_{max}} \frac{P_{max}}{P_2} = \frac{|S_{11}|^2}{|S_{21}|^2} \tag{2.57}$$

From eqn. (2.57), it is seen that

$$|\Gamma(j\omega)|^2 = \frac{1}{|S_{21}(j\omega)|^2} \tag{2.58}$$

2.7.2 Network Synthesis Procedure

The network synthesis for double terminated networks is accomplished by following these steps

- Determination of the attenuation constant, $\alpha(s)$.
- Determine the transfer and reflection polynomials $E(s)$, $P(s)$ and $F(s)$

$$S_{21}(s) = \frac{P(s)}{E(s)} \qquad (2.59a)$$

$$S_{11}(s) = \frac{F(s)}{E(s)} \qquad (2.59b)$$

- Determination of the transmission parameters
- Extraction of the circuit elements.

Each of these steps will be discussed in more detail in the following sections.

2.7.2.1 Determination of the attenuation constant

Usually the determination of the attenuation constant, $\alpha(s)$, starts with the determination of the transmission coefficient, $|S_{21}(j\omega)|^2$. The transmission coefficient for a Butterworth filter is defined by Rhodes [Rh 1976-a] to be

$$|S_{21}(j\omega)|^2 = \frac{1}{1 + \omega^{2n}} \qquad (2.60)$$

where n is the order of the filter. Using the definition of attenuation constant given by eqn. (2.9), $\alpha(j\omega)$ is

$$\alpha(j\omega) = 10\log(1 + \omega^{2n}) \qquad (2.61)$$

2.7.2.2 Determination of the Transmission and Reflection Polynomials

The determination of the transmission and reflection polynomials is based on the theory set fourth by Teme [TP 1977-b]. By definition, $S_{11}(s)$, $H(s)$, and $K(s)$ are all rational functions of s, with real coefficients. The transducer factor, $\Gamma(s)$, and $S_{11}(s)$ can be expressed as follows

$$\Gamma(s) = \frac{E(s)}{P(s)} \tag{2.62a}$$

$$S_{11}(s) = \frac{F(s)}{E(s)} \tag{2.62b}$$

where $E(s)$, $P(s)$ and $F(s)$ are polynomials. Substituting eqn. (2.62a) into eqn. (2.58), eqn. (2.63) results

$$S_{21}(s) = \frac{P(s)}{E(s)} \tag{2.63}$$

Substituting eqn. (2.62b) and eqn. (2.63) into eqn. (2.57), it is seen that

$$K(s) = \frac{F(s)}{P(s)} \tag{2.64}$$

Teme supply necessary conditions for the polynomials given by eqns. ((2.62a)-(2.64)) to realize the double terminated two-port. These conditions are

- $E(s)$ is a strictly Hurwitz polynomial (all zeros lie in the open left-halfplane).
- The degree of $E(s) \geq P(s)$.
- The degree of $F(s)$ is at most that of $E(s)$.

For a lossless terminated two-port, $S_{11}(s)$ is related to $S_{21}(s)$ by

$$|S_{11}(j\omega)|^2 + |S_{21}(j\omega)|^2 = 1 \tag{2.65}$$

Substitution of eqn. (2.62b) and eqn. (2.63) into eqn. (2.65) yields the following equation

$$|E(j\omega)|^2 = |F(j\omega)|^2 + |P(j\omega)|^2 \tag{2.66a}$$

or

$$E(s)E(-s) = F(s)F(-s) + P(s)P(-s) \tag{2.66b}$$

Dividing eqn. (2.65) by $|S_{21}(j\omega)|^2$ and using eqn. (2.57) yields the following equation

$$|K(j\omega)|^2 + 1 = \frac{1}{|S_{21}(j\omega)|^2} \tag{2.67}$$

Substitution of eqn. (2.60) into eqn. (2.67) yields the following equations

$$|K(j\omega)|^2 = \omega^{2n} = \frac{|F(j\omega)|^2}{|P(j\omega)|^2} = \frac{F(s)F(-s)}{P(s)P(-s)} \tag{2.68}$$

From eqn. (2.68), it is seen that

$$F(s)F(-s) = \omega^{2n} \tag{2.69a}$$

$$P(s) = 1 \tag{2.69b}$$

Substituting $\omega = \dfrac{s}{j}$ into eqn. (2.69a) yields

$$F(s)F(-s) = \left(\frac{s}{j}\right)^{2n} = (-1)^n s^{2n} \tag{2.70}$$

From eqn. (2.70), $F(s)$ and $F(-s)$ can be expressed as follows

$$F(s) = s^n \tag{2.71a}$$

$$F(-s) = (-s)^n \tag{2.71b}$$

Again, with the substitution of eqn. (2.69a) and eqn. (2.69b) into eqn. (2.66b) it follows

$$E(s)E(-s) = 1 + (-1)^n s^{2n} \tag{2.72}$$

The derivation of the roots for $(-1)^n s^{2n}$ presented here follows the approach of Su [Su 1996-c]. Let $E(s)E(-s) = 0$ in eqn. (2.72), then

$$s^{2n} = e^{jn\pi} e^{j(2k-1)\pi} \tag{2.73}$$

where k is any integer. Hence $2n$ zeros of $F(s)F(-s)$ are

$$s_k = e^{j\left(\frac{2k+n-1}{2n}\right)\pi} \tag{2.74}$$

where $k = 0, \pm 1, \pm 2, \ldots, n-1$. It follows that

$$E(s)E(-s) = (-1)^n (s - s_k) \tag{2.75}$$

The polynomial $E(s)$ consists of zeros that lie in the left-halfplane of the s-plane.

2.7.2.3 Determination of the Transmission matrix parameters

The [Z], [Y] and [S] parameter representations can be used to characterize a microwave network with any arbitrary ports, but in practice many microwave networks consist of two or more two-port networks. Due to that, it is convenient to define a $[2 \times 2]$ transmission, or ABCD matrix, for each two-port network.

Pozar [Po 1998-a] defines the ABCD matrix in terms of total voltages and currents as shown in Fig. 2.11 and the following equations

$$V_1 = AV_2 - BI_2 \qquad (2.76a)$$

$$I_1 = CV_2 - DI_2 \qquad (2.76b)$$

or in matrix form as

$$\begin{bmatrix} V_1 \\ I_1 \end{bmatrix} = \begin{bmatrix} A & B \\ C & D \end{bmatrix} \begin{bmatrix} V_2 \\ -I_2 \end{bmatrix} \qquad (2.77)$$
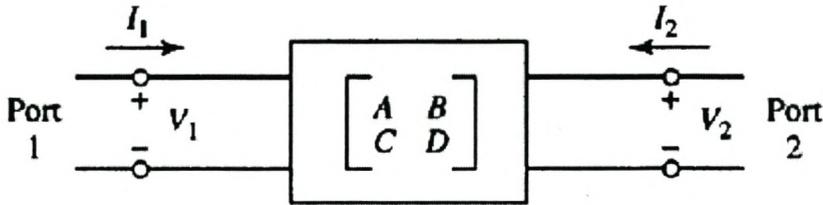
Figure 2.11 A two-port network

From eqn. (2.77), the transmission matrix, T, is given by

$$T = \begin{bmatrix} A & B \\ C & D \end{bmatrix} \qquad (2.78)$$

The T-matrix parameters can be obtained by first expressing the voltages and currents V_1, V_2, I_1 and I_2 as follows

$$V_1 = a_1 + b_1 \qquad (2.79a)$$

$$I_1 = a_1 - b_1 \qquad (2.79b)$$

$$V_2 = a_2 + b_2 \qquad (2.79c)$$

$$I_2 = a_2 - b_2 \qquad (2.79d)$$

Adding eqn. (2.79a) and eqn. (2.79b) and also eqn. (2.79c) and eqn. (2.79d), result to the following equations

$$a_1 = \frac{V_1 + I_1}{2} \tag{2.80a}$$

$$a_2 = \frac{V_2 + I_2}{2} \tag{2.80b}$$

Furthermore, subtracting eqn. (2.79b) from eqn. (2.79a) and also eqn. (2.79d) from eqn. (2.79c), the following equations results

$$b_1 = \frac{V_1 - I_1}{2} \tag{2.81a}$$

$$b_2 = \frac{V_2 - I_2}{2} \tag{2.81b}$$

It follows from eqn. (2.76a), eqn. (2.76b), eqn. (2.80b) and eqn. (2.81b) that

$$A = -\left. \frac{V_1}{V_2} \right|_{I_2 = 0} \tag{2.82a}$$

$$C = \left. \frac{I_1}{V_2} \right|_{I_2 = 0} \tag{2.82b}$$

$$a_2 = b_2 = \left. \frac{V_2}{2} \right|_{I_2 = 0} \tag{2.82c}$$

when port 2 is open-circuited. In addition it is seen from eqn. (2.76a), eqn (2.76b), eqn. (2.80b) and eqn. (2.81b) that

$$B = -\left. \frac{V_1}{I_2} \right|_{V_2 = 0} \tag{2.83a}$$

$$D = \left. \frac{I_1}{I_2} \right|_{V_2 = 0} \tag{2.83b}$$

$$a_2 = -b_2 = \frac{I_2}{2}\bigg|_{V_2=0} \tag{2.83c}$$

when port 2 is short-circuited.

The scattering matrix (eqn. (2.54)) can also be expressed as follows

$$b_1 = S_{11}a_1 + S_{12}a_2 \tag{2.84a}$$

$$b_2 = S_{21}a_1 + S_{22}a_2 \tag{2.84b}$$

Substitution of eqn. (2.80a), eqn. (2.81a) and eqn. (2.82c) into eqns. (2.84a) -(2.84b) yields

$$\frac{V_1 - I_1}{2} = S_{11}\frac{V_1 + I_1}{2} + S_{12}\frac{V_2}{2} \tag{2.85a}$$

$$\frac{V_2}{2} = S_{21}\frac{V_1 + I_1}{2} + S_{22}\frac{V_2}{2} \tag{2.85b}$$

Also, by substituting eqn. (2.80a), eqn. (2.81a) and eqn. (2.83c) into eqns. (2.84a)-(2.84b), it follows that

$$\frac{V_1 - I_1}{2} = S_{11}\frac{V_1 + I_1}{2} + S_{12}\frac{I_2}{2} \tag{2.86a}$$

$$-\frac{I_2}{2} = S_{21}\frac{V_1 + I_1}{2} + S_{22}\frac{I_2}{2} \tag{2.86b}$$

Eqn. (2.85a), eqn. (2.85b), eqn. (2.86a) and eqn. (2.86b) can also be expressed as follows

$$V_1(1 - S_{11}) + V_2(-S_{12}) = I_1(1 + S_{11}) \tag{2.87a}$$

$$V_1(-S_{21}) + V_2(1 - S_{22}) = I_1(S_{21}) \tag{2.87b}$$

$$V_1(1 - S_{11}) + I_2(-S_{12}) = I_1(1 + S_{11}) \tag{2.87c}$$

$$V_1(-S_{21}) + I_2(-1 - S_{22}) = I_1(S_{21}) \tag{2.87d}$$

Solving for I_1 from eqn. (2.87b) and eqn. (2.87d), respectively, yields

$$I_1 = -V_1 + V_2 \left[\frac{(1 - S_{22})}{S_{21}} \right] \tag{2.88a}$$

$$I_1 = -V_1 + I_2 \left[\frac{(-1 - S_{22})}{S_{21}} \right] \tag{2.88b}$$

Eqns. (2.89) result due to the substitution of eqn. (2.88a) and eqn. (2.88b) into eqn. (2.87a) and eqn. (2.87c), respectively.

$$2V_1 = V_2 \left[\frac{(1 - S_{22})(1 + S_{11})}{S_{21}} + S_{12} \right] \tag{2.89a}$$

$$2V_1 = I_2 \left[\frac{(1 + S_{11})(-1 - S_{22})}{S_{21}} + S_{12} \right] \tag{2.89b}$$

The transmission matrix elements A and B given by eqn (2.82a) and eqn. (2.83a) respectively, are obtained from eqns. (2.89) to be

$$A = \frac{V_1}{V_2} = \frac{1}{2S_{21}} \left[(1 + S_{11})(1 - S_{22}) + S_{12}S_{21} \right] \tag{2.90a}$$

$$B = -\frac{V_1}{I_2} = -\frac{1}{2S_{21}} \left[(1 + S_{11})(-1 - S_{22}) + S_{12}S_{21} \right] \tag{2.90b}$$

Furthermore, solving for V_1 from eqn. (2.87b) and eqn. (2.87d) yields

$$V_1 = \left[\frac{(1 - S_{22})}{S_{21}} \right] V_2 - I_1 \tag{2.91a}$$

$$V_1 = -I_1 + I_2 \left[\frac{(-1 - S_{22})}{S_{21}} \right] \tag{2.91b}$$

Substitution of eqn. (2.91a) into eqn. (2.87a) and eqn. (2.91b) into eqn. (2.87c) result to the following equations

$$2I_1 = V_2 \left[\frac{(1 - S_{22})(1 - S_{11})}{S_{21}} - S_{12} \right] \quad (2.92a)$$

$$2I_1 = I_2 \left[\frac{(-1 - S_{22})(1 - S_{11})}{S_{21}} - S_{12} \right] \quad (2.92b)$$

It follows that the transmission matrix elements C and D defined by eqn. (2.82b) and (2.83b), respectively, can be obtained from eqns. (2.92) to be

$$C = \frac{1}{2S_{21}} \left[(1 - S_{22})(1 - S_{11}) - S_{12}S_{21} \right] \quad (2.93a)$$

$$D = \frac{1}{2S_{21}} \left[(-1 - S_{22})(1 - S_{11}) - S_{12}S_{21} \right] \quad (2.93b)$$

Substitution of eqn. ((2.62b)-(2.63)) into the scattering matrix elements given by eqns. (2.90) and eqns. (2.93) with $S_{12} = S_{21}$ and $|S_{11}| = |S_{22}|$ result into the following equations for the transmission matrix elements

$$A = \frac{1}{2P(s)} \left[(E(s) + F(s))(E(s) \mp F_x) + P^2(s) \right]$$

$$B = \frac{1}{2P(s)} \left[(E(s) + F(s))(E(s) \pm F_x) + P^2(s) \right]$$

$$C = \frac{1}{2P(s)} \left[(E(s) - F(s))(E(s) \mp F_x) - P^2(s) \right]$$

$$D = \frac{1}{2P(s)} \left[(E(s) - F(s))(E(s) \pm F_x) + P^2(s) \right]$$

(2.94)

where $F_x = F(-s)$. Substitution of eqn. (2.94) into eqn. (2.78) and further simplification, result into the following T-matrix

$$[T] = \frac{1}{2PE} \begin{bmatrix} EE + EF \mp EF_x \mp FF_x + PP & E^2 + EF \pm EF_x \pm FF_x - PP \\ EE - EF \mp EF_x \pm FF_x - PP & EE - EF \pm EF_x \mp FF_x + PP \end{bmatrix} \quad (2.95)$$

where $F = F(s)$, $E = E(s)$ and $P = P(s)$.

For P even, $P = P_x$ and eqn. (2.66b) becomes

$$FF_x + PP_x = EE_x \tag{2.96a}$$

or

$$FF_x = EE_x - PP_x \tag{2.96b}$$

Also for P odd, $P = -P_x$ and eqn. (2.66b) becomes

$$FF_x = EE_x - PP_x \tag{2.97}$$

Substitution of eqn. (2.96b) and eqn. (2.97) into eqn. (2.95), respectively result to the following T-matrices

$$T = \frac{1}{2P} \begin{bmatrix} E+F+F_x+E_x & E+F+F_x+E_x \\ E-F-F_x+E_x & E-F+F_x-E_x \end{bmatrix} \text{ for } P \text{ even} \tag{2.98a}$$

$$T = \frac{1}{2P} \begin{bmatrix} E+F+F_x+E_x & E+F+F_x+E_x \\ E-F-F_x+E_x & E-F+F_x-E_x \end{bmatrix} \text{ for } P \text{ odd} \tag{2.98b}$$

The polynomial, $E(s)$, is composed of an odd part, E_0, and an even part, E_e, as follows

$$E = E_e + E_0 \tag{2.99a}$$

$$E_x = E(-s) = E_e(s) - E_0(s) \tag{2.99b}$$

Adding eqn. (2.99a) and eqn. (2.99b), and also subtracting eqn. (2.99b) from eqn. (2.99a) result into the following equations

$$E + E_x = 2E_e \tag{2.101a}$$

$$E - E_x = 2E_0 \tag{2.101b}$$

2-34

Substituting eqns. (2.101) into eqns. (2.98) result into the following T-matrices

$$T = \frac{1}{P}\begin{bmatrix} E_e + F_e & E_0 + F_0 \\ E_0 - F_0 & E_e + F_e \end{bmatrix} \text{ for } P \text{ even} \qquad (2.102a)$$

$$T = \frac{1}{P}\begin{bmatrix} E_0 + F_0 & E_e + F_e \\ E_e - F_e & E_0 + F_0 \end{bmatrix} \text{ for } P \text{ odd} \qquad (2.102b)$$

2.7.2.4 Extraction of Circuit Elements

The procedure presented for extracting circuit elements follows the theory set fourth by Li [Li 1978]. There are a variety of ways of removing elements from the overall transfer matrix. At each stage an element can be removed either from the left-hand side or the right hand side of the transfer matrix (except for the last element). The pattern choice depends on the amount of error that it produces. However, a pattern that has a lowest error rate is the removal of the elements constantly from the left-hand side of the transfer matrix.

The element extraction procedure is best shown by an example. Using the theory given in the preceding sections, the transfer matrix, T, for a 3rd-order Butterworth filter is given by

$$T = \begin{bmatrix} 2s^2 + 1 & 2s^3 + 2s \\ 2s & 2s^2 + 1 \end{bmatrix} \qquad (2.103)$$

A series inductance, L, will be removed from the left-hand side. This inductance has the inverse matrix given by

$$\begin{bmatrix} 1 & -sL \\ 0 & 1 \end{bmatrix} \qquad (2.104)$$

Premultiplying eqn. (2.103) by eqn. (2.104) gives

$$\begin{bmatrix} (2-2L)s^2 +1 & (2-2L)s^3 + (2-L)s \\ 2s & 2s^2 +1 \end{bmatrix} \tag{2.105}$$

Setting the coefficients of the highest powers in the A and B entries to zero can reduce the degree of this matrix. This procedure gives two estimates for L:

$$L_1 = 1 \tag{2.106a}$$

$$L_2 = 1 \tag{2.106b}$$

In practice, due to round-off error, the two estimates will be slightly different. They can be averaged together as shown in eqn. (2.107) to improve accuracy.

$$L = 0.5(L_1 + L_2) = 1 \tag{2.107}$$

After L is removed, eqn. (2.103) becomes

$$T = \begin{bmatrix} 1 & s \\ 2s & 2s^2 +1 \end{bmatrix} \tag{2.108}$$

A shunt capacitor, C, will next be removed from the left-hand side and this component has the inverse matrix

$$\begin{bmatrix} 1 & 0 \\ -sC & 1 \end{bmatrix} \tag{2.109}$$

Premultiplying eqn. (2.108) by eqn. (2.109) yields

$$\begin{bmatrix} 1 & s \\ s(2-C) & s^2(2-C)+1 \end{bmatrix} \tag{2.110}$$

The C and D entries give the two estimates $C_1 = C_2 = 2$. If the two estimates are slightly different, again they should be averaged together. After the shunt capacitor is removed, eqn. (2.108) becomes

$$T = \begin{bmatrix} 1 & s \\ 0 & 1 \end{bmatrix}$$

(2.111)

Eqn. (2.111) is identified as the matrix for a series inductance. The circuit resulted from this procedure is shown in Fig. 2.12.
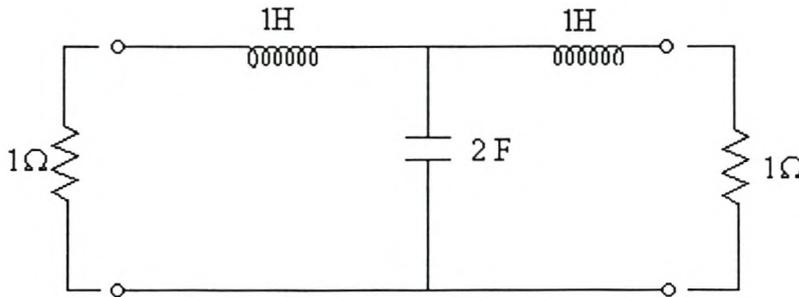
Figure 2.12 Third-order Butterworth Filter

The transfer coefficient for the circuit shown in Fig. 2.12 was obtained to be

$$S_{21}(s) = \frac{1}{2s^3 + 4s^2 + 4s + 2}$$

(2.112)

In addition, when $n = 3$ and $s = j\omega$ in eqn. (2.60), eqn. (2.113) will result

$$S_{21}(s) = \frac{1}{s^3 + 2s^2 + 2s + 1}$$

(2.113)

Fig. 2.13 shows the transfer coefficient given by eqn. (2.112) and analysis of Fig. (2.12).
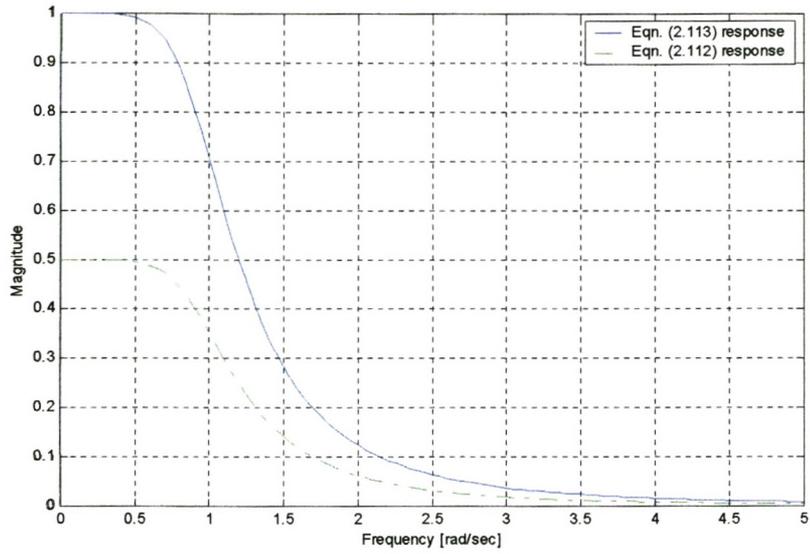
Figure 2.13 Transfer coefficient for a 3rd-order Butterworth Filter

2.8 Frequency Transformations

The attention in the preceding sections was paid to low-pass filters since there are techniques for deriving high-pass, band-pass, and band-reject filters from basic low-pass filters. The procedure for obtaining these filters from the low-pass filter presented here follows the approach of Su [Su 1996-d] and is known as frequency transformation.

The complex variable, s, for the normalized low-pass function is given by

$$s = \sigma + j\omega \qquad (2.114)$$

whereas the complex variable, S, for the transformed network function is given by

$$S = \sum + j\Omega \qquad (2.115)$$

where Ω is the normalized frequency.

In the following sections, the procedures for obtaining high-pass, band-pass and band-reject filters will be discussed.

2.8.1 High-Pass Filter

The starting point for obtaining a high-pass filter is a normalized low-pass prototype whose pass band is $0 < \omega < \omega_p$ and $\omega_p = 1$ with a network function $H_{LP}(s)$. The following transform is utilized

$$s = \frac{\Omega_0}{S} \qquad (2.116)$$

Substituting $s = j\omega$ and $S = j\Omega$ into eqn. (2.116), eqn. (2.117) is obtained

$$\omega = -\frac{\Omega_0}{\Omega} \qquad (2.117)$$

Substitution of eqn. (2.116) into a low-pass network function, $H_{LP}(s)$, a high-pass network function is obtained

$$H_{HP}(S) = H_{LP}\left(\frac{\Omega_0}{S}\right) \qquad (2.118)$$

Furthermore, the transform given in eqn. (2.116) implies that inductors transform to capacitors and capacitors transform to inductors as shown in Fig. 2.14.
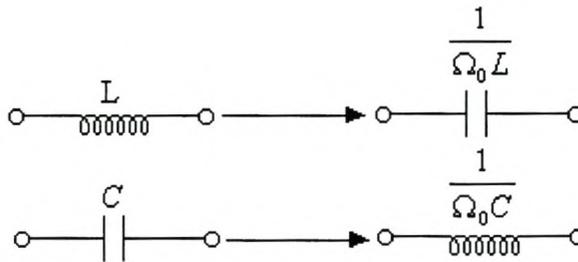
Figure 2.14 Low-pass to high-pass transformation of circuit elements.

In conclusion the transform given by eqn. (2.116) has an effect to the magnitude characteristics. To illustrate that, the low-pass magnitude characteristic, $|H(j\omega)|$, is transformed into the high-pass magnitude characteristic, $|H(j\Omega)|$, as shown in Fig. 2.15.
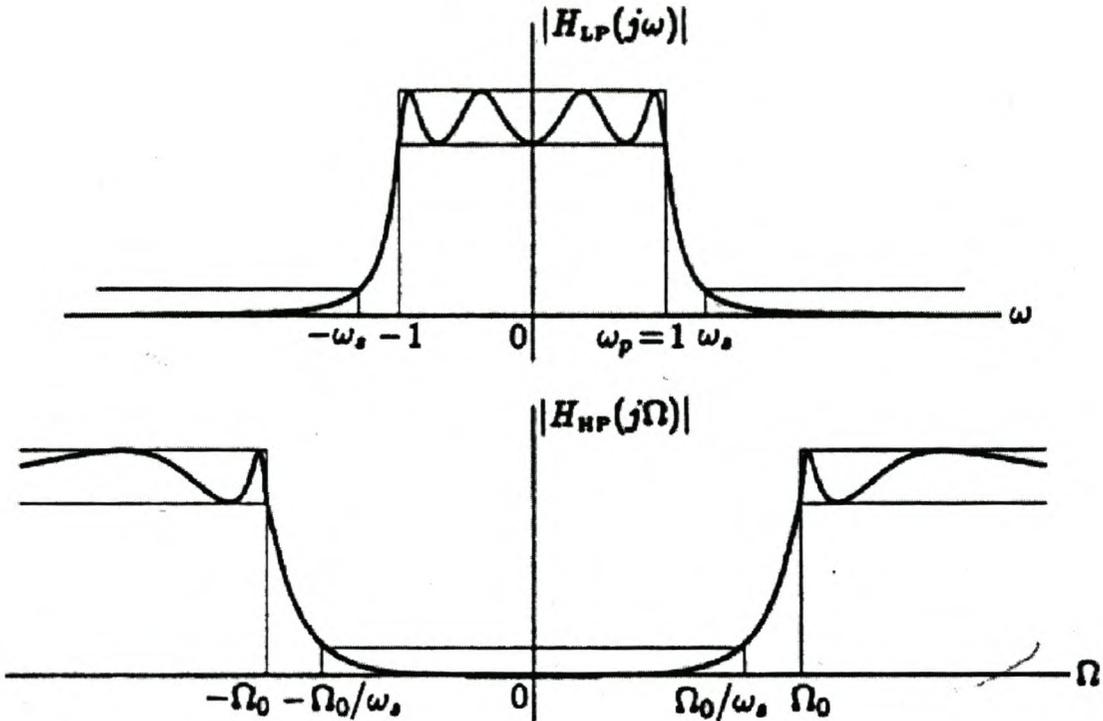
Figure 2.15 The low-pass-to-high-pass transformation

The points, $\omega = 1$, $\omega = -1$, $\omega = \omega_s$ and $\omega = -\omega_s$ are mapped to $\Omega = -\Omega_0$, $\Omega = \Omega_0$, $\Omega = -\Omega_0/\omega_s$ and $\Omega = \Omega_0/\omega_s$, respectively. Hence, not only the low-pass characteristic is transformed into a high pass characteristic, but there is also a flip-over of the positive and negative halves of the characteristic. Because of the symmetry of the magnitude characteristic, this transform puts the pass band in the range $\Omega_0 < \Omega < \infty$ and the stop band in $0 < \Omega < \Omega_0/\omega_s$.

2.8.2 Band-Pass Filter

Again, the starting point for obtaining the band-pass filter is the normalized ($\omega_p = 1$) low-pass prototype filter with the network function $H_{LP}(s)$. The required transformation for obtaining the band-pass filter from the low-pass filter is

$$s = \frac{S^2 + \Omega_0^2}{BS} \tag{2.119}$$

2-41

where B is the bandwidth of the band-pass filter and Ω_0 is the desired center frequency. Using the transformation given by eqn. (2.119), the band-pass filter function is given by

$$H_{BP}(S) = H_{LP}\left(\frac{S^2 + \Omega_0^2}{BS}\right) \qquad (2.120)$$

Substituting $s = j\omega$ and $S = j\Omega$ into eqn. (2.119), eqns. (2.121) results

$$j\omega = \frac{-\Omega^2 + \Omega_0^2}{Bj\Omega} \qquad (2.121a)$$

or

$$\Omega^2 - B\omega\Omega - \Omega_0^2 = 0 \qquad (2.121b)$$

When $\omega = 0$, eqn. (2.121b) becomes $\Omega = \pm\Omega_0$, which implies that the point $\omega = 0$ is mapped onto $\Omega = \pm\Omega_0$. Also the point $\omega = \pm\infty$ map onto $\Omega = 0$ and $\Omega = \pm\infty$. In addition, for $\omega = \omega_p = 1$, eqn. (2.121b) becomes

$$\Omega^2 - B\Omega - \Omega_0^2 = 0 \qquad (2.122)$$

Solving the quadratic eqn. (2.122) gives

$$\Omega = \frac{B}{2} \pm \sqrt{\frac{B^2}{4} + \Omega_0^2} \qquad (2.123)$$

The values obtained for Ω from eqn. (2.123) are positive and negative values, respectively. Let each value be expressed as follows

$$\Omega_2 = \frac{B}{2} + \left(\sqrt{\frac{B}{4} + \Omega_0^2}\right) \qquad (2.124a)$$

$$-\Omega_1 = \frac{B}{2} - \left(\sqrt{\frac{B^2}{4} + \Omega_0^2} \right) \qquad (2.124b)$$

where Ω_1 is the lower 3-dB frequency, and Ω_2 is the upper 3-dB frequency. Substituting $\omega = -1$ into eqn. (2.121b), two roots which are equal to Ω_2 and $-\Omega_1$ would be obtained. Hence a low-pass band is mapped onto two band-pass regions, when the roots are $\pm\Omega_2$ and $\mp\Omega_1$. This mapping is shown in Fig. 2.16.
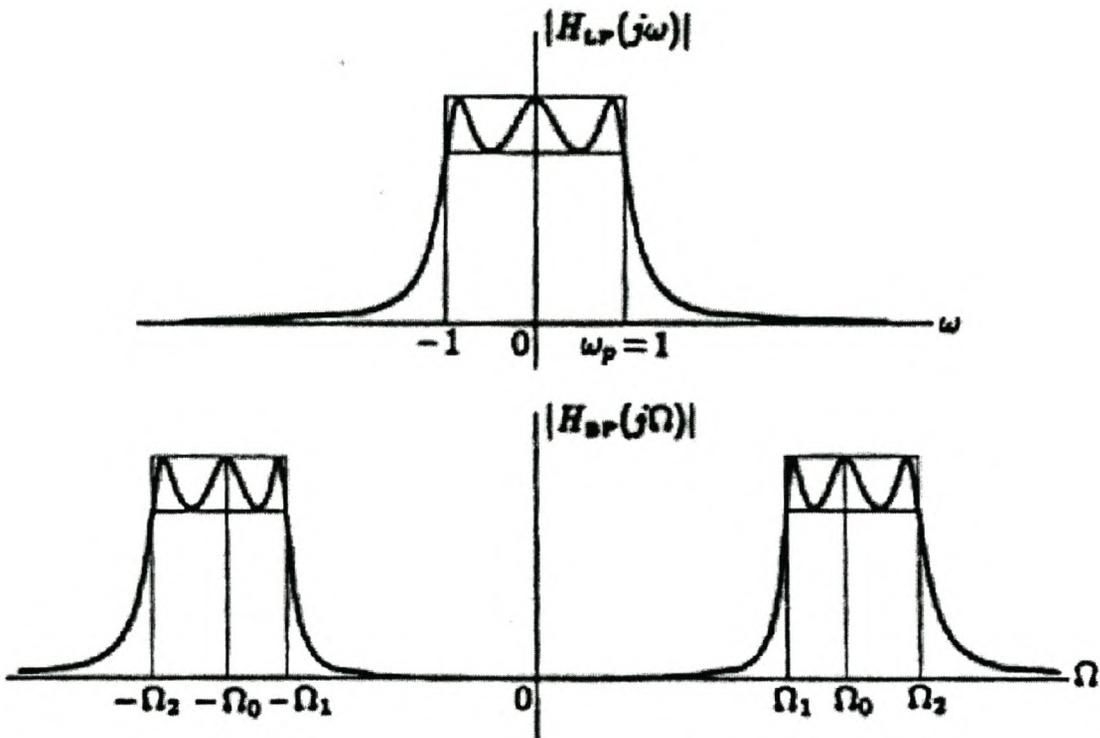
Figure 2.16 The Low-pass-to-band-pass transformation

Subtracting eqn. (2.124b) from eqn. (2.124a), eqn. (2.125) result

$$B = \Omega_2 - \Omega_1 \qquad (2.125)$$

where B is the bandwidth of the band-pass filter. Furthermore, multiplication of eqn. (2.124a) and eqn. (2.124b) result to the following equations

$$\Omega_1\Omega_2 = \left[\frac{B}{2} + \sqrt{\frac{B^2}{4} + \Omega_0^2}\right]\left[-\frac{B}{2} + \sqrt{\frac{B^2}{4} + \Omega_0^2}\right] = \Omega_0^2 \qquad (2.126a)$$

or

$$\frac{\Omega_0}{\Omega_1} = \frac{\Omega_2}{\Omega_0} \qquad (2.126b)$$

Hence Ω_2 and Ω_1 are geometrically symmetric about Ω_0. In fact it can be shown that the entire band-pass characteristic is geometrically symmetric about Ω_0. Thus, if the band-pass characteristic is plotted versus log Ω, then the entire curve will be symmetric about $\log(\Omega_0)$.

If the low-pass filter has a pole at s_k, then this transform maps it onto two poles. In addition, the use of this transformation implies that inductors transform to series resonant circuits and capacitors to parallel resonant circuits as shown in Fig. 2.17.
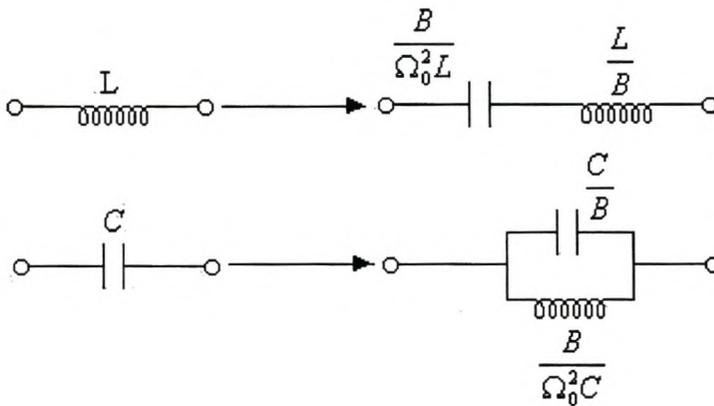
Figure 2.17 Low-pass to band-pass transformations of circuit elements.

The ratio of the center frequency to the bandwidth is known as the quality factor, Q, of the band-pass filter. That is

$$Q = \frac{\Omega_0}{B} \qquad (2.127)$$

The higher the Q, the narrower the bandwidth of a bandpass filter will be.

2.8.3 Band-Reject Filter

The band-reject filter is obtained from the low-pass prototype using the following transformation

$$s = \frac{B}{S^2 + \Omega_0^2} \qquad (2.128)$$

Along the imaginary axis

$$j\omega = \frac{Bj\Omega}{-\Omega^2 + \Omega_0^2} \qquad (2.129a)$$

or

$$\Omega^2 + \frac{B}{\omega}\Omega - \Omega_0^2 = 0 \qquad (2.129b)$$

More specifically in the band-pass filter, the focus is at the frequency band in which signals are rejected. Hence, it is most expedient that the low-pass prototype filter must first be normalized such that its stop band is $\omega > \omega_s = 1$ as shown in Fig 2.18
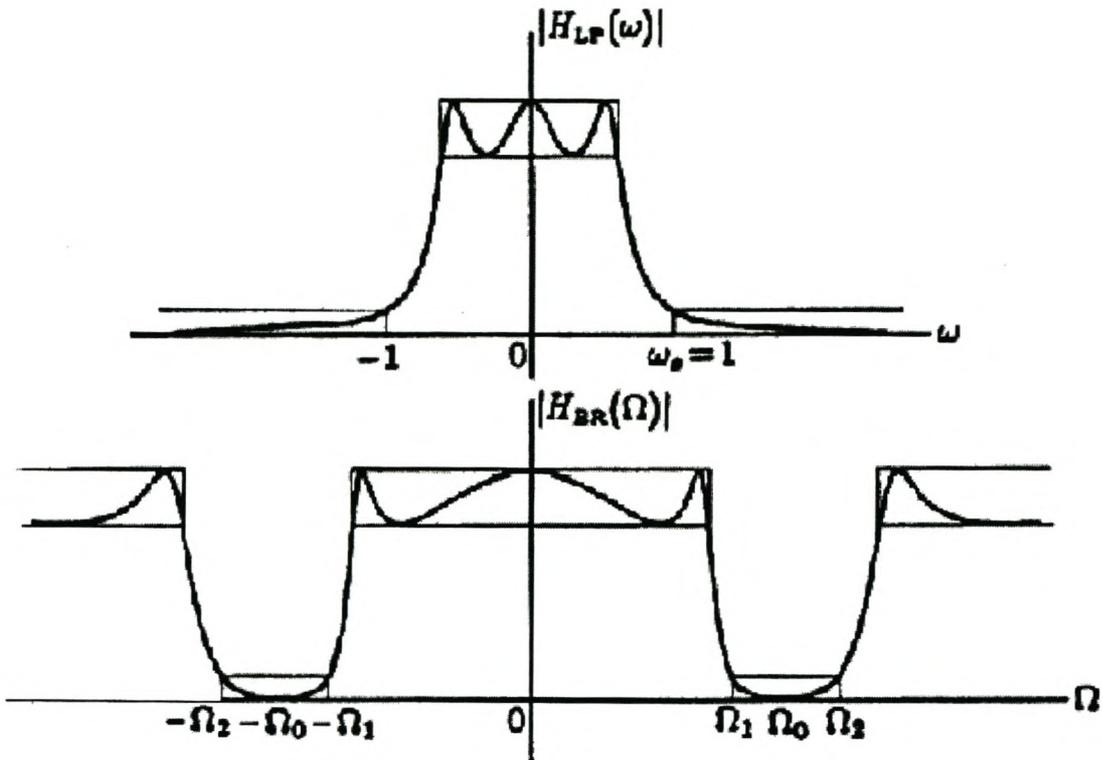
Figure 2.18 The low-pass-to-band-reject transformation

The points $\omega = \pm 1$ are mapped to $j\Omega$ axis by solving the quadratic equation

$$\Omega^2 \pm B\Omega - \Omega_0^2 = 0 \qquad (2.130)$$

The solution of these two equations will render four values of Ω which, if taken as a group, are identical to those equations given by eqn. (2.124a), eqn. (2.124b) and their negatives.

This implies that if the low-pass filter function has a pole (or a zero) at s_k, the locations of the corresponding poles (or zeros) of the band-reject filter function is obtained by solving eqn. (2.131)

$$S^2 - \frac{B}{s_k}S + \Omega_0^2 = 0 \qquad (2.131)$$

Furthermore, the use of this transform implies that inductors transform to parallel resonant circuits and capacitors transform to series resonant circuits as shown in Fig. 2.19.
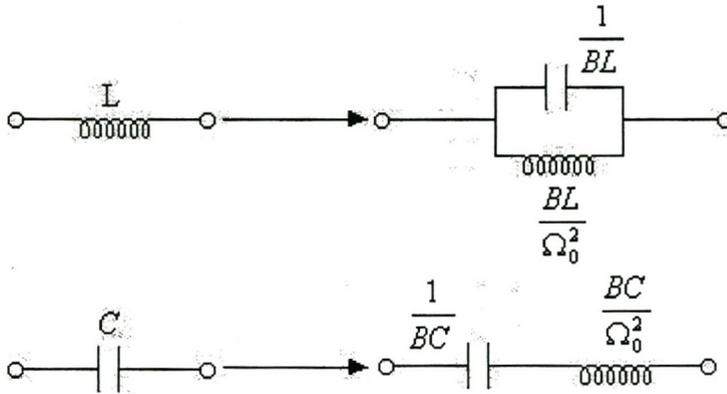
Figure 2.19 Low-pass to band-reject transformation of circuit elements

2.9 Conclusion

Location of poles and zeros determines the transfer function of a filter. The Butterworth low-pass filter has all its poles and zeros lying at infinite frequencies and zeros at DC.

The method presented for the synthesis of double terminated passive networks is accurate. Fig. 2.13 illustrates this.

Low-pass filter design methods provide the basis for all types of filters. These filters can be obtained from low-pass ones by applying frequency transformations presented.

The main emphasis will be on filters for wireless communication equipment that are often of the band-pass type. Such filters are discussed in the following chapter.

Chapter 3

Coupled Resonator Filters

3.1 Narrow Band Coupled Filters

The equivalent circuit of a general direct-coupled cavity is shown in Fig. 3.1 [AW 1971] and consists of n identical cavities tuned to the same normalized center frequency, $\omega_0 = 1$ rad/sec.
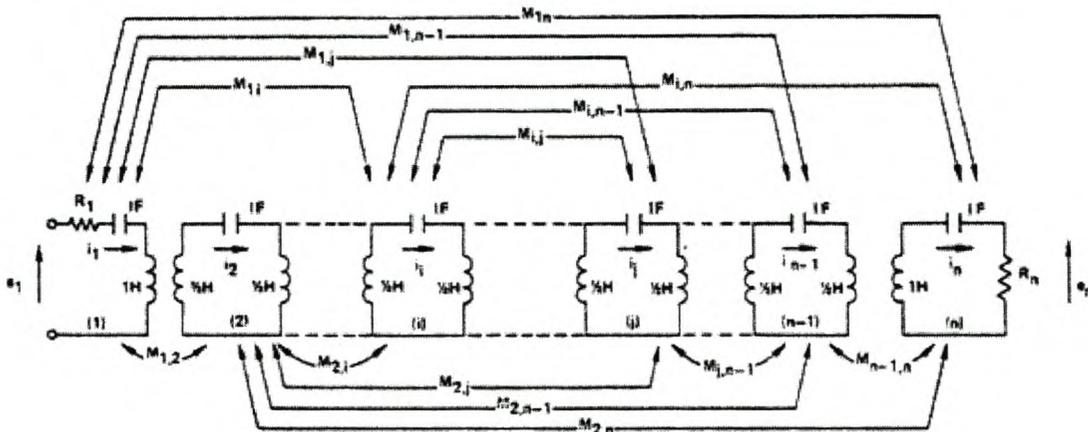
Figure 3.1 A general two-port network composed of synchronously tuned coupled cavities

The cavities are numbered 1,2,…, n, with the input applied to cavity 1 and the output to cavity n. The coupling coefficient , M_{ij} , between the *ith* and *jth* cavities are assumed to be frequency invariant, which is a valid assumption for narrow bandwidths. The circuit is completely described by the coupling matrix, M , which is a real $[n \times n]$ symmetric zero-diagonal matrix whose (i, j) entry is the value of the coupling coefficient M_{ij} .

3.2 Analysis of the Network

The loop equations of the network shown in Fig. 3.1, assuming a narrow bandwidth, can be expressed as follows:

$$
\begin{bmatrix} e_1 \\ 0 \\ 0 \\ 0 \\ \cdot \\ \cdot \\ \cdot \\ \cdot \\ e_n \end{bmatrix} = \begin{bmatrix} S+R_1 & jM_{12} & jM_{13} & \cdot & \cdot & \cdot & \cdot & jM_{1n} \\ jM_{12} & S & jM_{23} & \cdot & \cdot & \cdot & & \cdot \\ jM_{13} & jM_{23} & S & \cdot & \cdot & \cdot & & \cdot \\ \cdot & \cdot & \cdot & \cdot & \cdot & \cdot & \cdot & \cdot \\ \cdot & \cdot & \cdot & \cdot & \cdot & \cdot & \cdot & \cdot \\ \cdot & \cdot & \cdot & \cdot & \cdot & \cdot & \cdot & \cdot \\ \cdot & \cdot & \cdot & \cdot & \cdot & \cdot & S & jM_{n-1,n} \\ jM_{1n} & \cdot & \cdot & \cdot & \cdot & \cdot & S+R_n \end{bmatrix} \cdot \begin{bmatrix} i_1 \\ i_2 \\ i_3 \\ \cdot \\ \cdot \\ \cdot \\ \cdot \\ i_{n-1} \\ i_n \end{bmatrix} \qquad (3.1)
$$

or, in matrix form

$$[E]=[Z][I] \qquad (3.2)$$

where

$$S = j\left(\omega - \frac{1}{\omega}\right)$$
$$jM_{ij} \approx j\omega M_{ij} \approx j\omega_0 M_{ij} \ and \qquad (3.3)$$
$$\omega_0 = 1 \, rad/\sec$$

R_1 and R_n are the source and the load resistances, respectively.

The impedance matrix Z can be expressed in the form [AW 1972-a]:

$$Z = SI + M_R \qquad (3.4)$$

where I is an identity matrix and M_R is given by

3-2

$$M_R = R + jM \qquad (3.5)$$

where R is a $[n \times n]$ matrix whose elements are all zero, except $(1,1)$ and (n,n) entries which are equal to R_1 and R_n, respectively and the coupling, M, is a real symmetric matrix whose (i,j) entry is M_{ij}, for $i \neq j$, and $M_{ij} = 0$ for $i = j$.

When this circuit is considered as a two-port which is resistively terminated at the output port by the load R_n and driven at the input port by a source voltage e_1 with internal resistance R_1 it can be shown that the normalized low-pass voltage insertion loss ratio $|t(j\omega)|^2$ is defined as [AW 1974]

$$|t(j\omega)|^2 = \frac{4R_1}{R_n} \left| \frac{e_n(j\omega)}{e_1(j\omega)} \right|^2 \qquad (3.6)$$

where

$$e_1 = i_n \times R_n \qquad (3.7)$$

and

$$i_n = e_1 \frac{\left| cofactor\ Z_{1n} \right|}{|Z|} \qquad (3.8)$$

The synthesis of bandpass filters in waveguide cavities is most conveniently accomplished by assuming a symmetrical network [AW 1972-a], i.e. $R_1 = R_n = R$, and M is symmetrical about the antidiagonal (as well as about the main diagonal). Then eqn. (3.6) becomes

$$|t(j\omega)| = 2 \left| \frac{e_n(j\omega)}{e_1(j\omega)} \right| \qquad (3.9)$$

3-3

3.3 Synthesis of the Double Terminated Coupling Matrix

The starting point for the synthesis of M for the double terminated case are the transfer and reflection polynomials $E(s)$, $F(s)$ and $P(s)$, determined as

$$S_{21}(s) = \left(\frac{P(s)}{E(s)} \right)$$
$$S_{11}(s) = \left(\frac{F(s)}{E(s)} \right) \tag{3.10}$$

where $P(s)$ are the transmission zeros, $F(s)$ are the reflection zeros and $E(s)$ are the poles of the function.

For the transmission coefficient given in eqn. (3.10) to realize the doubly terminated network of Fig. 3.1, certain conditions must be met. These conditions are

- $E(s)$ is a Hurwitz polynomial in s of degree n,

- $P(s)$ is an even polynomial in s whose degree is $\leq (n-2)$.

In the general case the coefficients of $E(s)$ will be complex and those of $P(s)$ and $F(s)$ will alternate between purely real and purely imaginary.

The coupling matrix can be determined from the short-circuit characteristic of the network shown in Fig.3.2. Fig. 3.2(a) shows a two port lossless filter with a voltage source of internal impedance, R_1, on the left hand side and load, R_N, to the right hand side. The transformers at the input and output of Fig. 3.2(b) with turns ratio 1 : n_1 and n_2 : 1, respectively, are included to normalize the source and the load impedances.

3-4

(a)

(b)
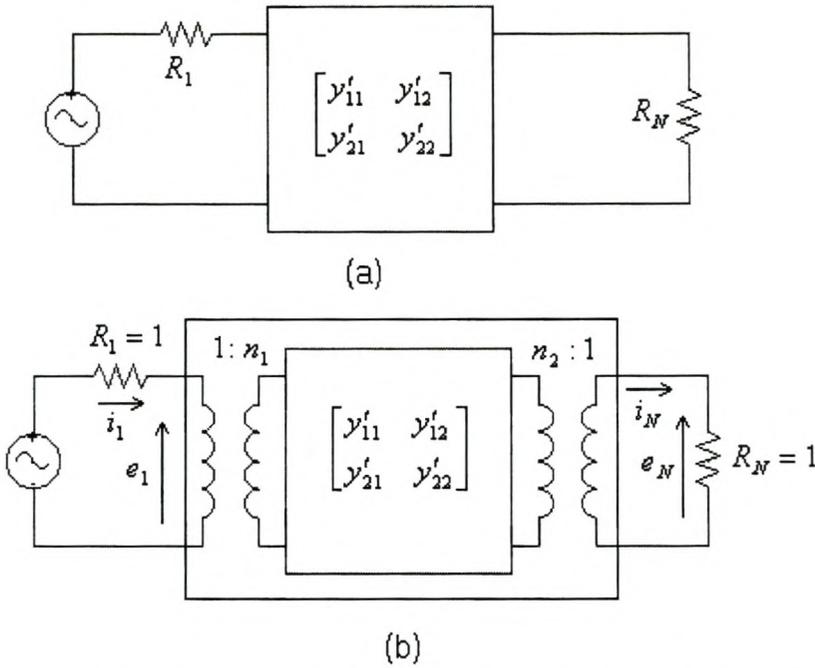
Figure 3.2 Short circuit equivalent admittance parameters of equivalent circuit (Fig. 3.1)

The two-port short-circuit admittance parameters relating to Fig. 3.2(b) are [Ca 1999]

$$\begin{bmatrix} i_1 \\ i_2 \end{bmatrix} = \begin{bmatrix} y_{11} & y_{12} \\ y_{21} & y_{22} \end{bmatrix} \cdot \begin{bmatrix} e_1 \\ e_2 \end{bmatrix} \tag{3.11}$$

The synthesis of bandpass filters in waveguide cavities is most conveniently done by assuming symmetrical networks, i.e., $y_{12} = y_{21}$. These parameters are scaled through transformers to represent the "inner" network of Fig. 3.1, giving

$$\begin{bmatrix} i_1 \\ i_2 \end{bmatrix} = \begin{bmatrix} n_1^2 y'_{11} & n_1 n_2 y'_{12} \\ n_1 n_2 y'_{21} & n_2^2 y'_{22} \end{bmatrix} \cdot \begin{bmatrix} e_1 \\ e_2 \end{bmatrix} \tag{3.12}$$

where the dashed parameters relate to the inner network of Fig. 3.2. The loop equations (eqn. (3.1)) of Fig. 3.1 can be expressed in the matrix form [AW 1971]

$$[jM + SI + R].[i_1, i_2, i_3, \cdots, i_N]^t = e_1[1, 0, 0, \cdots, 0]^t \qquad (3.13)$$

where R is an $[n \times n]$ matrix with all entries zero except at $R_{11} = R_1$ and $R_{NN} = R_N$, M is the $[n \times n]$ reciprocal coupling matrix and t represents the transpose of a matrix. The synthesis of M is most conveniently done by starting with a low-pass characteristic, which implies that $S = j\omega$. By putting R_1 and $R_N = 0$ (i.e., $R = 0$), the short-circuit admittance can be determined by solving eqn. (3.13) for i_N as follows

$$y_{21}(S) = \frac{i_N}{e_1}\Big|_{R_1, R_N = 0} = j[-M - \omega I]_{N1}^{-1} \qquad (3.14a)$$

and similarly by putting the voltage source at the other end of the network

$$y_{22}(S) = \frac{i_N}{e_N}\Big|_{R_1, R_N = 0} = j[-M - \omega I]_{NN}^{-1} \qquad (3.14b)$$

Since M is a real symmetric matrix, it can be diagonalized to its real eigenvalues by a real orthogonal matrix, T, as follows

$$-M = T \cdot \Lambda \cdot T^t \qquad (3.15)$$

where $\Lambda = diag[\lambda_1, \lambda_2, \lambda_3, \cdots, \lambda_N]$, λ_i are the eigenvalues of $-M$ and T^t is the transpose of T such that $T \cdot T^t = I$. Eqns. (3.14a), (3.14b) and (3.15) are the crux of the synthesis as it is through these equations that the physical network consisting of coupled cavities is mathematical related to the transfer function (eqn. (3.6)). Substitution of eqn. (3.15) into eqn. (3.14a) and eqn. (3.14b) yields the following equations

$$y_{21}(S) = j \left[T \cdot \Lambda \cdot T^t - \omega I \right]_{N1}^{-1} \tag{3.16}$$

and

$$y_{22}(S) = j \left[T \cdot \Lambda \cdot T^t - \omega I \right]_{NN}^{-1} \tag{3.17}$$

The general solution for an element i, j of an inverse eigenmatrix problem such as the right hand side of eqn (3.16) is

$$\left[T \cdot \Lambda \cdot T^t - \omega I \right]_{ij}^{-1} = \sum_{k=1}^{N} \frac{T_{ik} T_{jk}}{\omega - \lambda_k} \tag{3.18}$$

Substitution of eqn. (3.18) into eqn. (3.16) and eqn. (3.17), yields the following equations

$$y_{21}(S) = j \sum_{k=1}^{N} \frac{K_{21}}{\omega - \lambda_k} = j \sum_{k=1}^{N} \frac{T_{Nk} T_{1k}}{\omega - \lambda_k} \tag{3.19}$$

and

$$y_{22}(S) = j \sum_{k=1}^{N} \frac{K_{22}}{\omega - \lambda_k} = j \sum_{k=1}^{N} \frac{T_{Nk}^2}{\omega - \lambda_k} \tag{3.20}$$

Atia [AW 1974] supply necessary and sufficient conditions that the rational $[2 \times 2]$ matrix found in eqn. (3.11) is the desired admittance matrix for the two ports in Fig. 3.1. These conditions are

- The poles λ_k are simple and pure imaginary, and satisfy

$$\sum_{k=1}^{n} \lambda_k = 0; \tag{3.21}$$

- The residues of the partial fraction expansions (K_{21} and K_{22}) are real and symmetric

$$\sum_{k=1}^{N} \lambda_k K_{21} \text{ and } \sum_{k=1}^{n} \lambda_k K_{22} = 0 \tag{3.22}$$

From eqns. (3.19) and (3.20) it is clear that a partial expansion of $y_{21}(S)$ and $y_{22}(S)$ yields both the first and last rows of the T-matrix and the eigenvalues of the M-matrix, with

$$T_{Nk} = \sqrt{r_{22k}}$$
$$T_{NN} = \frac{r_{21k}}{T_{Nk}} = \frac{r_{21k}}{\sqrt{r_{22k}}}, \quad k = 1, 2, 3, \cdots, N. \tag{3.23}$$

The transformer turns ratios n_1 and n_2 can be determined by scaling the magnitudes of the row vectors T_{1k} and T_{Nk} to unity for the "inner" network of Fig. 3.2(b)

$$n_1^2 = R_1 = \sum_{k=1}^{N} T_{1k}^2, \ n_2^2 = R_n = \sum_{k=1}^{N} T_{Nk}^2 \tag{3.24}$$

Then,

$$T'_{1k} = \frac{T_{1k}}{n_1} \tag{3.25}$$

and

$$T'_{Nk} = \frac{T_{Nk}}{n_2} \tag{3.26}$$

With the first and the last rows of T' determined, the remaining rows may be constructed with the Gram-Schmidt orthonormalization process. This process is given in Appendix A. Finally the coupling matrix can be synthesized using eqn. (3.15).

However, the simplest method for determining the transformer turns ratios n_1 and n_2 is given by [AW 1971]. Since the denominator of $S_{21}(s)$ is of the form,

3-8

$$N(s) = \sum_{k=0}^{n} d_k s^{n-k} \tag{3.27}$$

then, by an algorithm [Fr 1964] for the computation of the inverse of the matrix $(\lambda I - A)$, one obtains

$$d_0 = 1$$
$$d_1 = -trace(-jR + M) = j(R_1 + R_N) \tag{3.28}$$

This means that the coefficient of the s^{n-1}-term of the denominator of $S_{21}(s)$ is related to the values of R_1 and R_N. Since a symmetrical network is assumed, $R = R_1 = R_N$ can be found from

$$R = n_1 = n_2 = \frac{coefficients(s^{n-1})}{2} \tag{3.29}$$

Furthermore, since the network is assumed to be symmetrical, it is advantageous to use the even and odd mode representation of the equivalent circuit to find the even-mode coupling matrix, M_e [AW 1974].

The procedure for obtaining M_e is equivalent to that described above (for obtaining M), with the exception that the admittance driving function become $Y_e(s)$ which is obtained from:

$$2Y_e = y_{21} + y_{22} \tag{3.30}$$

Also the elements for M_e are obtained by folding the full coupling matrix along the center line of the rows and columns as is illustrated in the following [AW 1974]:

$$M = \begin{bmatrix} 0 & M_{12} & 0 & M_{14} & 0 & M_{16} & \cdot\cdot & \cdot & M_{1n} \\ M_{12} & 0 & M_{23} & 0 & \cdot & \cdot & \cdot\cdot & \cdot & \cdot \\ 0 & M_{23} & 0 & M_{34} & \cdot & \cdot & \cdot\cdot & \cdot & \cdot \\ M_{14} & 0 & M_{34} & \cdot & \cdot & \cdot & \cdot\cdot & \cdot & \cdot \\ 0 & \cdot & \cdot & \cdot & \cdot & \cdot & \cdot\cdot & \cdot & \cdot \\ M_{16} & \cdot & \cdot & \cdot & \cdot & \cdot & \cdot\cdot & \cdot & \cdot \\ \cdot & \cdot & \cdot & \cdot & \cdot & \cdot & \cdot\cdot & \cdot & \cdot \\ \cdot & \cdot & \cdot & \cdot & \cdot & \cdot & \cdot\cdot & \cdot & \cdot \\ \cdot & \cdot & \cdot & \cdot & \cdot & \cdot & \cdot\cdot & \cdot & M_{n-1,n} \\ M_{1,n} & \cdot & \cdot & \cdot & \cdot & \cdot & \cdot 0 & M_{n-1,n} & 0 \end{bmatrix} \qquad (3.31)$$

$$M_e = \begin{bmatrix} M_{1,n} & M_{12} & M_{1,n-2} & M_{14} & M_{1,n-4} & \cdot\cdot & \cdot & M_{1,n/2} \\ M_{12} & M_{2,n-1} & M_{2,3} & \cdot & \cdot & \cdot\cdot & \cdot & \cdot \\ M_{1,n-2} & M_{2,3} & M_{3,n-2} & \cdot & \cdot & \cdot\cdot & \cdot & \cdot \\ \cdot & \cdot & \cdot & \cdot & \cdot & \cdot\cdot & \cdot & \cdot \\ \cdot & \cdot & \cdot & \cdot & \cdot & \cdot\cdot & \cdot & \cdot \\ \cdot & \cdot & \cdot & \cdot & \cdot & \cdot\cdot & \cdot & \cdot \\ \cdot & \cdot & \cdot & \cdot & \cdot & \cdot\cdot & \cdot & \cdot \\ \cdot & \cdot & \cdot & \cdot & \cdot & \cdot\cdot & \cdot & \cdot \\ M_{1,n/2} & \cdot & \cdot & \cdot & \cdot & \cdot\cdot & \cdot & M_{n/2,(n/2)+1} \end{bmatrix} \qquad (3.32)$$

From eqn. (3.32), it is clear that M_e represents an $n/2$ by $n/2$ matrix, implying that by working with a reduced matrix M_e, computation accuracy is greatly improved and the computation time is significantly reduced.

3.4 Finding the short-circuit admittance parameters

From the previous sections it is clear that the coupling matrix can be found from a partial expansion of the admittance driving functions $y_{21}(s)$ and $y_{22}(s)$.

In this section, two methods for determining the rational polynomials for the short-circuit admittance parameters, $y_{21}(y_{12})$ and y_{22}, from the transfer function will be presented.

The first method is called Darlington's Method. It is based on the theory originally presented by Darlington [Da 1939] and summarized by Valkenburg [Va 1960]. Finally, the second method is called Rhodes Method; it is based on the theory set fourth by Zabalawi [RZ 1980] and Rhodes [Rh 1976]

3.4.1 Darlington Method

Usually synthesis of most filter functions starts with the determination of the voltage transfer ratio with the required passband and stopband response. In this case a low pass prototype transfer ratio will be used.

This method starts by determining the reflection coefficient $S_{11}(s)$ from the transmission coefficient $S_{21}(s)$. For a lossless network, $S_{11}(s)$ is related to $S_{21}(s)$ by

$$\left|S_{11}(j\omega)\right|^2 = 1 - \left|S_{21}(j\omega)\right|^2 \qquad (3.33)$$

Replacing $j\omega$ by s yields the following equation

$$S_{11}(s)S_{11}(-s) = 1 - S_{21}(s)S_{21}(-s) \qquad (3.34)$$

where

$$S_{11}(s) = \frac{S_{11num}(s)}{S_{11den}(s)} \tag{3.35}$$

The denominator poles of $S_{11}(s)$ are the same as that of $S_{21}(s)$ and is therefore also a Hurwitz polynomial. Furthermore, the numerator zeros will alternate between pure real and pure imaginary as the power of s increases.

The input impedance for a double terminated network is related to $S_{11}(s)$ as follows [Su 1996]

$$Z_{in}(s) = R_1 \frac{1 \pm S_{11}(s)}{1 \mp S_{11}(s)} \tag{3.36}$$

Substitution of eqn. (3.35) into eqn. (3.36), result into eqn. (3.37)

$$Z_{in}(s) = R_1 \frac{S_{11den}(s) \pm S_{11num}(s)}{S_{11den}(s) \mp S_{11num}(s)} = \frac{Z_n^e + Z_n^o}{Z_d^e + Z_d^o} \tag{3.37}$$

where Z_n^e, Z_d^e, Z_n^o and Z_d^o are complex even and complex odd polynomials, respectively, in the variable s constructed from $E(s)$ and $F(s)$.

The driving point impedance for this network (Fig 3.1) in terms of its short and open-circuit parameters is [Va 1960]

$$Z_{in}(s) = \frac{z_{11}[1/y_{22} + R_N]}{z_{22} + R_N} = \frac{z_{11}[1/y_{22} + 1]}{z_{22} + 1} \tag{3.38}$$

Also, eqn. (3.37) can be expressed in the same form as that of eqn. (3.38) by bringing the odd parts outside the brackets of the numerator and denominator respectively, extracting either the even part or the odd parts and then multiplying by R_N.

For the even order case, the odd parts Z_n^o and Z_d^o are taken outside the brackets of the numerator and denominator, yielding

$$Z_{in}(s) = \frac{Z_n^o \left[R_N \dfrac{Z_n^e}{Z_n^o} + R_N \right]}{Z_d^o \left[R_N \dfrac{Z_d^e}{Z_d^o} + R_N \right]} \tag{3.39}$$

By comparing eqns. (3.38) and (3.39), it is seen that

$$y_{22}(s) = \frac{1}{R_N} \frac{Z_n^o}{Z_n^e} \tag{3.40}$$

and since the denominator of $y_{21}(s)$ is the same as that of $y_{22}(s)$, and the numerator of $y_{21}(s)$ has the same transmission zeros as $S_{21}(s)$

$$y_{21}(s) = \frac{1}{R_N} \frac{P(s)}{Z_n^e} \tag{3.41}$$

Similarly,

$$y_{22}(s) = \frac{1}{R_N} \frac{Z_n^e}{Z_n^o} \text{ and } y_{21}(s) = \frac{1}{R_N} \frac{P(s)}{Z_n^o}, \text{ for } N \text{ odd.} \tag{3.42}$$

Eqns. (3.40) and (3.41) can be used to determine either the full M-matrix or Y_e and the even coupling matrix discussed in section 3.4.1 above.

3.4.2 Rhodes Method

Due to the fact that the numerator of the reflection coefficient is either an even or an odd polynomial it is always possible to realize the filter as a symmetrical device. Using the bisection theorem [Va 1960], $S_{21}(s)$ can be expressed as follows [Rh 1976]

$$S_{21}(s) = \frac{Y_e - Y_o}{(1 + Y_e)(1 - Y_o)} \tag{3.43}$$

where Y_e and Y_o are even and odd mode admittances of a symmetrical network respectively. Also, $S_{21}(s)$ can be expressed as follows [Rh 1976]

$$S_{21}(s) = \frac{E(s)}{D_k(s)D_k^*(s)} \tag{3.44}$$

where $D_k^*(s)$ is $D_k(s)$ with the coefficients replaced by their complex conjugates, and

$$k = \frac{\text{order of denominator } S_{21}(s)}{2} \tag{3.45}$$

Comparing eqn. (3.43) and (3.44) gives

$$Y_o = Y_e^* \tag{3.46}$$

and the zeros of $1 + Y_o$ are the zeros of $D_k(s)$.

The poles of $S_{21}(s)$ lie in the left half plane and occur in complex conjugate pairs. Furthermore, the roots of $D_k(s)$ are chosen to be half the poles of $S_{21}(s)$ in the left plane

that is conjugate with $D_k^*(s)$. Then $D_k(s)$ can be expanded into the even and odd parts of its real and imaginary parts as follows

$$D_k(s) = E_1(s) + O_1(s) + j[E_2(s) + O_2(s)] \tag{3.47}$$

With the substitution of eqns. (3.44) and (3.47) into eqn. (3.43), it is seen that

$$Y_e(s) = \frac{E_1(s) + jO_2(s)}{O_1(s) + jE_2(s)} \quad \text{for } k \text{ odd} \tag{3.48}$$

or

$$Y_e(s) = \frac{O_1(s) + jE_2(s)}{E_1(s) + jO_2(s)} \quad \text{for } k \text{ even} \tag{3.49}$$

Eqns. (3.48) and (3.49) can then be used to determine the even-mode coupling matrix discussed in section 3.4.1.

3.5 Coupling Matrix Reduction

In general, the coupling matrix that emerges from the synthesis procedure described in section 3.4 has nonzero elements, implying that all the possible couplings are present. It is therefore necessary to find a way to transform the full coupling matrix into a realizable form by reducing the unwanted entries to zero.

Cameron [Ca 1999] presents a method known, as the folded canonical form to do this transformation and it will be discussed in the following section.

3.5.1 Folded canonical form

A similarity transform on the $[N \times N]$ coupling matrix, M, is carried out by pre-and post-multiplying it by an $[N \times N]$ rotation matrix, R_r, and its transpose, R_r^t:

$$M_r = R_r \cdot M_{r-1} \cdot R_r^t, \quad r = 1, 2, 3, \cdots, k \tag{3.50}$$

where k is the number of transformations required to reduce all unwanted elements to zero. All the elements of R_r are the same as the identity matrix, except that the pivot $[i, j]$ $(i \neq j)$ of R_r means that elements $R_{ii} = R_{jj} = R\cos\theta_r, R_{ji} = -R_{ij}\sin\theta_r$, $(i, j \neq 1 \ or \ n)$ and θ_r is the angle of rotation illustrated in Table 3.1.

3-16

Table 3.1 Example of 7th degree Rotation Matrix R_r pivot [3,5]

	1	2	3	4	5	6	7
1	1						
2		1					
3			c_r		s_r		
4				1			
5			s_r		c_r		
6						1	
7							1

where

$$c_r = \cos\theta_r$$
$$s_r = \sin\theta_r$$

$$(3.51)$$

Application of the similarity transform to the coupling matrix M_{r-1} changes the elements common to row i or j and columns i or j. The kth element in row or column i and j of the pivot $[i, j]$ will change according to the following formula:

$$M'_{ik} = c_r M_{ik} - s_r M_{jk}, \qquad \text{for an element in row } i. \qquad (3.52a)$$

$$M'_{jk} = s_r M_{ik} + c_r M_{jk}, \qquad \text{for an element in row } j. \qquad (3.52b)$$

$$M'_{ki} = c_r M_{ki} - s_r M_{kj}, \qquad \text{for an element in column } i. \qquad (3.52c)$$

$$M'_{kj} = s_r M_{ki} + c_r M_{kj}, \qquad \text{for an element in column } j. \qquad (3.52d)$$

where $k \ (\neq i, j) = 1, 2, 3, \ldots, n$, $c_r = \cos \theta_r$, $s_r = \sin \theta_r$, and the undashed matrix elements belong to the matrix M_{r-1}, and the dashed belong to M_r.

Two important elements of the similarity transform can be noted:

- Only the elements common in the rows and columns i and j of the pivot $[i, j]$ are influenced by the transformation.

- If two elements facing each other across the rows and the columns of the pivot are zero before the transformation, they will remain zero after the transformation. This imply that the reduction of unwanted elements procedure can be carried out without affecting the required elements.

This reduction procedure transforms the M-matrix into its folded canonical form and starts by reducing unwanted elements in the first row, then the n-th column, the second row, the $(n$-1$)$-th column and so fourth until all unwanted elements are zero.

The procedure discussed above is unconditionally valid for transformation of full coupling matrices. However, for even-mode matrices it is often necessary to reduce elements on the main diagonal, which cannot be handled by the method discussed above.

A similar method for the transformation of the even-mode matrix, using different reduction formulas, is derived for each individual case. An example of a third order even-mode matrix where M_{22} has to be reduced, is presented [RZ 1980]:

$$
\begin{bmatrix}
M_{11} & M_{12} & M_{13} \\
M_{12} & M_{22} & M_{23} \\
M_{13} & M_{23} & M_{33}
\end{bmatrix}
=
\begin{bmatrix}
M'_{11} & M'_{12} & M'_{13} \\
M'_{12} & 0 & M'_{23} \\
M'_{13} & M'_{23} & M'_{33}
\end{bmatrix}
\tag{3.53}
$$

The rotation matrix required to reduce M_{22} is given by

$$
R_r =
\begin{bmatrix}
1 & 0 & 0 \\
0 & c_1 & -s_1 \\
0 & s_1 & c_1
\end{bmatrix}
\tag{3.54}
$$

After the application of the transformation matrix, the following changes to the elements of the coupling matrix are observed:

$$M'_{12} = c_1 M_{12} - s_1 M_{13}, \quad M'_{13} = s_1 M_{12} + c_1 M_{13}$$
$$M'_{22} = c_1^2 M_{22} - 2 c_1 s_1 M_{23} + s_1^2 M_{33}$$
$$M'_{23} = c_1 s_1 M_{22} - s_1^2 M_{23} + c_1^2 M_{23} - c_1 s_1 M_{33} \tag{3.55}$$
$$M'_{33} = s_1^2 M_{22} + 2 c_1 s_1 M_{23} + c_1^2 M_{33}$$

To reduce M_{22} to zero the following must hold:

$$M_{33} t^2 - 2 M_{23} t + M_{22} = 0 \tag{3.56}$$

where $t = \tan \theta_1$ and θ_1 is the angle required to determine c_1 and s_1. Solving for t from eqn. (3.55), gives two possible solutions

$$t = \frac{M_{23} \pm \sqrt{M_{23}^2 - M_{22} M_{33}}}{M_{33}} \tag{3.57}$$

An extra realisability condition requires that $M_{23}^2 \geq M_{22} M_{33}$

Substituting the value of t back into eqn. (3.56) results into the final values for the elements of coupling matrix M.

3.6 Coupling Matrix Analysis

The coupling matrix analysis starts by assuming that a fourth-order band-pass filter with a center frequency at 1 rad/s and 2% bandwidth will be designed. Also four resonators will be needed, all of which are excited with a single mode. Fig. 3.3 shows an equivalent circuit (to Fig. 3.1) of a 4th order filter with the direct coupling.
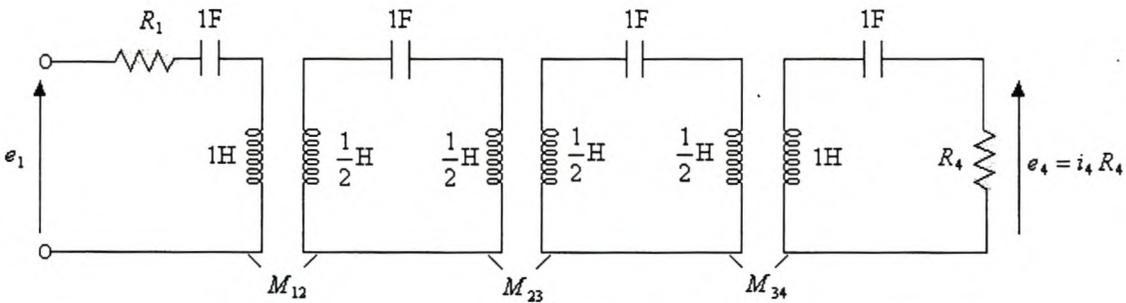
Figure 3.3 Equivalent 4th order filter

After applying the theory set fourth in section 3.4, the coupling matrix for a 4th order filter will be

$$M = \begin{bmatrix} M_{11} & M_{12} & M_{13} & M_{14} \\ M_{12} & M_{22} & M_{23} & M_{24} \\ M_{13} & M_{23} & M_{33} & M_{34} \\ M_{14} & M_{24} & M_{34} & M_{44} \end{bmatrix} \tag{3.58}$$

From eqn. (3.58), all the coupling terms for the full coupling matrix are non-zero. It can be seen that the coupling matrix obtained in eqn. (3.58) cannot be realized by the network shown in Fig. 3.3. Applying the coupling matrix reduction procedure discussed in section 3.5, eqn. 3.59 results

$$M = \begin{bmatrix} 0 & M_{12} & 0 & 0 \\ M_{12} & 0 & M_{23} & 0 \\ 0 & M_{23} & 0 & M_{34} \\ 0 & 0 & M_{34} & 0 \end{bmatrix} \tag{3.59}$$

which Fig 3.3 can realize.

The equivalent 4th order filter shown in Fig. 3.3 needs to be bandwidth scaled and impedance scaled to the bandwidth desired by the designer. This yields the circuit shown in Fig. 3.4.
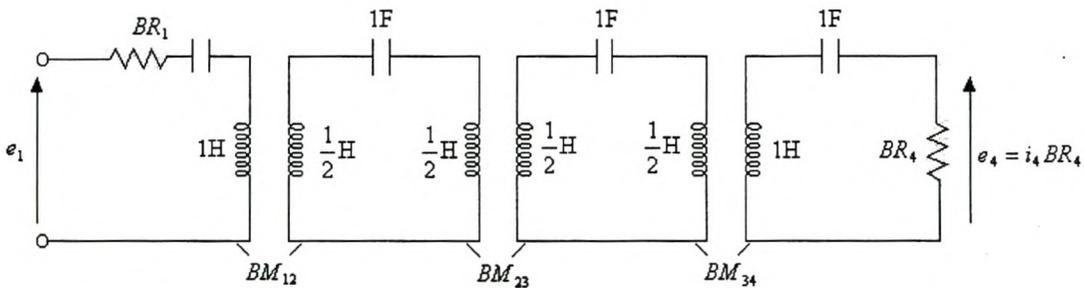
Figure 3.4 Bandwidth Scaling and Impedance Scaling

where B is the bandwidth. Then eqn. (3.59) become

$$M = \begin{bmatrix} 0 & BM_{12} & 0 & 0 \\ BM_{12} & 0 & BM_{23} & 0 \\ 0 & BM_{23} & 0 & BM_{34} \\ 0 & 0 & BM_{34} & 0 \end{bmatrix} \tag{3.60}$$

With the theory discussed above, a 4th order Butterworth band-pass filter coupling matrix was obtained. Fig. 3. 5 show the results of the analysis of the network shown in Fig. 3.4. The center frequency is at 1 rad/s and the bandwidth is 2%.
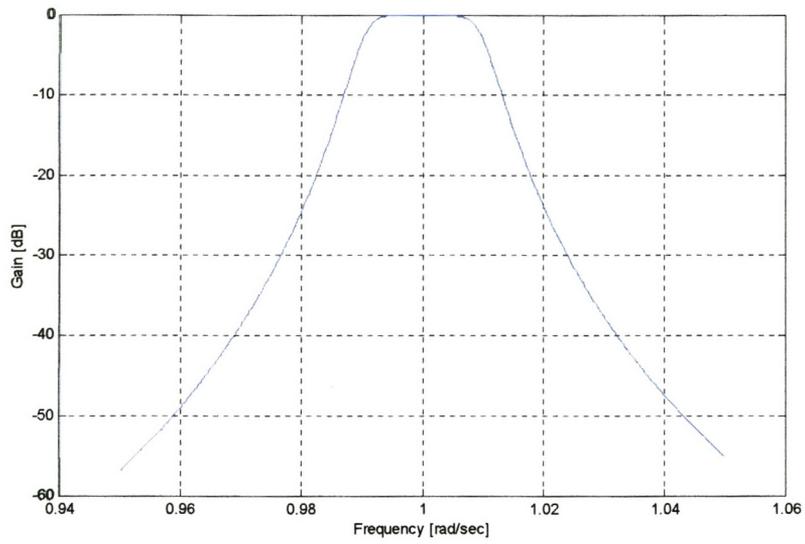
Figure 3.5 **Analysis of Coupling matrix for 4th-order Butterworth Filter.**

3.7 Conclusion

General methods have been presented for the direct synthesis of the coupling matrix for the double terminated two-port network shown in Fig. 3.1. The Rhodes method is very accurate as the even-mode admittance, $Y_e(s)$, is derived directly from $S_{21}(s)$ and there is no need to find the roots of $S_{11}(s)S_{11}(-s)$ as with the Darlington method.

The coupling matrix that emerges from the synthesis procedure has non-zero elements, implying all the possible couplings are present. With the use of folded canonical form, the coupling matrix can be made realizable by any structure of concern.

Application of theory presented to the filter design has been demonstrated through the synthesis of the coupling matrix for a fourth-order Butterworth filter. The obtained results are found to be in a good agreement with theory as illustrated in Fig. 3.5.

The only restriction in these filters is that the resonators that are coupled to each other must be identical. This restriction is placed on these filters by the equivalent circuit used.

In the following chapter the circuit theory, cavity, and the coaxial line resonators will be discussed.

4. Resonators

4.1 Introduction

Resonant circuits may be a combination of capacitors and inductors, which are small compared to a wavelength (lumped-element type), or distributed elements. They create, filter, and select frequencies in oscillators, amplifiers, and tuners. The advantage of using lumped elements is in their small size, but their Q-factor is lower than that of distributed elements, which causes higher insertion loss for filter applications. On the other hand, a circuit of distributed elements takes up more space.

Fields inside a resonator store energy at the resonant frequency where equal storage of electric and magnetic energies occurs. At the resonant frequency there is an exchange of stored energy between the capacitor and the inductor every quarter-cycle. There is also an exchange between stored electrical and magnetic energies every quarter-cycle in the distributed resonant circuit.

The figure of merit for assessing the performance or quality of a resonator is the quality factor, Q. It relates a resonant circuit's capacity for electromagnetic storage with its energy dissipation through heat. Q-factor of a resonant circuit is measured when the stored energy is a maximum in the inductor or capacitor. At microwave frequencies, Q-factors can be as high as 10,000 and at lower frequencies, the Q-factor is usually between 50 and 500. Furthermore, resonator bandwidth is inversely proportional to the Q-factor. Thus, high Q-factor resonators have narrow bandwidths.

Ideal lumped-elements are usually unattainable at microwave frequencies, so distributed elements are commonly used. Transmission lines with various lengths and terminations (usually open or short circuited) can be used to model series and parallel resonators of circuit theory.

Various implementations of the resonators at microwave frequencies using transmission lines, rectangular waveguides, cylindrical waveguides and coaxial lines will be discussed.

4.2 Quality Factor

The figure of merit for assessing the performance, or quality of a resonator is the quality factor, Q. The Q-factor is a measure of energy loss or dissipation per cycle as compared to the energy stored in the fields inside the resonator. Pozar [Po 1996-b] defines it as follows

$$Q = \omega_0 \frac{\text{energy stored}}{\text{average power dissipated}} = \frac{\omega_0 W_0}{P_\ell} \tag{4.1}$$

where ω_0 is the resonant radian frequency.

The properties of resonators derived in this context follows the theory set fourth by Kajfez [KG 1986]. The differential equation for a simple resonator is given by

$$\frac{d^2v}{dt^2} + 2 \times \sigma \frac{dv}{dt} + \omega_0^2 v = f(t) \tag{4.2}$$

where σ is the conductivity of the medium. The presence of $\sigma > 0$ corresponds to a resonator with losses. Laplace transforming eqn. (4.2) and solving for the transfer function, $H(s)$, yields the following equation

$$H(s) = \frac{V(s)}{F(s)} = \frac{1}{s^2 + 2 \times \sigma s + \omega_0^2} \tag{4.3}$$

Factoring the denominator of eqn. (4.3), eqn. (4.4) result

$$H(s) = \frac{j}{2 \times \omega_L} \left\{ \frac{1}{s + \sigma + j\omega_L} - \frac{1}{s + \sigma - j\omega_L} \right\} \tag{4.4}$$

where the loaded natural resonant frequency, ω_L, is

$$\omega_L = \sqrt{\omega_0^2 - \sigma^2} \qquad (4.5)$$

When $\sigma > 0$, a change in the resonant frequency, f_0, will result and this is called frequency pulling due to loss. Note that in eqn. (4.5), $\omega_L = \omega_0$ only when $\sigma = 0$. The natural response of the differential equation (eqn. (4.2)) is

$$v(t) = Ve^{-\sigma t}\sin(\omega_L t) \qquad (4.6)$$

The stored energy is proportional to the average value of $v^2(t)$, for small σ it is

$$W = \frac{1}{2} \times v^2(t)e^{-2 \times \sigma t} \qquad (4.7)$$

and the average power in the system is

$$P = -\frac{dW}{dt} = 2 \times \sigma W \qquad (4.8)$$

Solving for σ in eqn. (4.8), eqn. (4.9) results

$$\sigma = \frac{P}{2 \times W} \qquad (4.9)$$

Substituting eqn. (4.9) into eqn. (4.1), the quality factor becomes

$$Q = \frac{\omega_0}{2 \times \sigma} \qquad (4.10)$$

The loaded natural resonant frequency now becomes

$$\omega_L = \omega_0 \sqrt{1 - \frac{1}{4 \times Q^2}} \qquad (4.11)$$

Also substitution of eqn. (4.10) into eqn. (4.2) yields eqn. (4.12)

$$\frac{d^2v}{dt^2} + \frac{\omega_0}{Q}\frac{dv}{dt} + \omega_0^2 v = f(t) \qquad (4.12)$$

From eqn. (4.12), the following can be noted

- For a perfect resonator, $Q \longrightarrow \infty$, and the first derivative falls away.

- For a practical resonator, Q is finite and the first derivative must be retained.

Substituting $s = j\omega$ and $\sigma = \dfrac{\omega_0}{2 \times Q}$ into eqn. (4.3), the transfer function, $H(j\omega)$

becomes

$$H(j\omega) = \frac{1}{\omega_0^2 - \omega^2 + \dfrac{j\omega\omega_0}{Q}} \qquad (4.13)$$

The denominator of eqn. (4.13) can also be written as follows

$$\omega_0^2 - \omega^2 + \frac{j\omega\omega_0}{Q} = j\frac{\omega\omega_0}{Q}\left[1 + jQ\left[\frac{\omega}{\omega_0} - \frac{\omega_0}{\omega}\right]\right] \qquad (4.14)$$

Also, the ω-dependence term can be factored to give

$$\frac{\omega}{\omega_0} - \frac{\omega_0}{\omega} = \left(\frac{\omega - \omega_0}{\omega_0}\right)\left(\frac{\omega_0}{\omega} + 1\right) \tag{4.15}$$

Since for high Q, ω is very close to ω_0, $\frac{\omega_0}{\omega} + 1 = 2$. Therefore eqn. (4.15) becomes

$$\frac{\omega}{\omega_0} - \frac{\omega_0}{\omega} = 2 \times \left(\frac{\omega - \omega_0}{\omega_0}\right) \tag{4.16}$$

The approximate $H(j\omega)$ then becomes

$$H(j\omega) = \frac{-j\dfrac{Q}{\omega\omega_0}}{1 + 2 \times jQ\left(\dfrac{\omega - \omega_0}{\omega_0}\right)} \tag{4.17}$$

The half-power bandwidth is defined to be the frequency spread, $\Delta\omega$, where $\Delta\omega$ is defined by the difference in half-power frequencies ω_1 and ω_2, where

$$|H(\omega)| = \frac{1}{\sqrt{2}} \times |H(\omega_0)| \tag{4.18}$$

for $\omega = \omega_1$ and $\omega = \omega_2$. Using the approximate $H(j\omega)$, eqn. (4.18) becomes

$$\frac{\dfrac{Q}{(\omega\omega_0)}}{\sqrt{1 + 4 \times Q^2\left(\dfrac{\omega - \omega_0}{\omega_0}\right)^2}} = \frac{1}{\sqrt{2}} \times \frac{Q}{\omega_0^2} \tag{4.19}$$

Eqn. (4.19) is true only when

$$4 \times Q^2 \left(\frac{\omega - \omega_0}{\omega_0} \right)^2 = 1 \qquad (4.20)$$

The solution for the approximate half-power frequencies then becomes

$$\omega_i = \omega_0 \pm \frac{\omega_0}{2 \times Q}, \quad i = 1, 2 \qquad (4.21)$$

The approximate bandwidth, B, is defined as follows

$$B = \Delta \omega = |\omega_1 - \omega_2| = \frac{\omega_0}{Q} = 2\sigma \qquad (4.22)$$

To a very good approximation, then, quality factor is given by

$$Q = \frac{\omega_0}{\Delta \omega} = \frac{f_0}{\Delta f} \qquad (4.23)$$

Thus, the Q-factor as defined by eqn. (4.23) is the measure of the sharpness of the frequency response.

However, when a resonant circuit or cavity is used as a load in a microwave circuit, several different Q-factors can be defined. The first Q-factor is the unloaded Q-factor, Q_u, which indicates the figure of merit for the resonator itself. The next Q-factor is the external Q-factor, Q_e, which expresses the coupling condition between the external circuits and the resonator. Lastly, the loaded Q-factor, Q_L, which represents the total Q-factor including the resonator and external circuits, can be defined.

The unloaded Q-factor is defined by

$$Q_u = \frac{\omega_0 W}{P_u} \qquad (4.24)$$

where P_u is the internal power dissipation. For cavity resonators, power loss by conductors, P_c, dielectric fills, P_d, and radiation, P_r, contribute to Q_u. The total power in the cavity itself is the sum of these three individual internal components

$$P_u = P_c + P_d + P_r \qquad (4.25)$$

These losses can individually be accounted for by defining their Q-factors respectively, as follows

$$Q_c = \frac{\omega_0 W}{P_c} \qquad (4.26a)$$

$$Q_d = \frac{\omega_0 W}{P_d} \qquad (4.26b)$$

$$Q_r = \frac{\omega_0 W}{P_r} \qquad (4.26c)$$

Substituting eqn. (4.25) into eqn. (4.24), the unloaded Q-factor becomes

$$Q_u = \frac{\omega_0 W}{P_c + P_d + P_r} \qquad (4.27)$$

From eqn. (4.27), it is seen that with more power loss, a lower Q_u will result. Rearranging eqn. (4.27), the relationship between Q_u and Q_c, Q_d, and Q_r is found to be

$$\frac{1}{Q_u} = \frac{P_c}{\omega_0 W} + \frac{P_d}{\omega_0 W} + \frac{P_r}{\omega_0 W} = \frac{1}{Q_c} + \frac{1}{Q_d} + \frac{1}{Q_r} \qquad (4.28)$$

4-8

In order for the cavity to be useful, the cavity or resonator must deliver power to an external load. The power loss due to the presence of an external load in a cavity system results in the external Q-factor, defined by

$$Q_e = \frac{\omega_0 W}{P_e} \qquad (4.29)$$

where P_e is the power loss due to an external drain on the internal energy reserves.

The loaded Q-factor is the total Q-factor for the system including power losses both internal and external to the resonator system. The loaded Q-factor is defined by

$$Q_L = \frac{\omega_0 W}{P_T} \qquad (4.30)$$

Since $P_T = P_e + P_u$, Q_L becomes

$$\frac{1}{Q_L} = \frac{1}{Q_e} + \frac{1}{Q_u} \qquad (4.31)$$

One manifestation about eqn. (4.31) is that the smallest Q-factor dominates.

4.3 Transmission Line Resonators

Transmission lines are often schematically represented by a two-wire system, since it always have at least two conductors. Transmission lines supports transverse electromagnetic (TEM) waves. Since we are interested in the Q-factor of these resonators, lossy transmission lines will be considered.

Suppose that a transmission line, shorted at one end, is excited by a sinusoidal voltage at the other. Figure 4.1 shows a line terminated in a short-circuit, $Z_L = 0$, at z = 0.
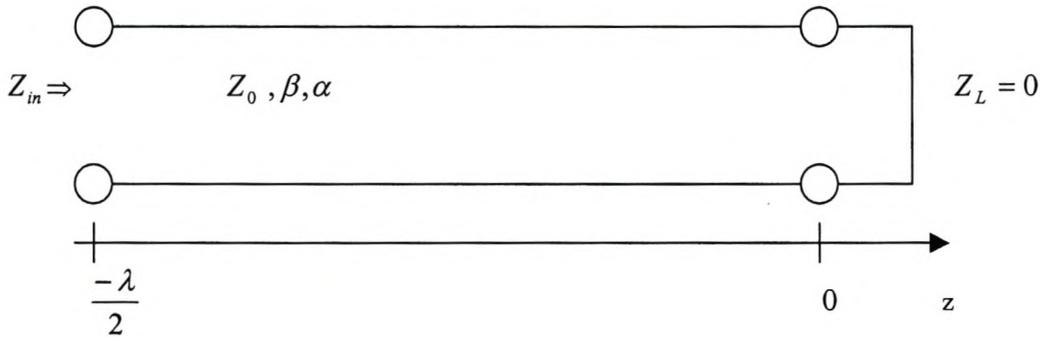

Figure 4.1 A transmission line terminated in a short circuit

The voltage and current wave on a lossless line [Po 1998-c] are given by

$$V(z) = V_0^+ [e^{-\gamma z} + \Gamma e^{\gamma z}] \qquad (4.32a)$$

$$I(z) = \frac{V_0^+}{Z_0} [e^{-\gamma z} - \Gamma e^{\gamma z}] \qquad (4.32b)$$

where Γ is the reflection coefficient of the load defined as follows

$$\Gamma = \frac{Z_L - Z_0}{Z_L + Z_0} \qquad (4.33)$$

4-10

with Z_0 the characteristic impedance of the line. $2V_0^+$ at $z = 0$ is the amplitude of the incident voltage and γ is the complex propagation constant, which is a function of frequency and is given by

$$\gamma = \alpha + j\beta \tag{4.34}$$

where α is the attenuation constant and β is the phase constant. The reflection coefficient for a short-circuit load is, from eqn. (4.33), $\Gamma = -1$, since $Z_L = 0$. The input impedance Z_{in} at a distance $-\ell$ from the load is the [Po 1998-c]

$$Z_{in}(-\ell) = \frac{V(-\ell)}{I(-\ell)} = Z_0 \frac{Z_L + Z_0 \tanh(\gamma\ell)}{Z_0 + Z_L \tanh(\gamma\ell)} = Z_0 \tanh(\gamma\ell) \tag{4.35}$$

Applying the identity

$$\tanh(x \pm jy) = \frac{\tanh x \pm j \tan y}{1 \pm \tanh x \tan y} \tag{4.36}$$

to eqn. (4.35) gives

$$Z_{in} = Z_0 \frac{\tanh(\alpha\ell) + j \tan(\beta\ell)}{1 + j \tan(\beta\ell)\tanh(\alpha\ell)} \tag{4.37}$$

For a lossless transmission line, $\alpha = 0$ and equation (4.37) becomes

$$Z_{in} = jZ_0 \tan(\beta\ell) \tag{4.38}$$

4.3.1 Quality Factor for Transmission Line Resonators.

In many practical cases the loss of the line is very small such that $\alpha\ell \ll 1$, which leads to $\tan(\alpha\ell) \approx \alpha\ell$. Let $\omega = \omega_0 + \Delta\omega$, where ω_0 is the resonant radian frequency and $\Delta\omega$ is small. For a TEM line the phase constant is,

$$\beta = \frac{\omega}{v_P} \tag{4.39}$$

where v_p is the phase velocity. This imply that

$$\beta\ell = \frac{\omega\ell}{v_p} = \frac{\omega_0\ell}{v_p} + \frac{\Delta\omega\ell}{v_p} \tag{4.40}$$

For $\ell = \dfrac{\lambda}{2} = \dfrac{\pi v_p}{\omega_0}$ and $\omega = \omega_0$, eqn. (4.40) becomes

$$\beta\ell = \pi + \frac{\Delta\omega\pi}{\omega_0} \tag{4.41}$$

which leads to the following result

$$\tan(\beta\ell) = \tan\left(\pi + \frac{\Delta\omega\ell}{\omega_0}\right) = \tan\left(\frac{\Delta\omega\pi}{\omega_0}\right) \approx \frac{\Delta\omega\pi}{\omega_0} \tag{4.42}$$

Substituting eqn. (4.42) into eqn. (4.37), the input impedance becomes

$$Z_{in} = Z_0 \frac{\alpha\ell + j\left(\dfrac{\Delta\omega\pi}{\omega_0}\right)}{1 + j\left(\dfrac{\Delta\omega\pi}{\omega_0}\right)\alpha\ell} \approx Z_0\left(\alpha\ell + j\frac{\Delta\omega\pi}{\omega_0}\right) \tag{4.43}$$

The input impedance [Po 1998-c] for a series resonator circuit is given by

$$Z_{in} = R + j2L\Delta\omega \qquad (4.44)$$

Comparing the input impedance given by eqn (4.43) and eqn. (4.44), the resonator resistance is

$$R = Z_0 \alpha \ell \qquad (4.45)$$

and the inductance is

$$L = \frac{Z_0 \pi}{2\omega_0} \qquad (4.46)$$

At resonance the capacitive reactance equals the inductive reactance, implying that the capacitance is given by

$$X_c = \frac{1}{\omega_0 C} = X_L = \omega_0 L \qquad (4.47a)$$

or

$$C = \frac{1}{\omega_0^2 L} \qquad (4.47b)$$

Solving for the radiant frequency, ω_0, from eqn. (4.47b) yields

$$\omega_0 = \frac{1}{\sqrt{LC}} \qquad (4.48)$$

The maximum energy stored by a resonator is expressed as follows

$$W_0 = W_m + W_e \qquad (4.49)$$

where W_m and W_e are the average energy stored by a series resonator in an inductor and capacitor respectively given by

$$W_m = \frac{1}{4} \times |I|^2 L \qquad (4.50a)$$

$$W_e = \frac{1}{4} \times |I|^2 \frac{1}{\omega^2 C} \qquad (4.50b)$$

and P_ℓ is the power dissipated by the resistor, R, given by

$$P_l = \frac{1}{2} \times |I|^2 R \qquad (4.51)$$

At resonance $W_m = W_e$, then eqn. (4.49) becomes

$$W_0 = 2 \times W_m \qquad (4.52)$$

Substituting eqn. (4.50a) and eqn. (4.52) into eqn. (4.1), the Q-factor for a short-circuited half-wavelength transmission line can be written as

$$Q = \omega_0 \frac{2W_m}{P_{loss}} = \frac{\omega_0 L}{R} = \frac{\pi}{2\alpha\,\ell} = \frac{\beta}{2\alpha} \qquad (4.53)$$

Resonant low-loss transmission lines can have Q's of thousands in the UHF range of frequencies.

4.4 Cavity Resonators

Waveguides, often consisting of a single conductor, supports transverse electric (TE) waves and/or transverse magnetic waves (TM), characterized by the presence of longitudinal magnetic or electric field components, respectively. The hollow rectangular waveguide can propagate TM and TE modes, but not TEM waves since only one conductor is present.

Hollow enclosures exhibit resonance behavior when excited by an electromagnetic field. These enclosures are known as cavity resonators and are widely used at frequencies above 3 GHz. The quality of these resonators can be quite high at microwave frequencies with typical values of unloaded Q ranging from 5000 to 50 000. As with the transmission line resonators described earlier, cavity resonators have an infinite number of resonant modes. These can be determined by solving Maxwell's equations and applying the boundary conditions appropriate to the particular configuration. This approach is used in the next section to analyze rectangular and cylindrical configuration.

4.4.1 The Rectangular Cavity Resonator

A rectangular resonator may be viewed as a rectangular waveguide shorted at both ends. This is illustrated in Fig. 4.2 for a guide of height b, width a and length d. The cavity is resonant at frequencies for which d is a multiple of $\frac{\lambda_g}{2}$, with λ_g being the guide wavelength for propagation along the z-axis.

The rectangular cavity shown in Fig. 4.2 is assumed to be lossless. This implies that the attenuation constant $\alpha = 0$, and thus that the propagation constant is given by $\gamma = j\beta$.

Determination of the field equations for the rectangular cavity resonator shown in Fig. 4.2 follows the theory set fourth by Pozar [Po 1998-d].

4-15
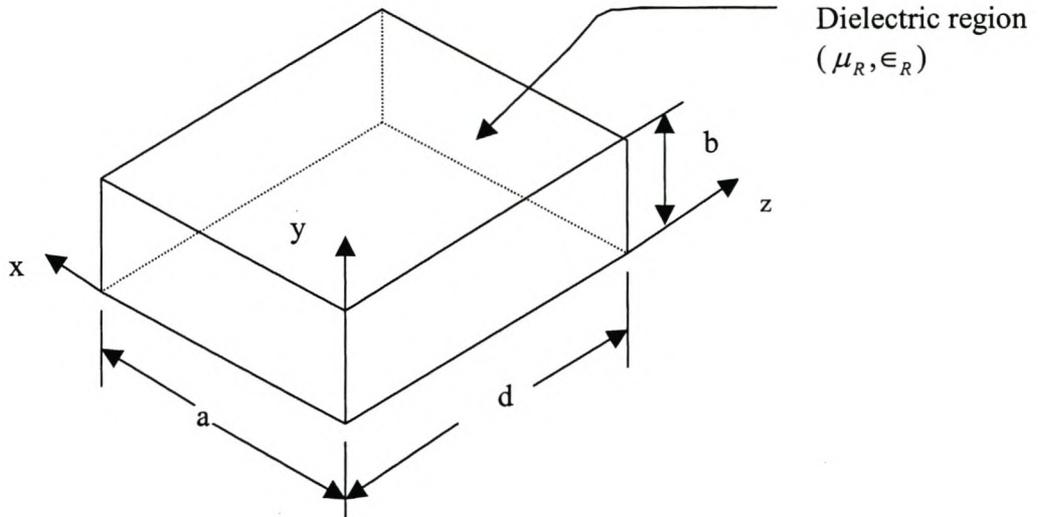
Figure 4.2   A rectangular cavity resonator

The TE and TM waveguide fields already satisfy the necessary boundary conditions on the side walls at (x = 0, a and y = 0, b) of the cavity. The transverse electric fields E_x and E_y must also be zero at the end walls at z = 0, d.

The transverse electric fields (E_x and E_y) of the TE_{mn} or TM_{mn} rectangular waveguide mode can be expressed as follows

$$\overline{E}_t(x,y,z) = \overline{e}(x,y)[A^+ e^{-j\beta_{mn}z} + A^- e^{-j\beta_{mn}z}] \qquad (4.54)$$

where $\overline{e}(x,y)$ is the transverse variation of the mode and A^+ and A^- are arbitrary amplitudes of the forward and backward traveling waves respectively. The phase constant β is defined as follows

$$\beta = \sqrt{k^2 - k_c^2} = \sqrt{k^2 - \left(\frac{m\pi}{a}\right)^2 - \left(\frac{n\pi}{b}\right)^2} \qquad (4.55)$$

where k_c is the cutoff wave number and

$$k = \omega\sqrt{\mu\varepsilon} = \omega\sqrt{\mu_0\mu_r\varepsilon_0\varepsilon_r} \qquad (4.56)$$

where μ_0 is the permeability of air and ε_0 is the permittivity of air. By applying the boundary conditions of the rectangular cavity to eqn. (4.54), A^+ and A^- can be found as follows:

At $z = 0$, $\overline{E}_t = 0$ implying that $A^+ = -A^-$. Also at $z = $ d, $\overline{E}_t = 0$, which leads to

$$\overline{E}_t(x,y,d) = -\overline{e}(x,y)A^+ 2j\sin\beta_{mn}d = 0 \qquad (4.57)$$

From eqn (4.57)

$$\beta_{mn}d = \ell\pi \quad \text{for } \ell = 1,2,3,... \qquad (4.58)$$

The cutoff wavenumber from equation (4.55) is given by

$$k_{mn\ell} = \sqrt{\left(\frac{m\pi}{a}\right)^2 + \left(\frac{n\pi}{b}\right)^2 + \left(\frac{\ell\pi}{d}\right)^2} \qquad (4.59)$$

Using the results obtained above, the resonant frequency of the $TE_{mn\ell}$ and $TM_{mn\ell}$ is defined as

$$f_{mn\ell} = \frac{ck_{mn\ell}}{2\pi\sqrt{\mu_r\varepsilon_r}} = \frac{c}{2\pi\sqrt{\mu_r\varepsilon_r}}\sqrt{\left(\frac{m\pi}{a}\right)^2 + \left(\frac{n\pi}{b}\right)^2 + \left(\frac{\ell\pi}{d}\right)^2} \qquad (4.60)$$

4.4.1.1 Determination of the Q-factor for the $TE_{mn\ell}$ mode

Selecting the TE_{mn} mode of the rectangular waveguide shown in Fig 4.2, addition of positive and negative traveling waves for H_z gives [RWV 1994]

$$H_z = (A^+ e^{-j\beta_{mn}z} + A^- e^{j\beta_{mn}z}) \cos \frac{m\pi x}{a} \cos \frac{n\pi y}{b} \qquad (4.61)$$

Since the normal component of the magnetic field, H_z, must be zero at $z = 0$ and $z = d$, this condition implies that $A^+ = -A^-$ and $\beta d = \pi \ell$ with ℓ an integer. Thus equation (4.61) becomes

$$H_z = C \cos \frac{m\pi x}{a} \cos \frac{n\pi y}{b} \sin \frac{\ell\pi z}{d} \qquad (4.62)$$

with $C = -2jA$. Substituting eqn. (4.62) into the TE equations, the following equations results

$$E_y = C \sin \frac{m\pi x}{a} \cos \frac{n\pi y}{b} \sin \frac{\ell\pi z}{d} \qquad (4.63a)$$

$$H_x = \frac{-C\beta k_x}{k_c^2} Cos \frac{m\pi x}{a} \cos \frac{n\pi y}{b} \sin \frac{\ell\pi z}{d} \qquad (4.63b)$$

$$H_z = \frac{j\pi C}{k\eta a} \cos \frac{m\pi x}{a} \cos \frac{n\pi y}{b} \sin \frac{\ell\pi z}{d} \qquad (4.63c)$$

These equations indicate the existence of a standing wave in the cavity.

The Q-factor now can be computed using eqn (4.1) for the TE_{mn} mode by finding the stored electric and magnetic energies and power lost in the conducting walls and

dielectric. The stored electric energy, stored magnetic and the power loss in the conducting walls are given by Pozar [Po 1998-b] to be

$$W_e = \frac{\varepsilon}{4} \int_V E_y E_y^* dv \qquad (4.64a)$$

$$W_m = \frac{\mu}{4} \int_V (H_x H_x^* + H_z H_z^*) dv \qquad (4.64b)$$

$$P_\ell = \frac{R_s}{4} \int_V |H_t|^2 ds \qquad (4.64c)$$

where ε is the permittivity of the material, μ is the permeability and

$$R_s = \sqrt{\frac{\omega \mu_0}{2\sigma}} \qquad (4.65)$$

The Q-factor at resonance can be determined using equation (4.1).

4.4.2 The Cylindrical Cavity Resonator

A circular waveguide shorted at both ends is widely used as a cavity resonator. The configuration is shown in Fig. 4.3 where a is the radius of the circular cylindrical cavity and d is its length. The circular cavities are usually constructed with a movable top wall to allow the mechanical tuning of the resonant frequency.

Resonance occurs where d is a multiple $\frac{\lambda_g}{2}$. A circular guide is capable of propagating TE_{nm} and TM_{nm} waves. The cavity modes are denoted by TE_{nmp} and TM_{nmp}, where p represents the number of half wavelengths in the z direction. Field patterns for some of the cavity modes are shown in Rizzi [Ri 1988]. The theory presented below follows the theory set fourth by Pozar [Po 1998-b].

Since cylindrical geometry is involved, it is appropriate to employ cylindrical coordinates
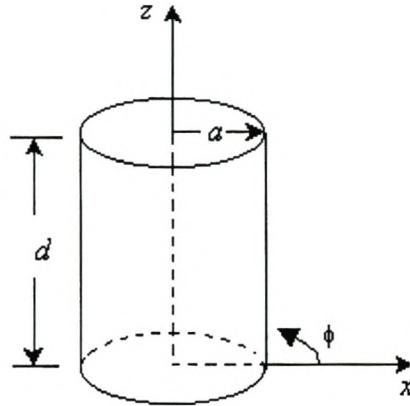

Figure 4.3 A cylindrical cavity resonator. (Diameter = D = 2a)

The transverse electric fields (E_ρ, E_ϕ) of the TE_{nm} and TM_{nm} modes for the circular waveguide are obtained from eqn. (4.54) to be

$$\overline{E}_t(\rho,\phi,z) = \overline{e}(\rho,\phi)[A^+ e^{-j\beta_{mn}z} + A^- e^{-j\beta_{mn}z}] \tag{4.66}$$

The propagation constants for the TE_{nm} and TM_{nm} mode are

$$\beta_{nm} = \sqrt{k^2 - \left(\frac{\rho'_{nm}}{a}\right)^2} \tag{4.67}$$

and

$$\beta_{nm} = \sqrt{k^2 - \left(\frac{\rho_{nm}}{a}\right)^2} \tag{4.68}$$

respectively, where ρ'_{nm} and ρ_{nm} are the mth roots of J'_{nm} and J_{nm}, and J_{nm} is the Bessel function of the first kind.

Applying the boundary conditions ($\overline{E}_t = 0$ at z = 0,d) to eqn. (4.66), the following result

$$A^+ = -A^- \text{ and } A^+ \sin \beta_{nm} d = 0 \tag{4.69}$$

Since the sine of π is equal to zero,

$$\beta_{nm} d = \pi\ell \quad \text{where } \ell = 0,1,2,3,..., \tag{4.70}$$

Thus, the resonant frequency of the $TE_{nm\ell}$ mode is

$$f_{nm\ell} = \frac{ck_{nm\ell}}{2\pi\sqrt{\mu_r\varepsilon_r}} = \frac{c}{2\pi\sqrt{\mu_r\varepsilon_r}}\sqrt{\left(\frac{\rho'_{nm}}{a}\right)^2 + \left(\frac{\ell\pi}{d}\right)^2} \tag{4.71}$$

where $k_{mn\ell}$ is the cut-off wavenumber for the cylindrical cavity, defined as:

$$k_{nm\ell} = \sqrt{\left(\frac{\rho'_{nm\ell}}{a}\right)^2 + \left(\frac{\ell\pi}{d}\right)^2} \tag{4.72}$$

Also, the resonant frequency for the $TM_{nm\ell}$ is given by:

$$f_{nm\ell} = \frac{ck_{nm\ell}}{2\pi\sqrt{\mu_r\varepsilon_r}} = \frac{c}{2\pi\sqrt{\mu_r\varepsilon_r}}\sqrt{\left(\frac{\rho_{nm}}{a}\right)^2 + \left(\frac{\ell\pi}{d}\right)^2} \tag{4.73}$$

From eqn. (4.71) and eqn. (4.73), the resonant frequency for any TE_{nm} and TM_{nm} mode propagating inside a cylindrical cavity can be determined.

4.4.2.1 Q-factor for the Cylindrical Cavity Resonator

It is assumed that the only mode propagating in the cylindrical cavity is the $TE_{nm\ell}$ mode. To determine the Q-factor of the $TE_{nm\ell}$ mode, the total energy stored and the power loss in the conducting walls of the cylindrical guide need to be determined. At resonance, the time average energy stored electric and magnetic energies stored are equal. The total energy is given be eqn (4.74)

$$W = W_e + W_m = \frac{\varepsilon}{2} \int_{z=0}^{d} \int_{\phi=0}^{2\pi} \int_{\rho=0}^{a} \left(|E_\rho|^2 + |E_\phi|^2 \right) \rho \, d\rho \, d\phi \, dz \qquad (4.74)$$

The fields of the $TE_{nm\ell}$ mode are [Po 1998-c]

$$E_\rho = \frac{jk\eta a^2 nH_0}{(p'_{nm})^2 \rho} J_n\left(\frac{p'_{nm}\rho}{a}\right) \sin n\phi \sin\frac{\ell\pi z}{d} \qquad (4.75a)$$

$$E_\phi = \frac{jk\eta aH_0}{(p'_{nm})} J'_n\left(\frac{p'_{nm}\rho}{a}\right) \cos n\phi \sin\frac{\ell\pi z}{d} \qquad (4.75b)$$

$$H_\rho = \frac{\beta aH_0}{p'_{nm}} J'_n(p'_{nm}\rho) \cos n\phi \cos\frac{\ell\pi z}{d} \qquad (4.75c)$$

$$H_\phi = \frac{-\beta a^2 nH_0}{(p'_{nm})^2 \rho} J'_n(p'_{nm}\rho) \sin n\phi \cos\frac{\ell\pi z}{d} \qquad (4.75d)$$

Substituting eqn. (4.75a) and eqn. (4.75b) into eqn. (4.74) and integrating will result in eqn (4.76)

$$W = W_m + W_e = 2W_e = \frac{\varepsilon k\eta^2 a^4 H_0^2 \pi d}{8(p'_{nm})^2}\left[1-(\frac{n}{p'_{nm}})^2\right]J_n^2(p'_{nm}) \qquad (4.76)$$

The power loss in the conducting walls is

$$P_\ell = \frac{R_s}{4} \int_V |H_t|^2 \, ds \qquad (4.77)$$

The Q-factor at resonance can thus be determined using equation (4.1)

4.5   Coaxial Line Resonators

A coaxial line consists of two conductors, where the inner conductor is at a certain potential, V_0, and the outer conductor is at a reference, say zero volts. The principal mode of propagation in a coaxial line is the TEM mode. There are, however, other ways in which electromagnetic energy can propagate along a coaxial line. These are called higher-order propagation modes. These higher-order modes can only propagate when the signal frequency exceeds a certain value. This value is known as the cutoff frequency of the mode and is denoted by f_c. When the frequency become so high that the wavelength is comparable with the distance between the conductors, other modes, of the kind found in hollow waveguides, exist. Fig. 4.4 shows two forms of coaxial line geometries. Fig. 4.4(a) shows a square coaxial line concentric with round inner conductor while Fig. 4.4(b) shows a circular coaxial line.


(a)   **(b)**
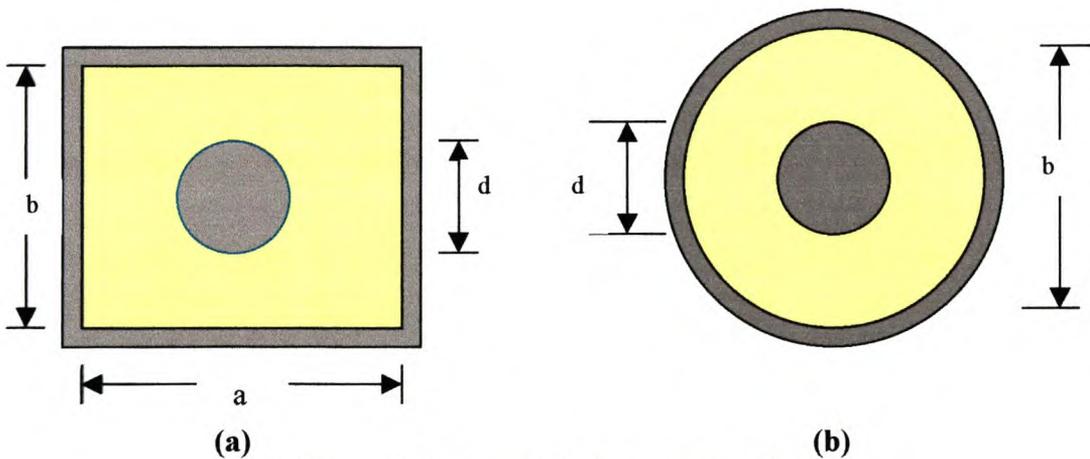
Figure 4.4   Coaxial line geometries

Hence, pure TEM mode propagation can only be assured if the dimensions of Fig 4.4(b) and the operating frequency are chosen to be such that the propagation wavelength, λ, obeys the following inequality [Gu 1972]

$$\lambda = \frac{\pi b}{2}\left(1 + \frac{d}{b}\right)$$
(4.78)

4.5.1 Rectangular Coaxial Line with Round Center Conductor

Fig. 4.5 shows a TEM coaxial line with a round inner conductor and a square outer conductor.
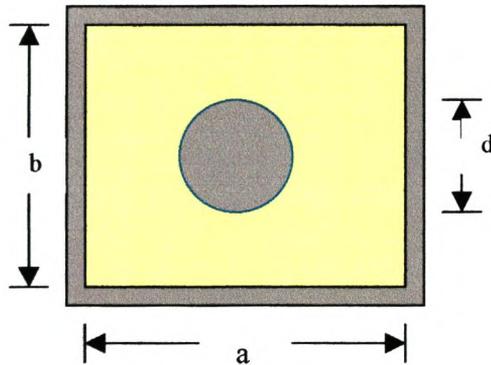
Figure 4.5   Square coaxial line concentric with round inner conductor

The characteristic impedance for the rectangular line with a round inner conductor is given by Lin [LIN 1985] as

$$Z_o = \sqrt{\frac{\mu}{\varepsilon}} \frac{\varepsilon}{C}$$
(4.79)

where C is the capacitance per unit length of the line given by

$$C = \frac{Q}{U_1}$$
(4.80)

Here Q is the charge per unit length and U_1 is the potential of the inner conductor given by

$$Q = 2\pi\varepsilon A \quad \text{and} \quad U_1 = A\ln\frac{R}{\rho} \tag{4.81}$$

Substituting eqn. (4.80) and eqn. (4.51) into eqn. (4.79), the following results

$$Z_o = \frac{1}{2\pi}\sqrt{\frac{\mu}{\varepsilon}}\ln\frac{R}{\rho} \tag{4.82}$$

with $\rho = \dfrac{d}{2}$ and the constant $R = (1.3211)^{\frac{1}{N}}\dfrac{b}{2}$. When $a = b$, eqn (4.82) becomes

$$Z_0 = 59.952\left(\ln\frac{b}{d} + \frac{0.27847}{N}\right) \tag{4.83}$$

where N is the number of sides of the outer conductor. For $N = 4$, eqn (4.83) becomes

$$Z_0 = 59.952\left(\ln\frac{b}{d} + 0.06962\right) \tag{4.84}$$

The impedance determined above is having a 1.5% error for $\dfrac{d}{b} < 0.80$.

Riblet [Ri 1983] re-examined the problem of determining the characteristic impedance of a concentric coaxial transmission line having a circular inner conductor and square outer conductor. The results were presented in terms of the outer "shield factor", R_{eff}, defined as the ratio of the diameter of an outer circle, having the same capacitance as the outer square, to the side of the outer square. This factor gives an error in the order of 0.02Ω for impedances greater than 3Ω. Fig 4.6 illustrates the definition of R_{eff}.

Given $\dfrac{d}{s}$, the characteristic impedance of the structure is given by eqn. (4.85)

$$Z_o = \frac{1}{2\pi}\sqrt{\frac{\mu}{\varepsilon}} \ln \frac{R_{eff} \times s}{d}$$

(4.85)

where s = b according to Fig. 4.5.
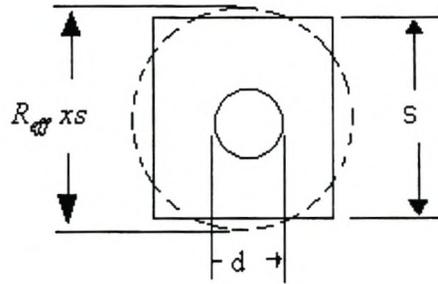
Figure 4.6   Illustration of R_{eff}

The attenuation constant, α, of a transmission line supporting a TEM mode is given by

$$\alpha = \frac{1.3273 \times 10^{-3}}{b} \frac{1}{\sigma\delta} \frac{\dfrac{b}{d} + f_N}{\ln\dfrac{b}{d} + \dfrac{0.27847}{4}}, \text{ neper/m}$$

(4.86)

where σ is the conductivity of the inner and outer conductors, δ is the skin depth and $f_N = 0.744186$ for $N = 4$.

The Quality factor for coaxial resonators is the same as that of transmission line resonators (eqn. (4.53)) and is given by

$$Q = \frac{\beta}{2\alpha}$$

(4.87)

where β is the propagation constant given by

$$\beta = \frac{2\pi}{\lambda} \qquad (4.88)$$

and λ is the wavelength of the line given by

$$\lambda = 2\ell \qquad (4.89)$$

Therefore, the quality factor is given by

$$Q = \frac{\pi}{2\alpha\ell} \qquad (4.90)$$

Using the results discussed above, the graph for the characteristic impedance versus the dimensions for the configuration shown in Fig. 4.5 can be obtained. This is illustrated in Fig. 4.7. The MATLAB code used to obtain this is given in Appendix B.3.

Also, the results discussed above can be used to show the effects of the line dimensions on the Q factor. This is illustrated in Fig. 4.8.
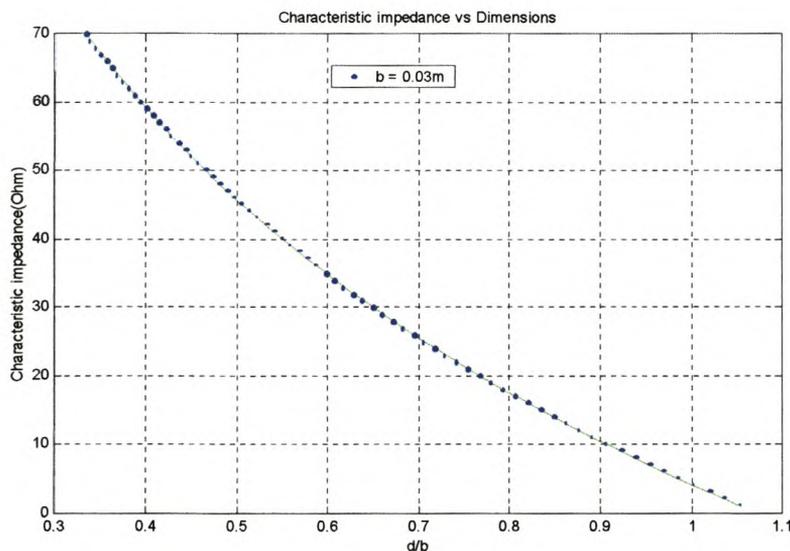

**Figure 4.7   The characteristic impedance as a function of the line parameters**

4-28
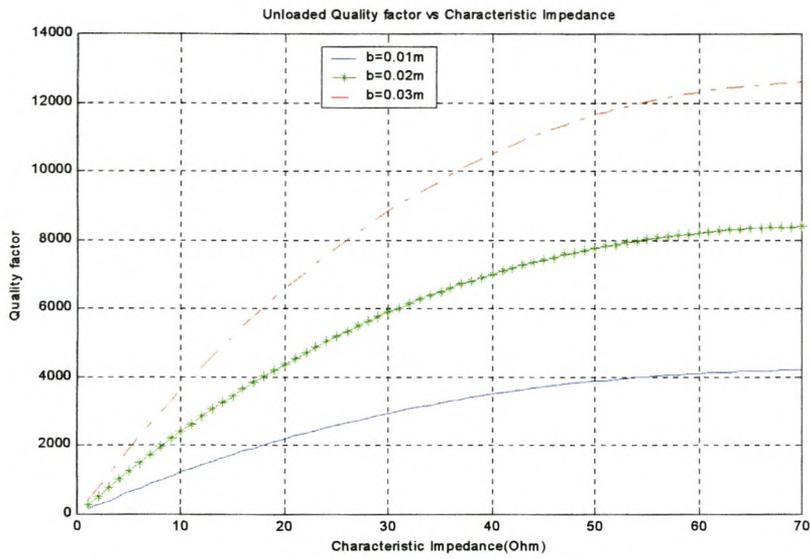
Figure 4.8 Effects of the line parameters on the Q factor

4.5.2 The Circular Coaxial Line

Fig. 4.9 shows the geometry of a coaxial line.
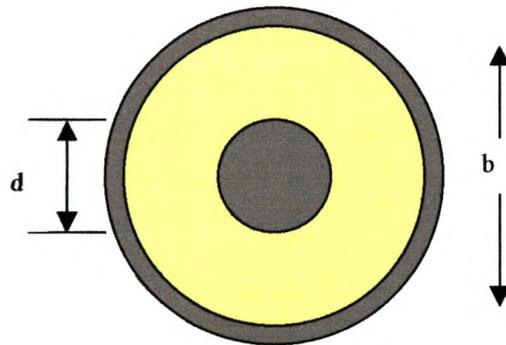
Figure 4.9   Coaxial line geometry

Gunston [Gu 1972] defines the characteristic impedance for the coaxial line as follows

$$Z_0 = \frac{1}{2\pi}\sqrt{\frac{\mu}{\varepsilon}}\ln\left(\frac{b}{d}\right) \tag{4.91}$$

where μ and ε are the magnetic permeability (H/m) and dielectric permittivity (F/m) of the insulating medium filling the space between the conductors, respectively.

The attenuation constant of the coaxial line supporting the TEM mode is given by Gunston [Gu 1972] as follows

$$\alpha = \frac{1}{2}\left(\frac{R}{Z_0} + GZ_0\right) \tag{4.92}$$

where R is the resistance due to finite conductivity of the conductors and G is the conductance due to dielectric loss in the material between the two conductors. R and G therefore represent loss and they are given by

$$R = \sqrt{\frac{f}{\pi}}\left(\frac{1}{b}\sqrt{\frac{\mu_b}{\sigma_b}} + \frac{1}{d}\sqrt{\frac{\mu_d}{\sigma_d}}\right) \tag{4.93}$$

and

$$G = \frac{2\pi}{1.8x10^{10}} \cdot \frac{\varepsilon_r f \tan\delta}{\ln\left(\dfrac{b}{d}\right)} \tag{4.94}$$

where f is the operating frequency, μ is the permeability of the medium, σ is the electrical conductivity of the conductors labelled by the subscripts "a" and "b" and $\tan\delta$ is the loss angle of the insulating medium.

The Q-factor for a $l = \dfrac{\lambda}{2}$ coaxial line resonator is given by

$$Q = \frac{\pi}{2\alpha\ell} \tag{4.95}$$

A code was written in Matlab (Appendix B.4) using the results obtained above to plot the graphs shown in Fig 4.8. The graph shown in Fig 4.10 can be used to calculate the characteristic impedance for any coaxial line with any dielectric filling.

Fig 4.11 shows the effects that the dimensions for the coaxial line have on the Q-factor. The operating frequency used is 3 GHz, length of the line $\ell = \frac{\lambda}{2}$ and aluminum conductivity.
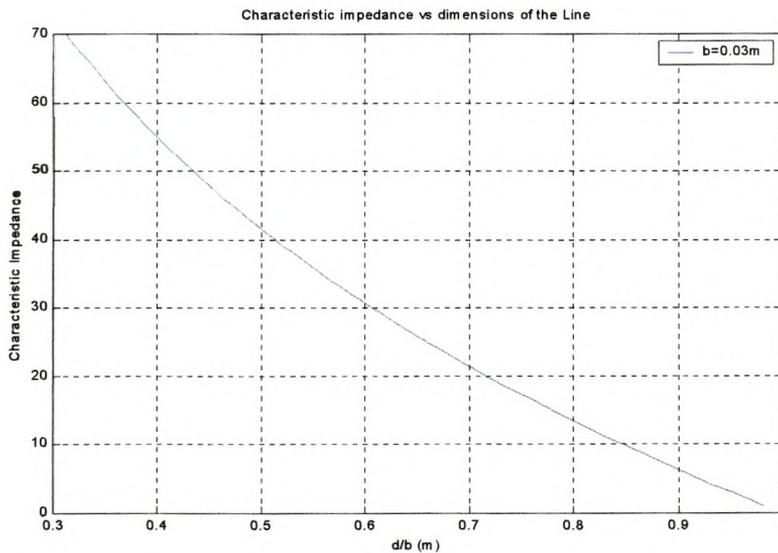

**Figure 4.10 Characteristic impedance of a circular coaxial line.**
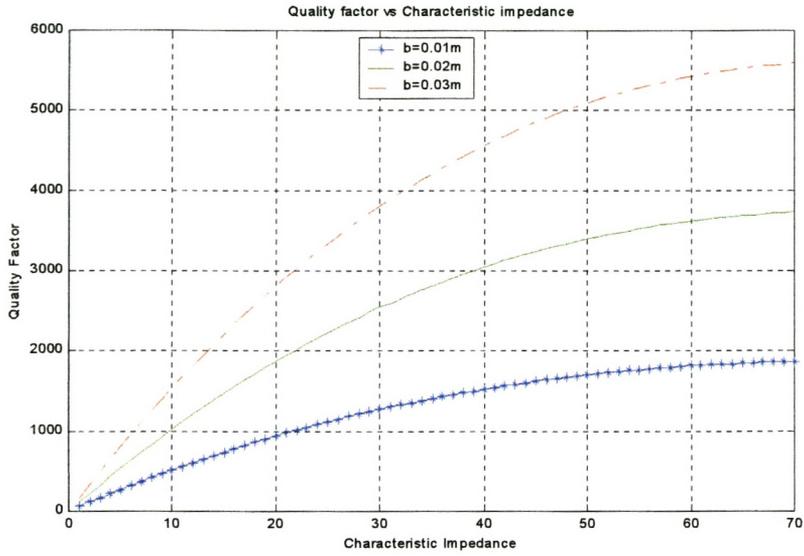
Figure 4.11 Effects of the line characteristic impedance on the Q-factor.

4.6 Resonator Perturbations

At resonance, average stored electric and magnetic energies are equal. If a small change of shape is made in resonator cavities, this will change one type of energy more than the other, and resonant frequency would then shift by an amount necessary to again equalize the energies. The perturbation theory [Pozar 1998-b] shows the amount of frequency shift when a small volume ΔV is removed from the resonator by pushing in the boundaries. The expression for a fractional change in resonant frequency is

$$\frac{\omega - \omega_0}{\omega_0} = \frac{\int_{v_0}(\mu|\overline{H}_0|^2 - \varepsilon|\overline{E}_0|^2)dv}{\int_{v_0}(\mu|\overline{H}_0|^2 + \varepsilon|\overline{E}_0|^2)dv} = \frac{\Delta W_m - \Delta W_e}{W_m + W_e} \qquad (4.96)$$

4.7 Insertion Loss

Insertion loss for a two-port system is defined by Rizzi [Ri 1988] as

$$L_I = 10 \ \log \left(\frac{P_{Lb}}{P_{La}} \right) dB \qquad (4.97)$$

where referring to Fig. 4.12, P_{Lb} is the power delivered to a specified load (Z_L) before inserting the network and P_{La} is the power delivered to the same load after insertion of the network.
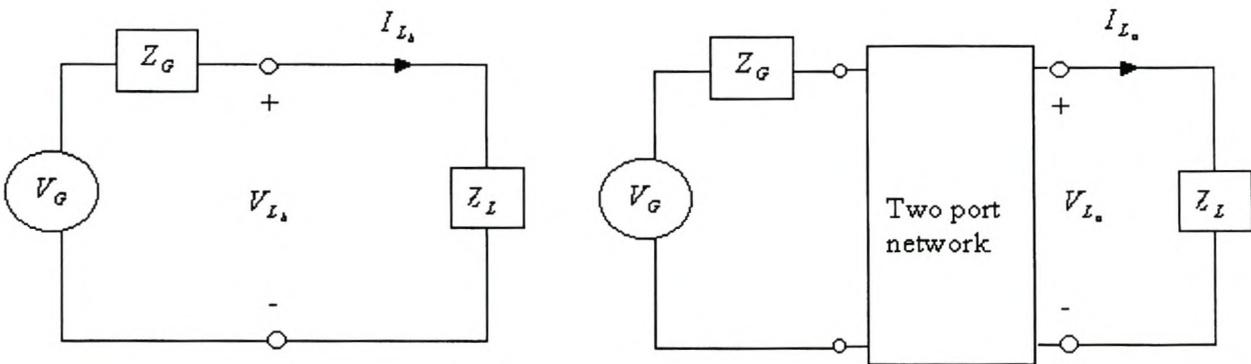

Figure 4.12 A description of the insertion loss and phase definition.

Since insertion loss is defined as a power ratio measured at the load (Z_L), eqn (4.97) can be expressed in terms of rms voltages as:

$$L_I = 20 \log \left(\frac{V_{Lb}}{V_{La}} \right) = 20 \times \log \left(\frac{1}{|S_{21}|} \right) \text{when} \, Z_G = Z_L \qquad (4.98)$$

where S_{21} is defined by eqn. (2.53) from Chapter 2 as follows

$$|S_{21}|^2 = 4\sqrt{\frac{R_G}{R_L}}\left|\frac{V_2}{E_G}\right|^2 \qquad\qquad (4.99)$$

Fig. 4.13 shows the Butterworth response for fourth-order band-pass filter losses. From this it can be seen that the insertion loss is inversely proportional to the Q-factor.
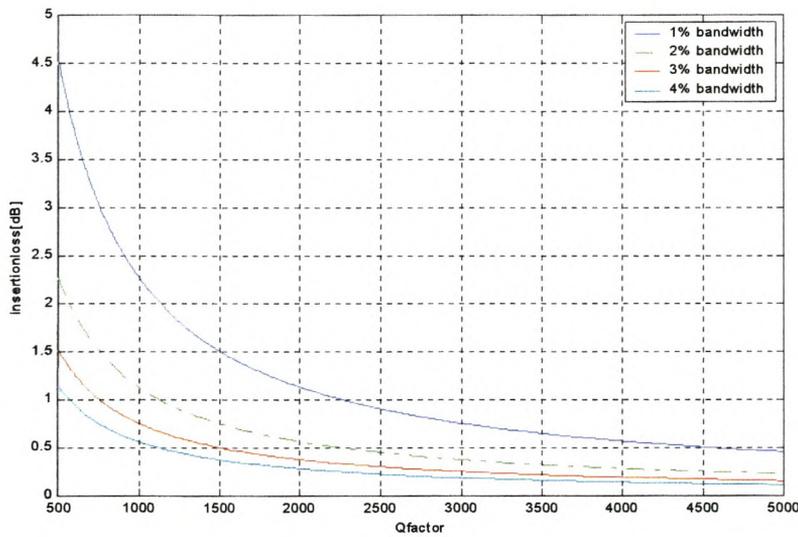

Figure 4.13 Butterworth response for fourth-order bandpass filter Losses at f_0

4.8 Resonator Transformation

The lumped series-resonant circuit of the series branch of the filter, is shown in Fig. 4.14(a). In ordinary distributed filter design, the resonant circuit is easily replaced by a one half wavelength resonator line as shown in Fig. 4.14(b)
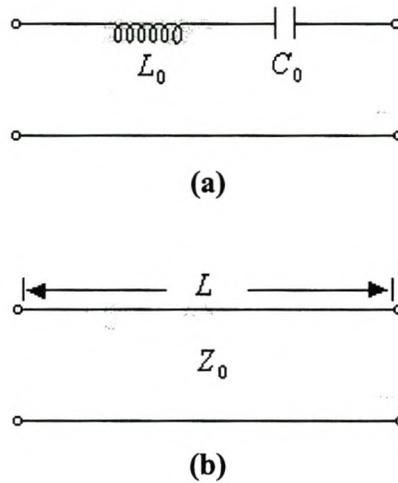

Figure 4.14 Transformation of *LC* resonator to distributed resonator

At the resonant frequency, ω_0, Inui [IN 1979] defines the relationship between the two circuits as follows

$$Z_0 = \frac{2\omega_0 L_0}{\pi}, L = \frac{\lambda_0}{2} \tag{4.100}$$

where L_0 is the inductance of lumped circuit, Z_0 is the characteristics impedance of the line, L is the physical length of the line and λ_0 is the wavelength in the medium of propagation at ω_0.

However the element given by eqn. (4.100) has the following problems

- The element size is somewhat large in the VHF range, due to long line length of $\frac{\lambda_0}{2}$.

- The element has repeating reactances at harmonic frequencies $((2n+1)\omega_0)$.

- The element has zero impedance at zero frequency.

With L_0, C_0 equals to unity and $\omega_0 = 1$, eqn. (4.100) becomes

$$Z_0 = \frac{2}{\pi} \qquad\qquad (4.101)$$

4.9 Conclusion

The rectangular coaxial resonator concentric with a circular conductor has a higher unloaded Q-factor compared with the circular coaxial resonator. Using these resonators, filters with lower insertion loss can be achieved.

In filter applications, identical resonators can be coupled to each other to yield coupled resonators as discussed in chapter 3. The basic coupling design for these resonators is discussed in chapter 5.

Chapter 5

Basic Coupling Design

5.1   Introduction

The determination of the electromagnetic that couples through a small aperture in a common wall between two regions is important in the design of coupled resonator filters. There are several methods that can be used to determine the coupling coefficient between two identical resonators, but only two of them are considered in this chapter.

The first method is based on Bethe's [Be 1944] theory and Cohn's [Co 1951 and Co 1952-a] experimental work. Bethe investigated the coupling through a small circular aperture in a common conducting plane wall of zero thickness and his solution utilizing equivalent electric and magnetic dipole moments has been extensively used in the design of coupled cavity and waveguide systems. Bethe's method of solution is applicable to small elliptical apertures as well as to circular apertures, but not to rectangles or more complicated geometrical shapes.

Since Bethe's theory only holds for very small apertures in walls of zero thickness, several correction factors were introduced to accomplish the effects of large apertures and non-zero wall-thickness. Cohn [Co 1951] gives a technique for accurately measuring the magnetic and electric polarizabilities of apertures and extensive magnetic polarizability data while similar data on electric polarizabilities are presented in Cohn [Co 1952-a].

The second method is based on the theory set fourth by Chang et al [CKZ 1991] and McDonald [Mc 1972]. From the knowledge of resonance frequencies determined using Ansoft Optimetrics, the coupling coefficient between two identical resonators can be determined.

Ansoft Optimetrics is an analytic tool that allows you to:

- Identify the basic design parameters that are to be varied during the simulation. These include the geometric parameters of the coupling cavity between two identical resonators, material properties and solution frequency.
- Specify the values to which each design parameter is set during the solution, generally by sweeping them through a range of values. This allows you to define a series of variations on the original structure, each of which will be solved during the parametric sweep.

The software then automatically sets the design parameters to the values that is specified, and computes the solution for each variation on the structure. After the parameter sweep is completed, the results can be analyzed the software post-processing functions.

In the preceding paragraphs, the introduction of coupling between two identical cavities was discussed without considering the means of injecting the electromagnetic energy into the resonator itself. The technique for exciting the cavity resonator was suggested by Wong [Wo 1979] and will be discussed in section 5.4.

5.2 Method Based on Bethe's theory and Cohn's experimental work

5.2.1 Fields Determination

Since the field distribution for the configuration shown in Fig. 5.1 is not fully available, field equations for a coaxial line were used to solve for these. Fig. 5.1(a) shows a 3D-view while Fig. 5.1(b) shows a cross cut in the x-z plane of Fig. 5.1(a). Consider a small rectangular aperture centered at the top of the broad wall of a waveguide. The TEM mode is assumed to be incident at $z < 0$ and the fields to be coupled to the next guide through the aperture can be computed in the following way. First, changing the position of the origin so that z = 0 will be at the center of the aperture, results to the following equations for the incident fields

$$E_r = \frac{E_0}{r} \sin \beta \left(z + L - \frac{1}{2} \Delta L \right)$$ (5.1)

$$H_\phi = \frac{H_0}{r} \cos \beta \left(z + L - \frac{1}{2} \Delta L \right)$$ (5.2)

only for $L = \frac{\lambda}{2}$. The excitation field at the center of the aperture (z = 0) is then

$$E_r = \frac{E_0}{r} \sin \left[\beta \left(L - \frac{1}{2} \Delta L \right) \right]$$ (5.3)

$$H_\phi = \frac{H_0}{r} \cos \left[\beta \left(L - \frac{1}{2} \Delta L \right) \right]$$ (5.4)
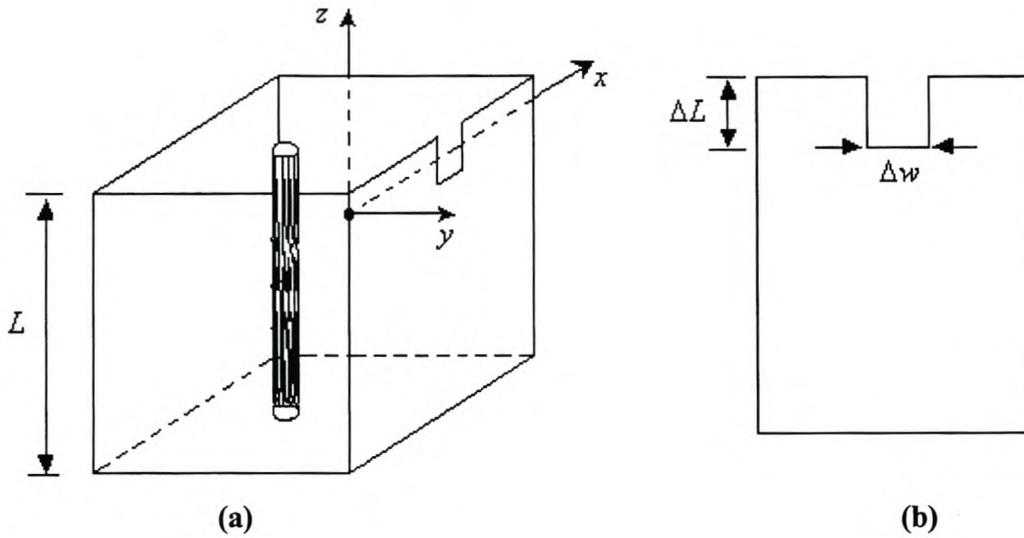
Figure 5.1 Rectangular coaxial line concentric with circular center conductor.

5.2.2 Aperture polarizability

The theory developed originally by Bethe for a circular aperture and later generalized by Collin [Co 1960], shows that if a field exists on one side of a conducting plane wall of zero thickness and a small aperture is cut in the wall, the field in the second region is the same as that from an electric dipole moment, P_e, normal to the wall and a magnetic dipole moment, M_m, tangential to the wall, both at the center of the aperture. The electric and magnetic dipole moments are given by McDonald [Mc 1972] to be

$$\mathbf{P}_e = \varepsilon_0 \mathbf{P}_0 E_n \qquad\qquad (5.5)$$

$$\mathbf{M}_m = \mathbf{M}_0 H_t \qquad\qquad (5.6)$$

where $\mathbf{P}_0$ and $\mathbf{M}_0$ are the electric and magnetic polarizabilities of a small aperture and E_n and H_t are the normal electric field and the tangential magnetic field vector, respectively. The magnitude of the dipole moments depends on the strength of the

tangential H-fields and normal E-fields. The polarizability of an aperture can be calculated analytically for simple geometries [AH 1983], but usually the design of slot apertures (rectangular, round ended and single or cross shaped) is conveniently done using Cohn's [Co 1951 and Co 1952-a] experimentally determined polarizabilities (P_0 and M_0). The graph for three different apertures is given in Fig. 5.2.
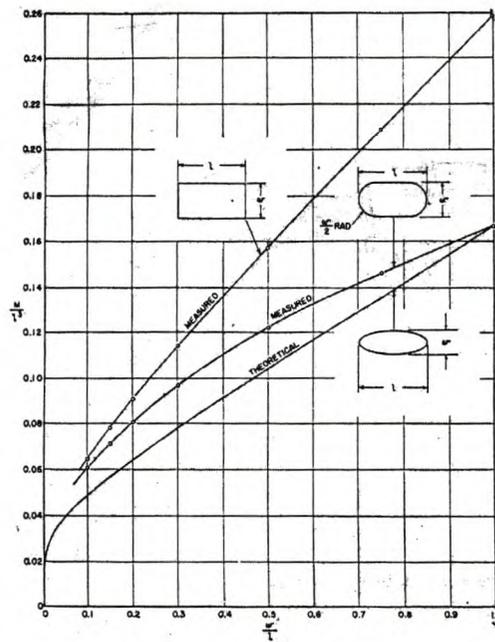

Figure 5.2 Magnetic polarizability of three different apertures

Since Bethe's theory only holds for very small apertures in walls of zero thickness, several correction factors were introduced to accomplish the effects of large apertures and non-zero wall-thickness. The aperture dimensions result from the corrected polarizabilities, which are derived from the true polarizabilities (M_0 and P_0) and the correction factors (c_1, c_2, c_3) for the real design case.

The first correction factor, c_1, concerns the influence of the iris resonance effect on the coupling and is determined by [Co 1952-b]:

$$c_1 = \frac{2f_r}{\pi f} \tan\left(\frac{\pi f}{2f_r}\right) \tag{5.7}$$

where f_r is the resonance frequency of the aperture given by

$$f_r = \frac{c}{2l}\sqrt{1 + \frac{4w^2}{\lambda_g^2}}, \tag{5.8}$$

where f is the frequency of operation, w is the width of the aperture and λ_g is the wavelength in the cavity. Also c is the phase velocity given by

$$c = \frac{1}{\sqrt{\mu\varepsilon}} \tag{5.9}$$

The correction factor for finite iris thickness, is [MYJ 1980]:

$$c_2 = 10^{\frac{2.73tA}{\lambda_c}\sqrt{1-\frac{\lambda_c}{\lambda}}} \tag{5.10}$$

where A is an empirical constant determined from the case of a round aperture. For a rectangular aperture of length l in an iris with a thickness t, A is about 3 if $t \prec 0.02l$. A decreases as t becomes larger. Also, λ_c is the free space wavelength at the cutoff frequency for the lowest order mode in a waveguide that has the same cross section as the aperture.

A third correction factor is added for the effect of the variation of field strength over the iris [Le 1980].

$$c_3(H_t) = \frac{\int_l |H_t|^2 . dx}{|H_{t\,max}|^2 . l} \tag{5.11}$$

Therefore, the corrected polarizabilities becomes

$$P = c_1 c_2 c_3 P_0 \tag{5.12}$$

$$M = c_1 c_2 c_3 M_0 \tag{5.13}$$

5.2.3 Coefficient of Coupling

The aperture polarizability concept is applied to the coupling between two lossless, symmetrical oriented, identical resonant cavities coupled by a rectangular aperture in a plane common wall as shown in Fig. 5.3. The most general equation relating the coupling coefficient, k, between two identical cavities connected by an aperture in a common wall is given by Rosenberg [UBR 1993]:

$$k = \frac{\text{Energy lost through aperture per cycle}}{2 \times \text{Energy stored by degeneracy}} \tag{5.14}$$

The term above is derived from Bethe's theory and the denominator is the total energy stored in the resonator. Eqn. (5.14) can now be written as [Mc 1974]

$$k = M \frac{|H_t|^2}{\iiint |H|^2 \, dv} + P \frac{|E_n|^2}{\iiint |E|^2 \, dv} \tag{5.15}$$

Eqn. (5.15) shows how the coupling coefficient is related to the electric and magnetic polarizabilities. The first term in equation (5.15) represent the magnetic coupling which is accomplished by tangential H-field coupling in the aperture and the second term is the electric field coupling which is accomplished by normal E-field coupling through the

aperture. The normalizing integrations in the denominators of equation (5.15) are over the volume v of one cavity.
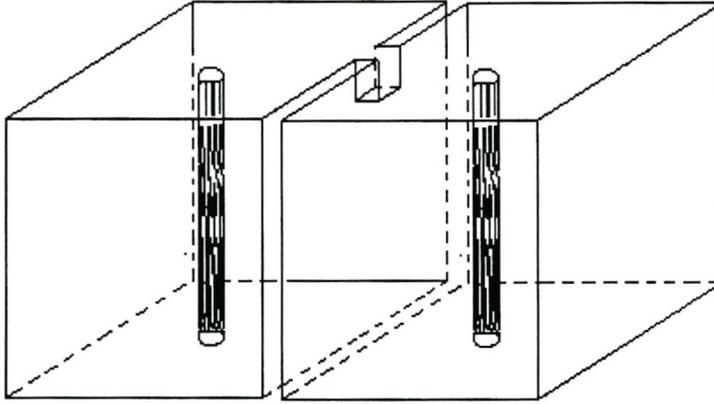

Figure 5.3 Two identical cavities coupled by a rectangular aperture.

5.3 Iris Design with Ansoft Optimetrics

Another formulation of the coupling coefficient is proposed by Chang et al [CKZ 1991] and MacDonald [Mc 1972]. Two identical resonant cavities coupled by a small aperture in a plane common wall are shown in Fig .5.4. The interior of each half of the structure is divided into two regions, a cavity region and an aperture region, by a plane surface s. The aperture region and the cavity region are uniformly filled with air (i.e., μ_0, ε_0)
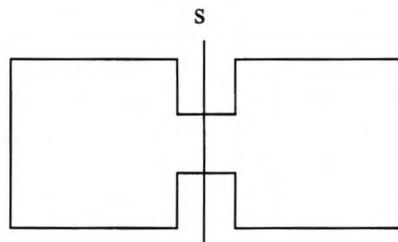

Figure 5.4 Two identical cavities coupled by an aperture in a plane common wall

The two cavities coupled by the small aperture will exhibit the behavior of two lightly coupled identical resonant circuits, for which a general representation is given in Fig. 5.4.
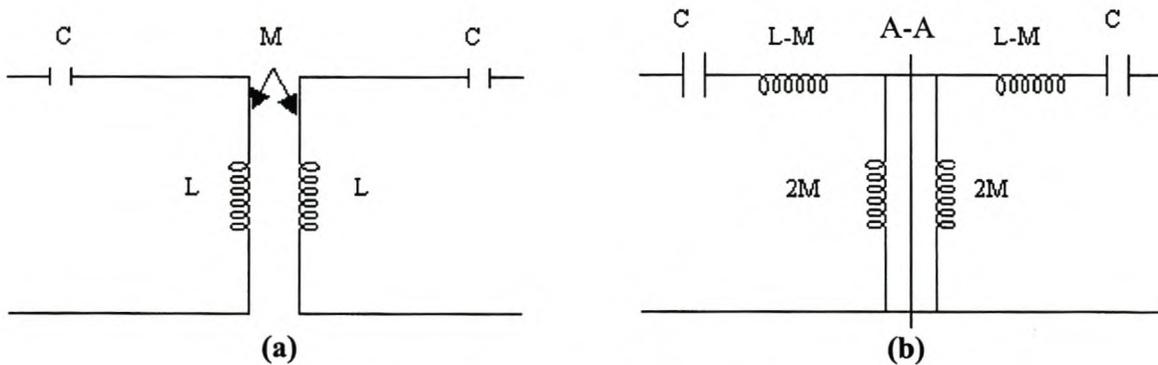

Figure 5.5 Equivalent circuit of coupling structure

A coupled cavity structure such as that in Fig. 5.4 has two oscillation states for each cavity resonance. One state corresponds to an electric wall boundary condition on the

symmetry plane in Fig. 5.4 or a short circuit on the symmetry line A-A of Fig. 5.5(b). The resulting circuit is shown in Fig. 5.6.
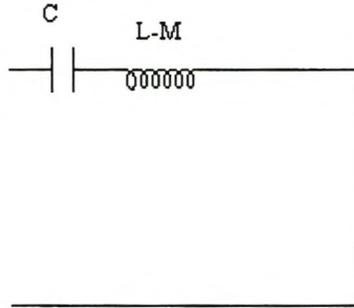
Figure 5.6 Circuit resulting by placing an electrical wall boundary

The other oscillation state corresponds to a magnetic wall boundary condition on the symmetry plane on Fig. 5.4 or an open circuit on the symmetry line A-A in Fig. 5.5(b) resulting in the circuit shown in Fig. 5.7.
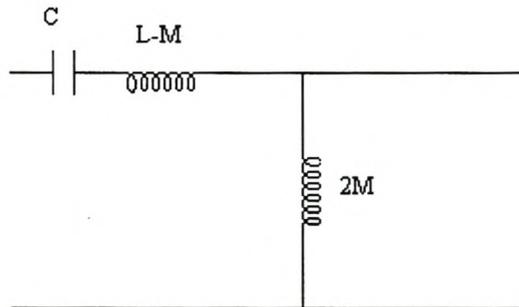
Figure 5.7 Circuit resulting from placing a magnetic wall boundary

From the theory of transformers, the coupling between two resonators is:

$$k = \frac{M}{\sqrt{L_i L_j}} = \frac{M}{L_T} \qquad (5.15)$$

5-10

where M is the coupling coefficient between the cavities and L_T is the total inductance of the circuit. From the symmetry of the structure, it is possible to calculate M from knowledge of the resonant frequencies f_e, corresponding to Fig. 5.6 and f_m, corresponding to Fig. 5.7. Here f_e and f_m represent the resonant frequencies assuming the plane A-A to be a perfect electric conductor (PEC) and a perfect magnetic conductor (PMC), respectively.

At resonance, the radian frequency, w_0 (eqn. 4.48), is given by

$$w_0 = \frac{1}{\sqrt{LC}} \tag{5.16}$$

Substituting $w_0 = 2\pi f_0$ into eqn. (5.16) gives

$$f_0 = \frac{1}{2\pi\sqrt{LC}} \tag{5.17}$$

where f_0 is the resonant frequency. Using eqn. (5.17), the resonant frequencies f_e and f_m corresponding to Fig.5.6 and Fig.5.7 respectively, are obtained to be

$$f_e^2 = \frac{1}{4\pi^2 C(L-M)} \tag{5.18}$$

$$f_m^2 = \frac{1}{4\pi^2 C(L+M)} \tag{5.19}$$

Substituting eqn. (5.15) into eqn. (5.18) and eqn. (5.19), the following equations results

$$f_e^2 = \frac{1}{4\pi^2 C(1-k)L} \tag{5.20}$$

$$f_m^2 = \frac{1}{4\pi^2 C(1+k)L} \tag{5.21}$$

From eqn. (5.20),

$$\frac{1}{4\pi^2 LC} = (1-k)f_e^2 \tag{5.22}$$

Substituting eqn. (5.22) into eqn. (5.21) result in the following equation

$$f_m^2 = \frac{(1-k)f_e^2}{(1+k)} \tag{5.23}$$

Then from eqn. (5.23), the coefficient of coupling is obtained to be

$$k = \frac{f_e^2 - f_m^2}{f_e^2 + f_m^2} \tag{5.24}$$

By placing a PEC or a PMC in the midway plane of the coupling waveguide, only half of the structure, shown in Fig. 5.4, needs to be analyzed. The Ansoft Optimetrics software can be used to analyze half of the structure shown in Fig.5.4, i.e., to calculate f_e (with the PEC at the center) and f_m (with the PMC at the center). An Ansoft Optimetrics procedure for determining these resonant frequencies is given in Appendix A. Then eqn. (5.24) is used to obtain the coupling coefficient, k.

To achieve unequal couplings, three cavity parameters (i.e., the height, width, and length of the coupling cavity) can be varied.

5.4 Tap Point Design

The purpose of designing a tap point position is to match the input impedance of the generator with the filter characteristic impedance. This will yield the maximum transfer of power from the source to the filter itself. The theory presented follows the theory set fourth by Wong [Wo 1979]. The schematic diagrams of the two common types of tapped-line filters are depicted in Fig. 5.8.

Fig. 5.8 (a) shows a series of n identical resonators, which are parallel, coupled to one another, short circuited at one end and are called interdigital filters.

The resonators shown in Fig. 5.8(b) are short circuited on both ends and they are called combline filters.


(a)

(b)
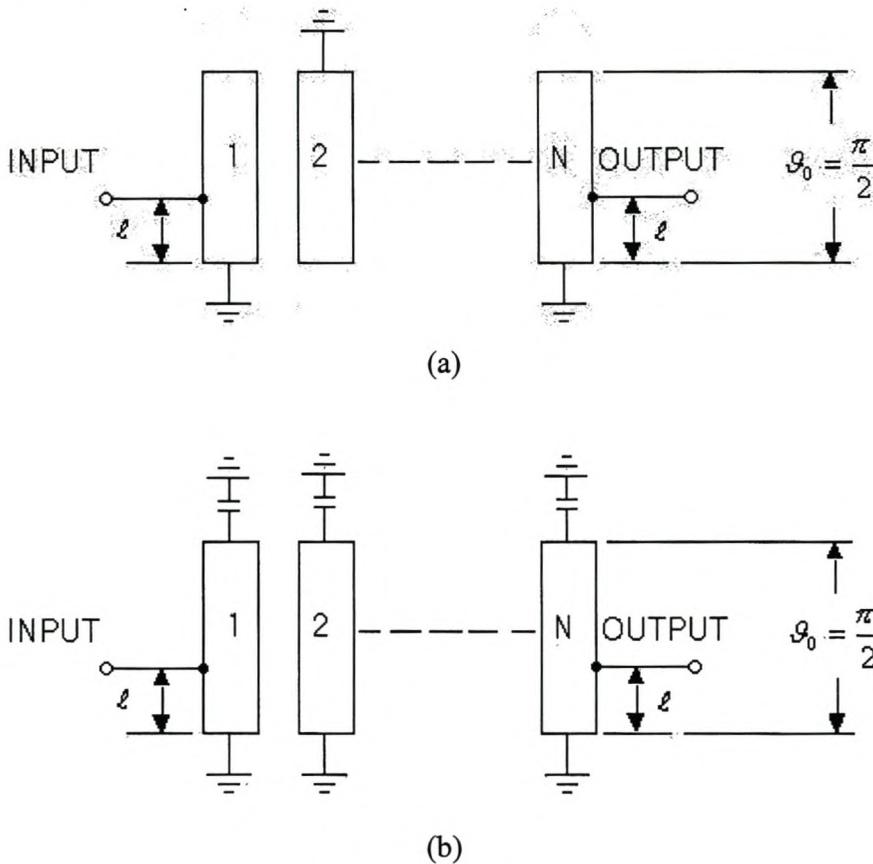
Figure 5.8 Tapped-line resonators

In order to design the tap point position, the following parameters are required:

- The single loaded Q-factor, Q_s, of the first resonator and the last resonator,
- The characteristic impedance, Z_0.

Once these parameters are known, the tap point $\dfrac{\ell}{L}$ can be calculated from

$$\frac{Q_s}{\dfrac{R}{Z_0}} = \frac{\pi}{4\sin^2\left(\dfrac{\pi\ell}{2L}\right)} \tag{5.25}$$

where R is the generator impedance and Z_0 is the characteristic impedance of the filter.

5.5 Conclusion

One problem that has not been addressed is coupling between dissimilar cavities. Both techniques described above assume identical cavities, which is a restriction placed on the filter by the equivalent circuit given in Chapter 3. Investigation into this problem is currently underway and could further reduce the size and weight of coupled resonator filters.

Chapter 6

Design and Measurement of a 4th-Order band-pass Butterworth filter

6.1 Introduction

The foregoing sections of the thesis discussed the design of coupled cavity filters. This section illustrates this theory through an example of a 4th-order Butterworth filter.

6.2 Design Specifications

The design specification is summarized in Table 6.1.

Table 6.1   Design Specifications for coupled cavity band-pass filter

Filter Response	4th-order Butterworth filter
Center frequency Ω_0	3 GHz
Bandwidth	2%
Insertion loss	0.5 dB
Q-factor	2500
Waveguide	Rectangular Coaxial line with circular Center conductor

6.3 Design Procedure

The design procedure for a coupled cavity filter is in essence the determination of the coupling matrix and the dimensions of the cavities and the coupling irises coupling them. Determination of the cavity dimensions depends on the center frequency and the Q-factor, while the dimensions of the coupling irises depend on the coupling coefficient between these cavities.

A design procedure for a coupled cavity filter follows the following steps:

- Coupling matrix synthesis.
- Determination of the Tap point position.
- Determination of the cavity dimensions.
- Determination of the coupling irises dimensions.

Each of these steps will now be discussed in more details.

6.3.1 Coupling Matrix Synthesis

The determination of the coupling matrix follows the Darlington's method stated in Chapter 3 (section 3.4.1). A 4th-order filter consists of four identical resonators, excited with a single-mode. An equivalent circuit for a fourth order low-pass filter with the direct coupling is shown in Fig. 6.1.
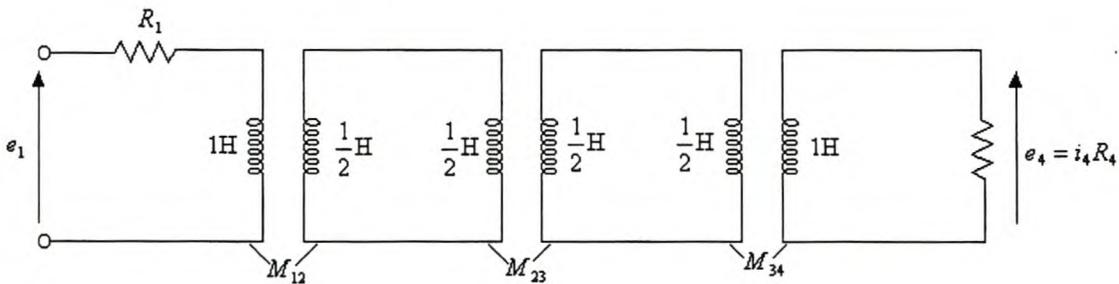

Figure 6.1 Equivalent 4th- order low-pass filter

The Butterworth filter low-pass characteristics magnitude is defined in Section 2.7.2.1 of Chapter 2 as follows

$$|H(j\omega)|^2 = \frac{1}{1+\omega^{2n}}$$ (6.1)

where n is the order of the filter. With the substitution of $\omega = s/j$ into eqn. (6.1), eqn. (6.2) results

$$|H(s)|^2 = \frac{1}{1+(-s^2)^n}$$ (6.2)

For a fourth-order filter $(n = 4)$, eqn (6.2) becomes

$$|H(s)|^2 = \frac{1}{1+s^8}$$ (6.3)

Using the method discussed in Section 2.7.2.2 to solve for the poles of eqn. (6.3), yields the following equation

$$|H(s)|^2 = \frac{1}{s^4 + 2.6131s^3 + 3.414214s^2 + 2.613126s + 1}$$ (6.4)

After obtaining eqn. (6.4), the Darlington's method, which is discussed in Section 3.4.1, is used to obtain the admittance parameters. The transfer polynomials are obtained to be

$$S_{21}(s) = \frac{P(s)}{E(s)} = \frac{1}{s^4 + 2.6131s^3 + 3.414214s^2 + 2.613126s + 1}$$ (6.5)

where $P(s) = 1$ and

$$E(s) = s^4 + 2.6131s^3 + 3.414214s^2 + 2.613126s + 1$$ (6.6)

From $E(s)$, R_1 and R_n are extracted according to eqn. (3.29) as

$$R_1 = R_n = \frac{2.6131}{2} = 1.31\Omega \tag{6.7}$$

The reflection polynomials, $E(s)$ and $F(s)$, are obtained to be

$$S_{11}(s) = \frac{F(s)}{E(s)} = \frac{s^4}{s^4 + 2.6131s^3 + 3.4142s^2 + 2.6131s + 1} \tag{6.8}$$

The input impedance for the double terminated network (Fig. 6.1) is

$$
\begin{aligned}
Z_{in}(s) &= R_1 \frac{S_{11den}(s) - S_{11num}(s)}{S_{11den}(s) + S_{11num}(s)} \\
&= \frac{2s^4 + 2.6131s^3 + 3.4142s^2 + 2.6131s + 1}{2.6131s^3 + 3.4142s^2 + 2.6131s + 1}
\end{aligned}
\tag{6.9}
$$

Subsequently the admittance parameters for n even are

$$
\begin{aligned}
y_{22}(s) &= \frac{1}{R_1} \frac{Z_n^o}{Z_n^e} \\
&= \frac{2.6131s^3 + 2.6131s}{2s^4 + 3.4142s^2 + 1}
\end{aligned}
\tag{6.10a}
$$

$$
\begin{aligned}
y_{21}(s) &= \frac{1}{R_1} \frac{P(s)}{Z_n^e} \\
&= \frac{1}{2s^4 + 3.4142s^2 + 1}
\end{aligned}
\tag{6.10b}
$$

The partial fraction expansion required by eqn. (3.19) and eqn. (3.20) yield the following:

$$
\begin{aligned}
K_{22}^1 &= 0.2266 & \lambda_1 &= 1.1540j \\
K_{22}^2 &= 0.2266 & \lambda_2 &= -1.1540j \\
K_{22}^3 &= 0.4267 & \lambda_3 &= 0.6128j \\
K_{22}^4 &= 0.4267 & \lambda_4 &= 0.6128j
\end{aligned}
\tag{6.11a}
$$

and

$$
\begin{aligned}
K_{21}^1 &= -0.2266 & \lambda_1 &= 1.1540j \\
K_{21}^2 &= 0.2266 & \lambda_2 &= -1.1540j \\
K_{21}^3 &= -0.4267 & \lambda_3 &= 0.6128j \\
K_{21}^4 &= 0.4267 & \lambda_4 &= -0.6128j
\end{aligned}
\tag{6.11b}
$$

The first and the last rows of the full T-matrix are

$$
\begin{aligned}
T_1 &= \begin{bmatrix} -0.4164 & 0.4164 & 0.5715 & -0.5715 \end{bmatrix} \\
T_4 &= \begin{bmatrix} -0.4164 & 0.4164 & 0.5715 & 0.5715 \end{bmatrix}
\end{aligned}
\tag{6.12}
$$

The other rows for the full T – matrix are found from the Gram-Schmidt orthonormalisation process with any two linearly independent unit vectors. In this section [1, 0, 0, 0] and [0, 1, 0, 0] are used to form the general transformation matrix

$$
T = \begin{bmatrix}
-0.4164 & 0.4164 & 0.5715 & -0.5715 \\
0.8082 & 0.0000 & 0.0000 & -0.5889 \\
0.0000 & 0.8082 & -0.5889 & 0.0000 \\
-0.4164 & 0.4164 & 0.5715 & 0.5715
\end{bmatrix}
\tag{6.13}
$$

From eqn. (6.13) the full coupling matrix is determined to be

$$
M = \begin{bmatrix}
0.0000 & 0.5946 & 0.5946 & 0.0000 \\
0.5946 & -0.5412 & 0.0000 & -0.5946 \\
0.5946 & 0.0000 & 0.5412 & 0.5946 \\
0.0000 & -0.5946 & 0.5946 & 0.0000
\end{bmatrix}
\tag{6.14}
$$

Usually all coupling elements M_{ij} are non-zero. It can be seen that the coupling matrix obtained in eqn. (6.14) cannot be realized by the network shown in Fig. 6.1. Further steps needs to be taken to ensure the realization of the coupling matrix by Fig. 6.1. This can be accomplished by using the coupling matrix reduction method given in Section 3.5. The rotation matrix, which can be applied in this case, is given below

$$R = \begin{bmatrix} 0 & 0 & 0 & 0 \\ 0 & c_r & s_r & 0 \\ 0 & -s_r & c_r & 0 \\ 0 & 0 & 0 & 0 \end{bmatrix} \qquad (6.15)$$

where c_r and s_r can be determined from the following equations

$$c_r = \cos\theta_r$$
$$s_r = \sin\theta_r \qquad (6.16)$$

with

$$\theta_r = \tan^{-1}\left(\frac{M_{13}}{M_{12}}\right) \qquad (6.17)$$

The reduced coupling matrix, M_r, is given by eqn. (6.18)

$$M_r = \begin{bmatrix} 0 & 0.8409 & 0.0000 & -0.0000 \\ 0.8409 & -0.0000 & 0.5412 & -0.0000 \\ 0.0000 & 0.5412 & 0.0000 & 0.8409 \\ 0 & -0.0000 & 0.8409 & 0 \end{bmatrix} \qquad (6.18)$$

The equivalent 4th-order filter shown in Fig. 6.1 needs to be bandwidth scaled and impedance scaled to the 2% bandwidth. This yields the circuit shown in Fig. 6.2.
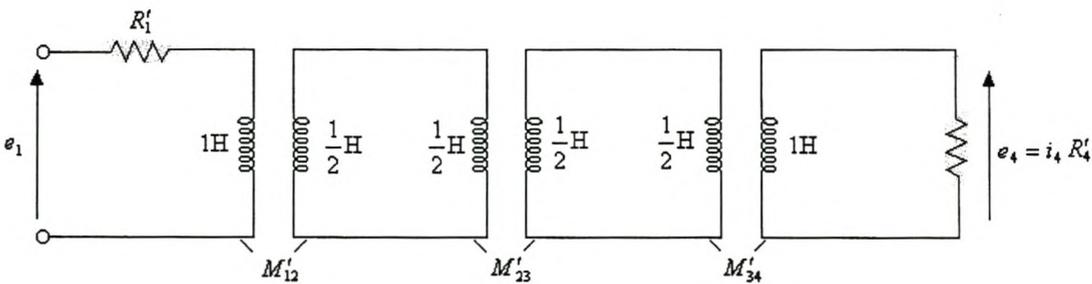

Figure 6.2 Bandwidth Scaling and Impedance Scaling

where

$$R_1' = R_4' = BR_1 = BR_4 = 0.0262, \qquad (6.19)$$

M_{12}', M_{23}' and M_{34}' are given by eqn. (6.20)

$$M' = \begin{bmatrix} 0.0000 & 0.0168 & 0.0000 & -0.0000 \\ 0.0168 & -0.0000 & 0.0108 & -0.0000 \\ 0.0000 & 0.0108 & 0.0000 & 0.0168 \\ 0.0000 & -0.0000 & 0.0168 & 0.0000 \end{bmatrix} \qquad (6.20)$$

Applying the low-pass to band-pass transformation discussed in Section 2.8.2 to Fig. 6.2 result to the circuit shown in Fig. 6.3.
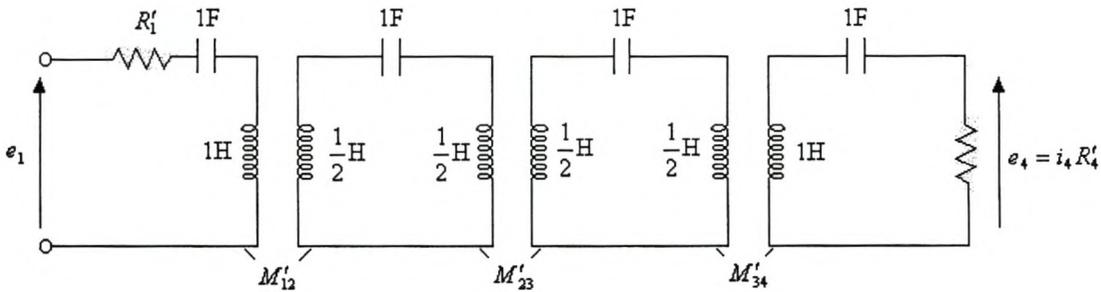

Figure 6.3 An equivalent fourth-order band-pass filter

However, the circuit shown in Fig. 6.3 above can be transformed into an ordinary distributed filter shown in Fig. 6.4 as discussed in Section 4.8.
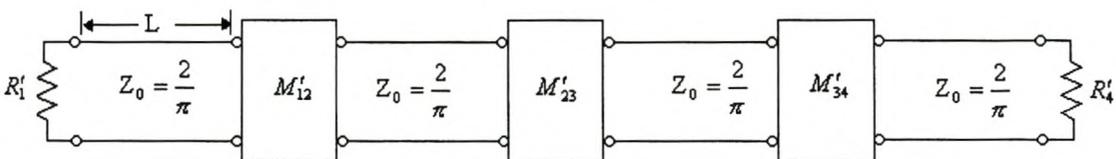

Figure 6.4 Distributed filter representation.

The comparison between the response of the lumped element fourth-order Butterworth band-pass filter and an equivalent distributed filter response is shown in Fig. 6.5.
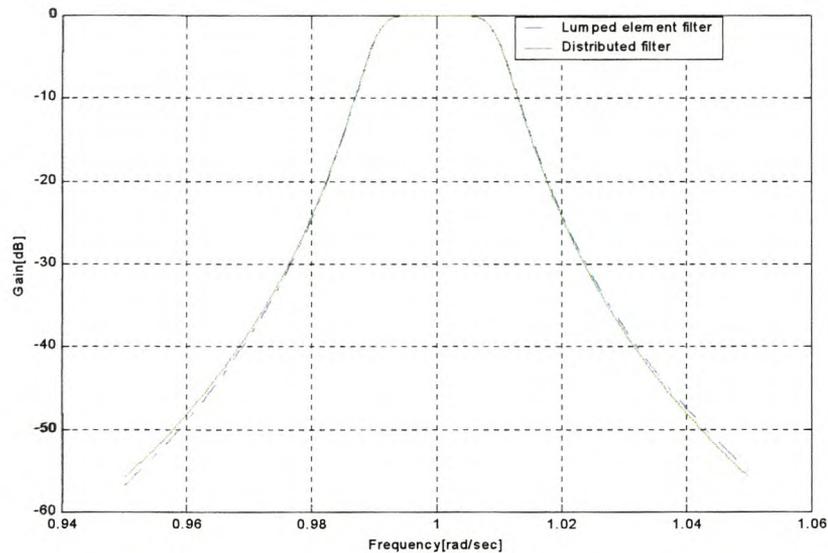
Figure 6.5 Comparison between lumped and distributed filter response.

From Fig. 6.5, the response of the lumped element filter and distributed filter are symmetrical over the entire pass-band. Hence, a lumped element filter can be transformed into a distributed element filter.

6.3.2 Determination of the Tap point position

The tap point position must be determined such that the filter input impedance is matched to the source impedance.

A distributed filter circuit that is used for the determination of the tap point position is shown in Fig. 6.6.
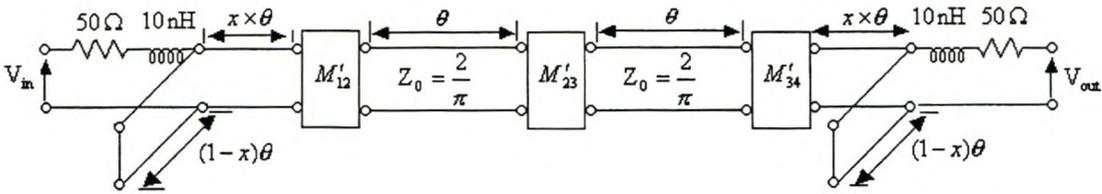
Figure 6.6 Representation of the Tap point position.

Here, θ is the electrical length given by

$$\theta = \beta L = \frac{2\pi}{\lambda}\frac{\lambda_0}{2} = \omega\pi,$$ (6.21)

L is the physical length of the cavities, ℓ from Fig. 5.8 is the position of the tap point from the bottom of the cavity to the center and x is the ratio of this position to the physical length of the cavities, $\dfrac{\ell}{L}$, given by

$$\frac{\ell}{L} = x = 0.0556$$ (6.22)

The comparison (ratio to the physical length) between the distributed filter response without the tap point position and with the tap point position is shown in Figure 6.7.
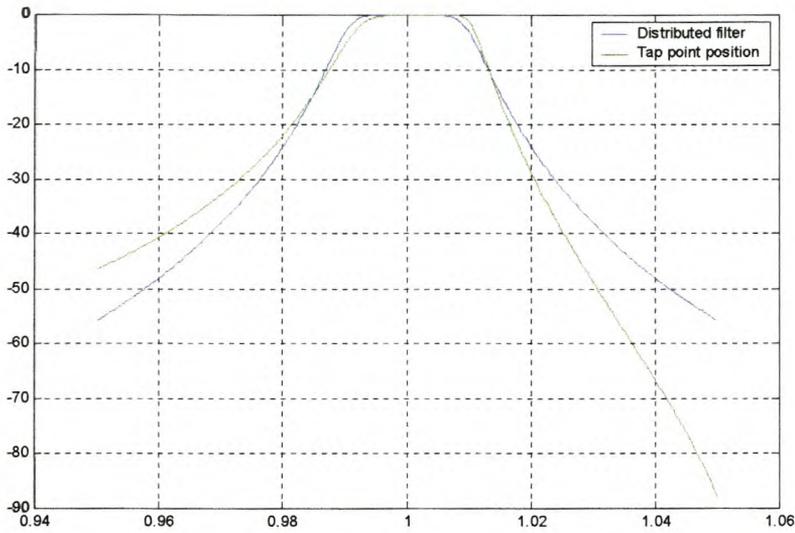
Figure 6.7 Tap point position response.

From Figure 6.7, it is seen that the distributed filter with $\dfrac{\ell}{L}$ suppresses higher frequencies more than the distributed filter without $\dfrac{\ell}{L}$. Their response compares well in terms of the center frequency.

6.3.3 Determination of the cavity dimensions

Since the equivalent circuit analyzed in the previous section consists of four identical resonators, each resonator will be replaced with a waveguide structure shown in Fig. 6.8. Fig. 6.8(a) shows a 3D-view, while Fig. 6.8(b) shows the top view of Fig. 6.8(a).

(a)   **(b)**
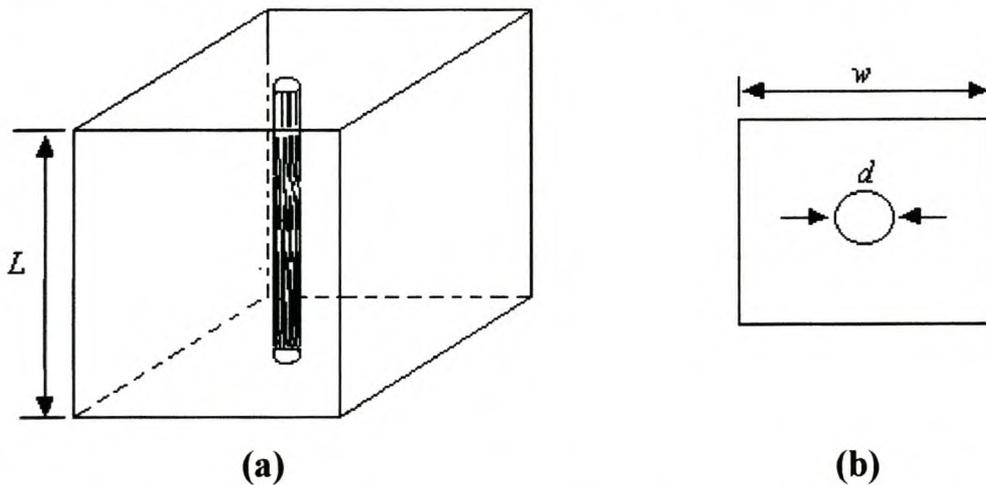
Figure 6.8 Square coaxial line concentric with round inner conductor.

Table 6.3.3 shows the cavity dimensions that are obtained using the theory set fourth in section 4.5.1 with a characteristic impedance of 70Ω used.

**Table 6.3.3 Cavity dimensions.**

Length(L)	Width(w)	Diameter(d)
50mm	30mm	10mm

6.3.4 Determination of coupling iris dimensions

The 4th-order Butterworth filter have been analyzed on the basis of an equivalent circuit shown in the previous sections, i.e., on the basis of the parameters R, Z_0, $\dfrac{\ell}{L}$, M_{12}, M_{23} and M_{34}. It is now necessary to design the coupling slot between the first and the second cavities, the second and third cavities and finally the third and fourth cavities that will reproduce the parameters M_{12}, M_{23} and M_{34}.

The coupling parameters can be produced by cutting a rectangular aperture on the broad wall of each waveguide structure as shown in Fig. 6.9. Fig 6.9(a) shows the 3D-view while Fig. 6.9(b) and Fig. 6.9(c) shows a top-view and side view cut of Fig. 6.9(a), respectively.


(a)   **(b)**   **(c)**
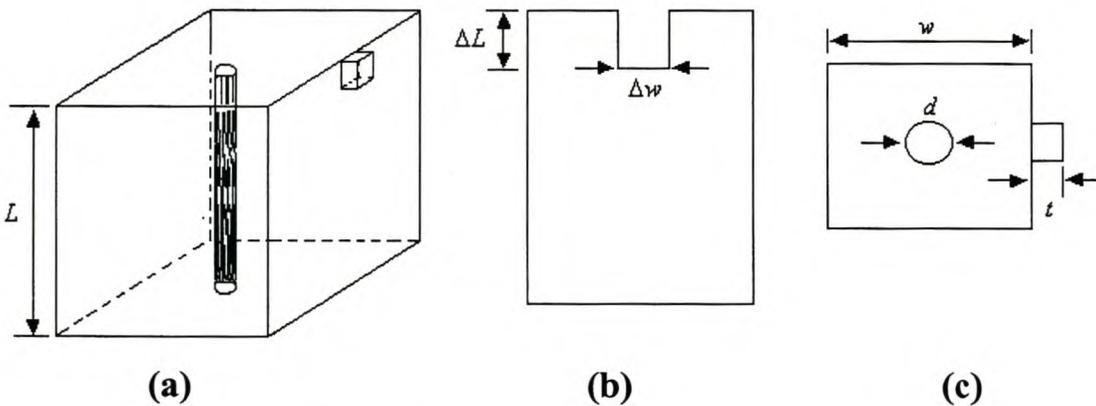
Figure 6.9 Dimensions of the coupling irises

The parameters L, w and d are given in Table 6.3.3 while the other dimensions can be determined using the method based on Bethe's theory and Cohn's experimental work or iris design with Ansoft Optimetrics method discussed in Chapter 5.

Table 6.3.4.1 shows the results that were obtained using iris design with Ansoft Optimetrics method. The resonant frequency was expected to decrease as the iris width, Δw, increases. However, the resonant frequencies obtained with this method are fluctuating as seen from table 6.3.4.1

In conclusion, this method fails to determine the resonant frequency. Hence, it cannot be used to determine the dimensions of the coupling irises.

Table 6.3.4.1 Ansoft Optimetrics results

Δw [mm]	f_e [GHz]	f_m [GHz]	ΔL [mm]	t [mm]
0.5	2.99783	2.99783	3	0.5
1	3.00124	3.00030	3	0.5
1.5	3.00160	2.99933	3	0.5
2	2.99674	2.99674	3	0.5
2.5	3.00149	2.99938	3	0.5
3	3.00086	3.00009	3	0.5
3.5	3.00107	2.99949	3	0.5
4	3.00123	2.99950	3	0.5
4.5	3.00082	2.99934	3	0.5
5	3.00069	2.9934	3	0.5

The results shown in Table 6.3.4.2 are obtained using the method based on Bethe's theory and Cohn's experimental work and were used in the filter mechanical structure.

Table 6.3.4.2 Bethe's theory and Cohn's experimental work

Δw [mm]	ΔL [mm]	k	t[mm]
1	2.3898	0.0108	0.5
1	2.5589	0.0168	0.5

6.4 Measurement Results of the Filter

A fourth order coaxial resonator waveguide coupled cavity filter was designed and manufactured using the above theory. Fig. 6.10 shows the coaxial resonator coupled cavity waveguide filter with four single mode cavities supporting a TEM mode.
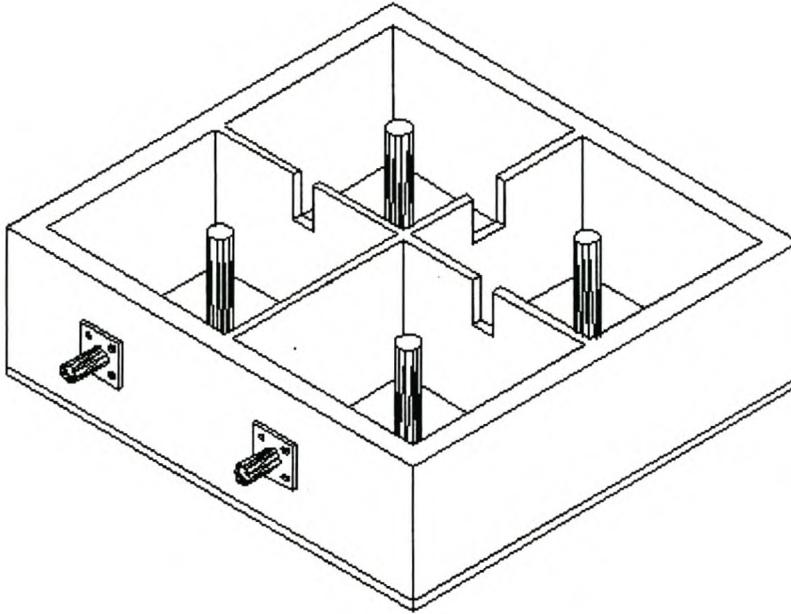
Figure 6.10 Co-axial resonator filter waveguide structure.

The experimental set-up is shown in Fig. 6.11. The experiment was performed by measuring system S-parameters on a full 2-port calibrated HP8753C Network Analyzer in the frequency range from 2.9 GHz to 3.1 GHz, using 201 sample points and the averaging was off. (i) and (ii) are the reference calibration planes which connects to plane (a) and (b), respectively.
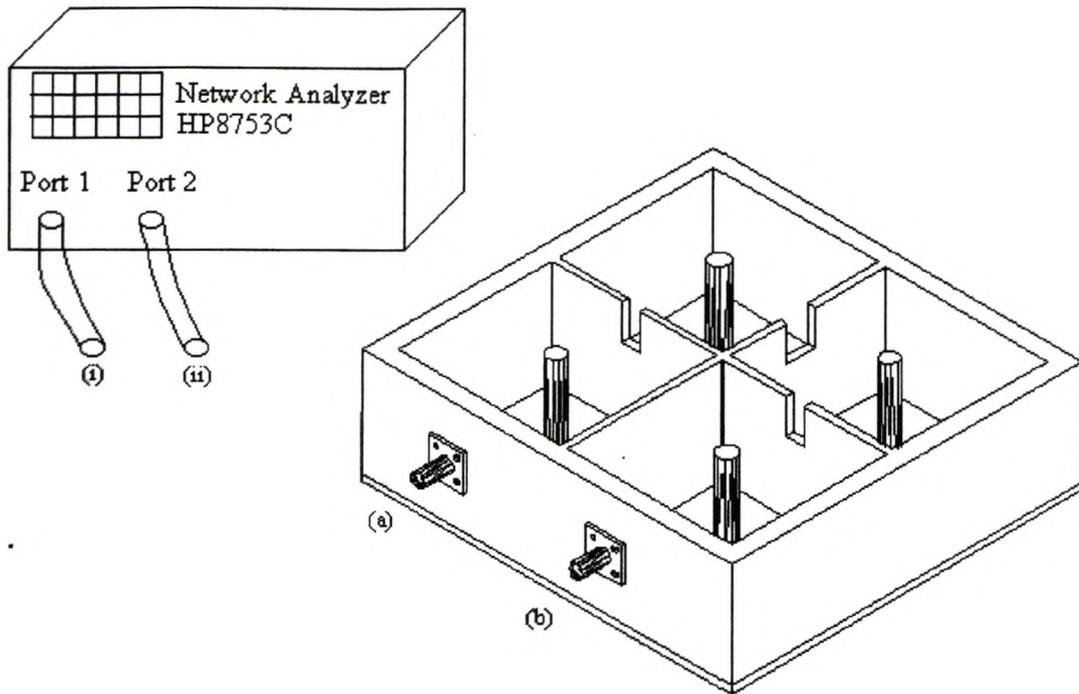
Figure 6.11 The experimental configuration

The measured response for the filter is shown in Fig. 6.12.
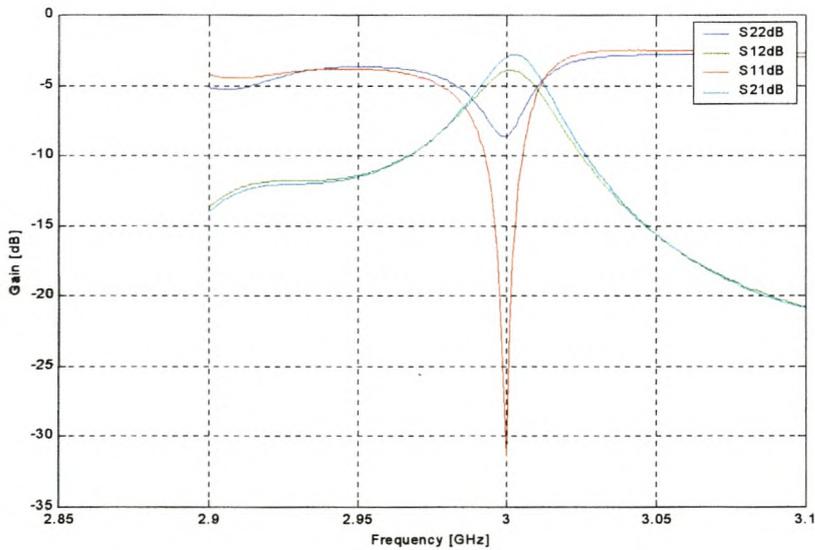
Figure 6.12 Measured filter response.

The reflection coefficients S_{22} reflects more than S_{11}, and this may have been caused by the connector at port 2 that were found to be damaged some time after the measurements were done. This is also why the magnitude of S_{12} and S_{21} differ. Unfortunately there was not any time to repeat these measurements.

A comparison between the measured response and design specification is summarized in Table 6.4

Table 6.4 Comparison between the measured response and design Specification.

	Desired	Measured
Center frequency	3GHz	3GHz
Bandwidth	2%	1%
Insertion loss	0.5 dB	3 dB

6.5 Theoretical Model For the Filter

Fig 6.13 shows the theoretical model that was used to predict the measured filter response shown in Fig. 6.12 above.
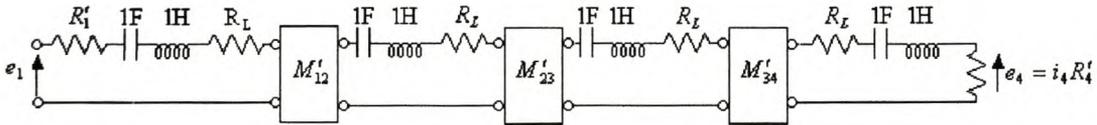
Figure 6.13 Filter theoretical model.

Here $M'_{12} = M'_{34} = 0.0108$, $M'_{23} = 0.0048$, $R'_1 = R'_4 = 0.0262$ and $R_L = 0.00131$. From Williams [Wi 1970] the loaded Q-factor of the filter is given by

$$Q = \frac{1}{R_L} = 763.359 \qquad (6.23)$$

A comparison of the predicted filter response and the measured filter response is shown in Fig. 6.14.
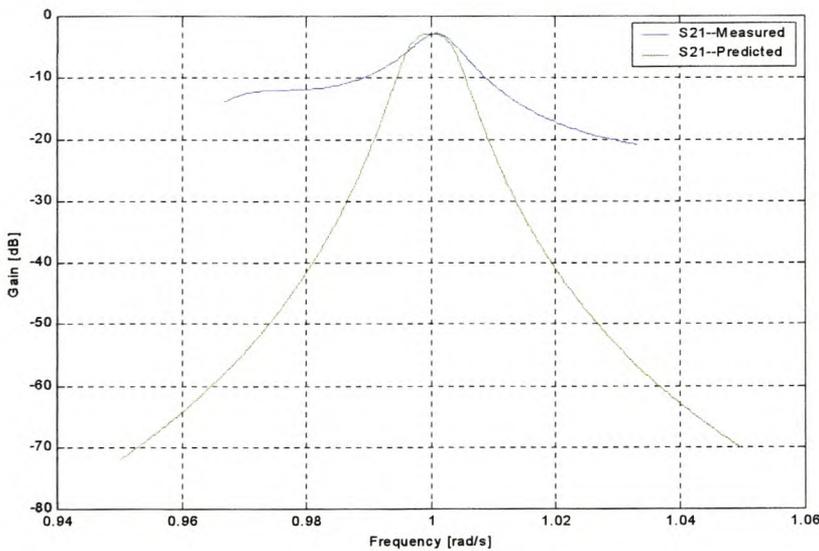
Figure 6.14 Comparison between measured filter and theoretical model responses.

The theoretical model is in good agreement with the measured results in terms of the center frequency.

6.6 Conclusion

A satisfactory filter response has been achieved especially regarding the center frequency and the insertion loss. The following parameters, however, has not been attained

- Bandwidth: It is believed that recalculation of the coupling coefficient can be used to obtain the necessary bandwidth.
- Coupling parameters M'_{12}, M'_{23} and M'_{34}: These are not attained due to non-existence of the field equation for a rectangular coaxial line. For this filter design, the field equation for a coaxial line are used to determine the dimensions of the coupling irises that realize the parameters M'_{12}, M'_{23} and M'_{34}.
- Q-factor: The desired Q-factor is 2500 and the predicted one is 763.359. The two points mentioned above can improve the Q-factor and in addition the mechanical filter structure might have losses due to construction tolerances causing the top wall not to make a proper contact to the sidewalls.

Nevertheless, a valuable experience has been gained from this exercise, i.e. Ansoft Optimetrics has been utilized in the determination of iris dimensions, even though it failed to determine the resonant frequency.

Chapter 7

Conclusions and Recommendations

7.1   Introduction

The objective of the project was to design a coupled coaxial resonator filter starting with the approximation function and ending up with a prototype filter.

This chapter gives a summary of the most important findings in this study. The thesis ends with the recommendations for future work.

7.2   Conclusions

A study of basic dynamics of filters with the emphasis on the Butterworth filter approximation function is given in Chapter 2. Furthermore, this approximation function was used in the synthesis of a doubly terminated coupling matrix.

The synthesis of a doubly terminated coupling matrix and calculation of the terminating resistance for the equivalent circuit (Fig. 3.1) was performed using Darlington's method. Usually the resulting coupling matrix has nonzero elements, but due to the restriction placed by the filter equivalent circuit, some of the elements had to be reduced with a coupling matrix reduction method. An analysis of the coupling matrix was made and a satisfactory response was achieved.

An investigation was performed on a half-wavelength rectangular coaxial resonator with a round center conductor. Since field equations for these resonators are not fully available, field equations for a coaxial line was used to solve for these.   These resonators were directly coupled to each other through rectangular apertures that was formed in the broad wall of each resonator. The dimensions of these apertures were determined using the method based on Bethe's theory and Cohn's experimental work.

In order to couple the input and output resonators to the external circuit, a part was added to the first and last resonators in the form of an SMA connector.

From the theory mentioned in the preceding paragraphs, a 4th-order coaxial resonator filter was designed. The measured response was in excellent agreement with theory in terms of the center frequency, but disagree in terms of the coupling coefficient, bandwidth and Q-factor. The reasons for this was given in section 6.6.

7.3   Future Work

To enhance the co-axial resonator filter performance, the following can be investigated:

- Experimental determination of the coupling iris dimensions.
- Bandwidth: The necessary bandwidth can be obtained by achieving the correct coupling iris dimensions.
- Q-factor: The two points mentioned above can improve the Q-factor and in addition the filter mechanical structure needs to be improved.
- Accurate simulation of the filter prior to construction.

Finally, the coupling between dissimilar cavities has not been addressed.   Both techniques presented in Chapter 5 assume identical cavities, which are a restriction placed on the filter by the equivalent circuit used.

References

[AH 1983]   E. Arvas, R. F. Harrington, " Computation of Magnetic Polarizability of Conducting Disks and the Electric Polarizability of Apertures ", IEEE Trans. on Antennas and Propagation, Vol.AP-35, No 5, Sept. 1983, pp. 719-724.

[AW 1967]   T. A. Abele and H.Wang, "An adjustable Narrow Band Microwave Delay Equalizer", IEEE Transactions on Microwave Theory and Techniques, MTT-15, No 10, Oct. 1967, pp. 566-574.

[AW 1971]   A. E. Atia, A. E. Williams, "New types of waveguide bandpass filters for satellite transponders", COMSAT Tech. Rev., vol. 1, no. 1, 1971, pp. 21-43.

[AW 1972-a]   A. E. Atia, A. E. Williams, "Narrow-Bandpass Waveguide Filters", IEEE Trans on MTT, Vol. MTT-20, April 1972, pp. 258-265.

[AW 1972-b]   A. E. Atia, A. E. Williams, "Nonminimum Phase Optimum-Amplitude Bandpass Waveguide Filter", IEEE Trans on MTT, Vol. MTT-22, April 1974, pp. 425-431.

[AW 1974]   A. E. Atia, A. E. Williams, "Narrow-Band Multiple-Coupled Cavity Synthesis", IEEE Transactions on Circuits and Systems, Vol. CAS-21, September 1974, pp. 649-655.

[Be 1944]   H. A. Bethe, "Theory of Diffraction by small holes", Phys. Rev., Vol. 66, Oct. 1944, pp. 163-182.

[BM 1970]   A. L. Berman and C. E. Mahle, "Nonlinear Phase Shift in Traveling wave Tubes as Applied to Multiple Access Communications Satellites", IEEE Transactions on Communication Technology , COM-18, No 1, Feb, 1970, pp. 37-48.

[BZ 1976]   Herman J. Blinchikoff, Anatol I. Zverev, "Filtering in the Time Domain and Frequency Domains", John Wiley & Sons, 1976.

[Ca 1999]   Richard J. Cameron, "General Coupling Matrix Synthesis Method for Chebyschev Filtering Functions", IEEE Trans on MTT, Vol. MTT-47, No 4, April 1999.

[Co 1951]   S.B. Cohn, "Determination of aperture parameters by Electrolytic-Tank Measurements", Proceedings of the IRE, Vol. 39, Nov. 1951, pp. 1416-1421.

[Co 1952-a]   S. B. Cohn, "The Electric Polarizability of Apertures of Arbitrary Shape", Proceedings of the IRE, Vol, 1952., pp. 1069-1071.

[Co 1952-b]   S. B. Cohn, "Microwave Coupling by Large Apertures", Proceedings of the IRE, Vol. 7, June 1952, pp. 696–699.

[Co 1957]   S.B Cohn, "Direct-coupled resonator filters" Proc. IRE, vol. 45, no. 2, February 1957, pp. 187-196.

[Co 1960]   R. E. Collin, " Field Theory of Guided Waves", New York, McGraw-Hill, 1960.

[Co 1968]   S. B. Cohn, "Microwave Bandpass Filters Containing High-Q Dielectric Resonators", IEEE. Trans on MTT, Vol. MTT-16, No. 4, April 1968.

[CKZ 1991]   Hsin-Chin Chang, Kawthar A. Zaki, "Evanescent-Mode Coupling Rectangular Waveguide Filters", IEEE Trans. on Microwave Theory and Techniques, Vol 39, No. 8, August 1991, pp. 1307-1312.

[Da 1939]   S. Darlington, "Synthesis of Reactance 4-Poles which Produce Prescribed Insertion Loss Characteristics", Journal of Mathematics and Physics, Vol. 18, No. 4, 1939, pp. 257-353.

[FPN 1994]   Gene F. Franklin, J. David Powell, Abbas Emami-Naeini, "Feedback Control of Dynamic Systems", Third Edition, Addison-Wesley, 1994.

[Gu 1972]   M.A.R. Gunston, "Microwave Transmission -Line Impedance Data", Van Nostrand Company, London, 1972, pp 5-8.

[IN 1979]   Osamu Inui and Junichi Nagai, "Miniaturization of Wide-Band VHF filters by using Spiral Resonators", Proc. IEEE, vol. 67, no. 1, January 1979, pp. 20-24.

[KG 1986]   D. Kajfez, P. Guillon, "Dielectric Resonators", Artech House, Chapter 1, 1986

[Le 1980]   R. Levy, "Improved Single and Multi-aperture Waveguide Coupling Theory, Including Explanation of Mutual Interactions", IEEE. Transactions on Microwave Theory and Techniques, Vol. MTT-28, No. 4, April 1980, pp.331–338.

[Li 1951]   W. G. Lin, "Microwave Filters Employing a Single Cavity Excited in More Than One Mode", Journal of Applied Physics, Vol.22, No. 8, August 1951, pp. 989-1001.

[Li 1978]   Larry F. Lind, "Accurate Cascade Synthesis", IEEE. Trans. on Circuits and Systems, Vol. CAS-25, No 12, December 1978.

[LIN 1985]   Weigan Lin, "Polygonal Coaxial Line with a Round Center Conductor", IEEE Trans. MTT-33, no. 6, June 1985, pp. 545-549.

[Mc 1972]   N. A. McDonald, "Electric and Magnetic Coupling through small apertures in Shield Walls of Any Thickness", IEEE Transactions on Microwave Theory and Techniques, Vol. MTT-20, No. 10, October 1972, pp. 689–695.

[MH 1994]   G. L. Matthaei, G. L. Hey-Shipton, "Concerning the Use of High-Temperature Superconductivity in Planar Microwave Filters", IEEE. Trans on MTT, Vol. 42, July 1994, pp. 1287-1293.

[MY 2001]   M. Makimota, S. Yamashita, "Microwave Resonators and Filters for Wireless Communication: theory, design and application", Springer-Vela Berlin Heidelberg New York, 2001, pp. 1-9.

[MYJ 1980]   G. Matthaei, L. Young, E. M. T. Jones, " Microwave filters, Impedance-Matching Networks, and Coupling Structures", Artech House, Dedham Massachusetts, 1980.

[Og 1990]   Katsuhiko Ogata, "Modern control Engineering", Second Edition Prentice Hall International Editions, 1990.

[PM 1975]   John D. Paliouras, Douglas S. Meadows, "Complex variables for Scientists and Engineers", Second Edition, MacMillan Publishing Company, New York, 1975, pp. 4-14.

[Po 1998-a]   David M. Pozar, "Microwave Engineering", Second Edition, John Willey and Sons, 1998, pp. 182-243.

[Po 1998-b]   David M. Pozar, "Microwave Engineering", Second Edition, John Willey and Sons, 1998, pp 300-343.

[Po 1998-c]   David M. Pozar, "Microwave Engineering", Second Edition, John Willey and Sons, 1998, pp. 56-96.

[Po 1998-d]   David M. Pozar, "Microwave Engineering", Second Edition, John Willey and Sons, 1998, pp. 104-176.

[Rh 1976]   J. D. Rhodes, "Theory of Electrical Filters", Wiley-Interscience, 1976.

[Ri 1939]   R. D. Richtemeyer, "Dielectric resonator", J.Appl.Phys, vol. 10, June 1939, pp. 391.

[Ri 1983]   H. J. Riblet, "An Accurate Approximation of the Impedance of a Circular Cylinder Concentric with an External Square Tube", IEEE.Trans.MTT-31, no.10, October 1983, pp. 841-844.

[Ri 1988]   Peter A. Rizzi, "Microwave Engineering Passive Circuits", Prentice Hall, Eaglewood, New Jersey 07632.

[RZ 1980]   R. J. Rhodes, I. H. Zabalawi, "Synthesis of Symmetrical Dual Mode Inline Prototype Networks", Circuit theory and Applications, Vol. 8, 1980, pp. 145-160.

[RWV 1994] S. Ramo, J. R. Winnery and T. Van Duzer, "Fields and Waves in Communication Electronics", Third Edition, John Willey and Sons, N. Y, 1994.

[Su 1996-a]   Kendal L. Su, "Analog Filters", Kluver Academic Publishers, 1996, pp. 1-18.

[Su 1996-b]   Kendal L. Su, "Analog Filters", Kluver Academic Publishers, 1996, pp. 23-41.

[Su 1996-c]   Kendal L. Su, "Analog Filters", Kluver Academic Publishers, 1996, pp. 47-72.

[Su 1996-d]   Kendal L. Su, "Analog Filters", Kluver Academic Publishers, 1996, pp. 75-86

[Su 1996-e]   Kendal L. Su, "Analog Filters", Kluver Academic Publishers, 1996, pp. 91-116.

[Su 1996-f]   Kendal L. Su, "Analog Filters", Kluver Academic Publishers, 1996, pp. 143-165.

[TL 1977-a]   Gabor C. Temes, Jack W. LaPatra, "Introduction to Circuit Synthesis and Design", McGraw-Hill, Inc, 1977, pp. 1-25.

[TL 1977-b]   Gabor C. Temes, Jack W. LaPatra, "Introduction to Circuit Synthesis and Design", McGraw-Hill, Inc, 1977, pp. 194-241.

[UBR 1993]   J. Uher, J. Bornemann, U. Rosenberg, "Waveguide Components for antenna Feed Systems: Theory and CAD", Artech House, Boston, 1993.

[Va 1960]   M. E. Van Valkenburg, "Introduction to Modern Network Synthesis", New York: Wiley, 1960.

[Wi 1971]   Albert. E. Williams, "A Four-Cavity Elliptic Waveguide Filter", IEEE Trans. on Microwave Theory and Techniques, Vol. MTT-18, December 1970, pp. 1109-1114.

[Wo 1979]   Joseph S. Wong, " Microstrip Tapped-Line Filter Design ", IEEE Trans. on Microwave Theory and Techniques, Vol. MTT-27, No.1, January 1979, pp. 44-50.

Appendix A

Gram Schmidt Orthonormalisation Method

Orthogonal sets of vectors simplify mathematical manipulations. The Gram Schmidt process uses a set of linearly independent vectors to construct an orthogonal basis. If the given set of linearly independent vectors are X_i, the corresponding vectors V_i by a recursive formula [La 1996]:

$$V_i = X_i - \frac{X_i \cdot V_i}{V_1 \cdot V_1} - \frac{X_i \cdot V_2}{V_2 \cdot V_2} - \cdot \quad \cdot \quad \cdot - \frac{X_i \cdot V_{i-1}}{V_1 \cdot V_{i-1}} V_{i-1}$$

These vectors need to be normalized to unit vectors to produce a set of orthonormal vectors.

Appendix B

Listing of Matlab Routines

B.1 Coupling matrix synthesis

```
y22n = 2.6131259*[1 0 1 0];
y22d = [2 0 3.4142134 0 1];
y21n = j*1;

[R22,P22,K22] = residue(y22n,y22d);
[R21,P21,K21] = residue(y21n,y22d);

n = sqrt(sum(R22));
TN = sqrt(R22')/n;
T1 = R21'./(TN*n^2)

% Completion of T-matrix by Gramm-Schmidt process
x1 = T1;
x2 = TN;
u3 = [1 0 0 0];
u4 = [0 1 0 0];
v3 = u3-(u3*x2')*x2-(u3*x1')*x1;
x3 = v3/sqrt(v3*v3');
v4 = u4-(u4*x3')*x3-(u4*x2')*x2-(u4*x1')*x1;
x4 = v4/sqrt(v4*v4');

T = [T1;x3;x4;TN];
M = T*j*diag(P22)*T';

Rt = eye(4);
theta = -atan2(M(1,3),M(1,2));
Rt(2,2) = cos(theta);
Rt(3,3) = cos(theta);
Rt(2,3) = -sin(theta);
Rt(3,2)=sin(theta);

M = Rt*M*Rt';
M = M1
Q = 2000;
Qm = eye(4)*1/Q;
wo = 1;
B = 0.02;

Ro = n^2;
M = M*B
```

```
Ro = Ro*B;

R = zeros(4,4);
R(1,1) = Ro;
R(4,4) = Ro;

w = [0.0001:0.001:2];
s=j*w;

for n=1:size(s,2),

    Zbandpass=((s(n)^2+1)/(s(n)))*eye(4)+R+j*wo*M+Qm;
    Zlowpass=s(n)*eye(4)+R+j*wo*M;
    I=inv(Zbandpass)*[1 0 0 0]';
    V2bandpass(n)=I(4)*Ro;
    I=inv(Zlowpass)*[1 0 0 0]';
    V2lowpass(n)=I(4)*Ro;

end

plot(w,20*log10(2*abs(V2lowpass)));
xlabel('frequency(rad/s)');
ylabel('transmission coefficient(dB)');
grid;
figure;
plot(w,20*log10(2*abs(V2bandpass)));
xlabel('frequency(rad/s)');
ylabel('transmission coefficient(dB)');
grid;
```

B.2 Determination of the Tap point position

```
clear all;

w = [0.95:0.0001:1.05];

for n = 1:size(w,2),

s = j*w(n);
Zo = 2/pi;
Rs = 0.0262; Ro=0.0262;
R = 50;
Ts = [1 Rs;0 1];
To = [1 0;1/Ro 1];

theta = pi*w(n);
Tr = [cos(theta) j*Zo*sin(theta); j*sin(theta)/Zo cos(theta)];
```

```
M = 0.01682;
Tk12 = [0 -s*M;1/(s*M) 0];

M = 0.01082;
Tk23 = [0 -s*M;1/(s*M) 0];

TF = Ts*Tr*Tk12*Tr*Tk23*Tr*Tk12*Tr*To;
S21f(n)= 2/TF(1,1);
y =  (abs(S21f(n))).^2;
S11f(n) = -sqrt(1-y);


% Determination of the correct tap point position

Zt = 70*pi/2;
R = 50;
K12=0.0168*Zt; K23=0.0108*Zt;
Ts = [1 R;0 1];
Tk12 = [0 j*K12; j/K12 0];
Tk23 = [0 j*K23; j/K23 0];
To = [1 0;1/R 1];
Zo = Zt*2/pi;
Tr = [cos(theta) j*Zo*sin(theta); j*sin(theta)/Zo cos(theta)];
x = 0.0556;
theta1 = theta*x;
Tr1 = [cos(theta1) j*Zo*sin(theta1); j*sin(theta1)/Zo cos(theta1)];
thetapar = (1-x)*theta;
Tpar = [1 0; 1/(j*Zo*tan(thetapar)) 1];
Tx = [1 j*0;0 1];
TF = Ts*Tx*Tpar*Tr1*Tk12*Tr*Tk23*Tr*Tk12*Tr1*Tpar*Tx*To;
S21ff(n) = 2/TF(1,1);

end

plot(w,20*log10(abs([S21ff])),w,20*log10(abs([S21f])));
xlabel('Frequency[rad/s]')
ylabel('Gain[dB]')
legend('distributed filter','Tap point position')
grid on;
```

B.3 Rectangular Coaxial line concentric with a circular center conductor

```
clear all
b1=1    %input('b(in cm) = ');
b1=b1/1e2
```

```
b2=2;
b2=b2/1e2;

b3=3;
b3=b3/1e2;

muo = 4*pi*(10^(-7));
mur=1;
mu = muo*mur;
epso=8.854e-12;
epsr = 1;
eps=epso*epsr;
f= 3e9;
sigma=3.816e7;
c = 2.997525e8;
lamda = c/f;
L = lamda/2;
delt= 1/sqrt(pi*f*sigma*muo);
  n=1;

for Zo = 1:1:70,
  bd1(n) = exp(Zo/(59.952)-0.06962);
  db1(n) = 1./(exp(Zo/(59.952)-0.06962));
  d1 = b1*db1(n);
  alph1 = (1.3273e-3/(b1))*(1/(sigma*delt));
  alph2 = (bd1(n) + 0.744186)./(log(bd1(n))+0.06962);
  alpha1(n) = alph1.*alph2;
  Q1(n)      = pi./(2*alpha1(n)*L);

  bd2(n) = exp(Zo/(59.952)-0.06962);
  db2(n) = 1./(exp(Zo/(59.952)-0.06962));
  d2 = b2.*db2(n);
  alph3 = (1.3273e-3/(b2))*(1/(sigma*delt));
  alph4 = (bd2(n) + 0.744186)./(log(bd2(n))+0.06962);
  alpha2(n) = alph3.*alph4;
  Q2(n)      = pi./(2.*alpha2(n).*L);

  bd3(n) = exp(Zo/(59.952)-0.06962);
  db3(n) = 1./(exp(Zo/(59.952)-0.06962));
  d3 = b3.*db3(n);
  alph5 = (1.3273e-3/(b3))*(1/(sigma*delt));
  alph6 = (bd3(n) + 0.744186)./(log(bd3(n))+0.06962);
  alpha3(n) = alph5*alph6;
  Q3(n)      = pi./(2.*alpha3(n).*L);
  n = n+1;
end

Z  = [1:1:70];
plot(db3,Z,'.',db3,Z)
title('Characteristic impedance vs Dimensions')
```

```
legend ('b = 0.03m')
xlabel('d/b(m)')
ylabel('Characteristic impedance(Ohm)')
grid on
figure
plot(Z,Q1,'-',Z,Q2,'-*',Z,Q3,'-.')
title('Unloaded Quality factor vs Characteristic Impedance')
legend ('b=0.01m','b=0.02m','b=0.03m')
xlabel('Characteristic Impedance(Ohm)')
ylabel('Quality factor')
grid on
```

B.4 Circular Coaxial Line

```
clear all,
b1= 1;
b1=b1/1e2;

b2=2;
b2=b2/1e2;

b3=3;
b3=b3/1e2;

muo = 4*pi*(10^(-7));
mur=1;
mu = muo*mur;
epso=8.854e-12;
epsr = 1;
eps=epso*epsr;
f = 3e9;
sigma=3.816e7;
c = 2.997525e8;
lamda = c/f;
L = lamda/2;
delt= 1/sqrt(pi*f*sigma*muo);
tand=tan(delt);
A=sqrt(mu/eps)
   n=1;

for Zo= 1:1:70
```

%for a cylindrical coaxial line

```
bd1(n)=exp(Zo.*2.*pi/A);
db1(n)=1./(exp(Zo.*2.*pi/(A)));
d1(n)=b1./bd1(n);
G = 4*pi^2*eps*tand./(log(bd1(n)));
R = sqrt(f*mu/(pi*sigma))*(1/(b1)+ 1./(d1(n)));
alpha1(n)=0.5.*(G.*Zo+R./Zo);
Q1(n)=pi/(2.*alpha1(n).*L);

bd2(n)=exp(Zo.*2.*pi/A);
db2(n)=1./(exp(Zo.*2.*pi/(A)));
d2(n)=b2./bd2(n);
G2 = 4*pi^2*eps*tand./(log(bd2(n)));
R2 = sqrt(f*mu/(pi*sigma)).*(1/(b2)+ 1./(d2(n)));
alpha2(n)=0.5.*(G2.*Zo+R2./Zo);
Q2(n)=pi/(2.*alpha2(n).*L);

bd3(n)=exp(Zo.*2.*pi/A);
db3(n)=1./(exp(Zo.*2.*pi/(A)));
d3(n)=b3./bd3(n);
G3 = 4*pi^2*eps*tand./(log(bd3(n)));
R3 = sqrt(f*mu/(pi*sigma)).*(1/(b3)+ 1./(d3(n)));
alpha3(n)=0.5.*(G3.*Zo+R3./Zo);
Q3(n)=pi/(2.*alpha3(n).*L);


n=n+1;

end
Z=1:1:70;

plot(Z,Q1,'-*',Z,Q2,'-',Z,Q3,'-.')
legend ('b=0.01m','b=0.02m','b=0.03m')
title('Quality factor vs Characteristic impedance')
xlabel('Characteristic Impedance');
ylabel('Quality Factor');
grid on
save impedance Z Q2  -ascii -double -tabs
figure
plot(db3,Z)
title('Characteristic impedance vs dimensions of the Line')
ylabel('Characteristic Impedance');
xlabel('d/b (m)');
legend ('b=0.03m')
grid on
```